REPORT DOCUMENTATION PAGE

Form Approved
OMB NO. 0704-0188

1. AGENCY USE ONLY (Leave Blank)	2. REPORT DATE	3. REPORT TYPE AND DATES COVERED
	June 30, 2004	Final Report 4/1/01-3/31/04

4. TITLE AND SUBTITLE
Control of Systems with Periodic Coefficients, with Application to Active Rotor Control

5. FUNDING NUMBERS
DAAD19-01-1-0415
[redacted]

6. AUTHOR(S)
Roberto Celi, Marco Lovera, and Patrizio Colaneri

7. PERFORMING ORGANIZATION NAME(S) AND ADDRESS(ES)
Department of Aerospace Engineering
University of Maryland, College Park, MD 20742

8. PERFORMING ORGANIZATION REPORT NUMBER
None

9. SPONSORING / MONITORING AGENCY NAME(S) AND ADDRESS(ES)
U. S. Army Research Office
P.O. Box 12211
Research Triangle Park, NC 27709-2211

10. SPONSORING / MONITORING AGENCY REPORT NUMBER
41569.2-EG

11. SUPPLEMENTARY NOTES
The views, opinions and/or findings contained in this report are those of the author(s) and should not be construed as an official Department of the Army position, policy or decision, unless so designated by other documentation.

12 a. DISTRIBUTION / AVAILABILITY STATEMENT
Approved for public release; distribution unlimited.

12 b. DISTRIBUTION CODE

13. ABSTRACT (Maximum 200 words)

The project focused on the analysis and synthesis of active rotor controls. The rotor was modeled as a periodic system. The key accomplishments are:

(i) First systematic study of the effect of zeros in rotorcraft aeromechanics. The "zeros" play a key role in the closed-loop behavior of the system. As rotor active controls become feasible, the calculation of zeros needs to become a routine design step.

(ii) First study of the effects of closed-loop HHC/IBC on the aeroelastic stability of a helicopter rotor including, for example, the in-plane damping. This is especially important for configurations with inherently low inplane damping such as bearingless rotors.

(iii) Presentation to the rotorcraft community of techniques for the analysis of periodic systems developed in other areas of engineering, e.g., in the signal processing and control engineering communities.

(iv) First study of the effects of closed-loop HHC/IBC on the aeroelastic stability of a helicopter, including the effects of the discrete elements, and of different sampling and update rates in the system.

In all cases, a realistic mathematical model was used, with typically more than 35 degrees of freedom, including blade flexibility and nonlinear rigid body dynamics.

14. SUBJECT TERMS
Helicopter aeroelasticity
Helicopter rotor control
Helicopter aeroservoelasticity

15. NUMBER OF PAGES
[redacted]
174

200 PRICE CODE

200 SECURITY CLASSIFICATION OF REPORT	18. SECURITY CLASSIFICATION ON THIS PAGE	200 SECURITY CLASSIFICATION OF ABSTRACT	(1) LIMITATION OF ABSTRACT
UNCLASSIFIED	UNCLASSIFIED	UNCLASSIFIED	UL

REPORT DOCUMENTATION PAGE (SF298)
(Continuation Sheet)

Papers submitted under ARO sponsorship during the reporting period:

Lovera, M., Colaneri, P., Malpica, C., and Celi, R., "Closed-Loop Aeromechanical Stability Analysis for a Hingeless Rotor Helicopter With HHC or IBC," ***Proceedings of the 29th European Rotorcraft Forum***, Friedrichshafen, Germany, September 2003; accepted for publication in the ***Journal of Guidance, Control, and Dynamics***.

Lovera, M., Colaneri, P., and Celi, R., "Periodic Control Issues in the Higher Harmonic Control of Helicopter Rotors," ***Proceedings of the American Control Conference***, Denver, CO, May 2003.

Colaneri, P., Celi, R., and Bittanti, S., "Constant-Coefficient Representations of Periodic-Coefficient Discrete Linear Systems," ***Proceedings of the AHS 4th Decennium Specialist Conference on Aeromechanics***, San Francisco, CA, January 2004.

Lovera, M., Colaneri, P., Malpica, C., and Celi, R., "Discrete-Time, Closed-Loop Aeromechanical Stability Analysis of Helicopters With Higher Harmonic Control," ***Proceedings of the 60th Annual Forum of the American Helicopter Society***, Baltimore, MD, June 2004.

(this is only a partial list of publications, please see the full Final Report for a complete list)

Scientific personnel supported by this project:

Dr. Roberto Celi, and Mr. Carlos Malpica, University of Maryland, College Park; Dr. M. Lovera, Dr. P. Colaneri, and Dr. S. Bittanti, Politecnico di Milano, Milan, Italy.

Report of inventions

None

Scientific progress and accomplishments

The project focused on the analysis and synthesis of active rotor controls. The rotor was modeled as a periodic system. The key accomplishments are:

(i) First systematic study of the effect of zeros in rotorcraft aeromechanics. The "zeros" play a key role in the closed-loop behavior of the system. As rotor active controls become feasible, the calculation of zeros needs to become a routine design step.

(ii) First study of the effects of closed-loop HHC/IBC on the aeroelastic stability of a helicopter rotor including, for example, the in-plane damping. This is especially important for configurations with inherently low inplane damping such as bearingless rotors.

(iii) Presentation to the rotorcraft community of techniques for the analysis of periodic systems developed in other areas of engineering, e.g., in the signal processing and control engineering communities.

(iv) First study of the effects of closed-loop HHC/IBC on the aeroelastic stability of a helicopter, including the effects of the discrete elements, and of different sampling and update rates in the system.

In all cases, a realistic mathematical model was used, with typically more than 35 degrees of freedom, including blade flexibility and nonlinear rigid body dynamics.

Technology transfer

Interactions with Drs. Mark Tischler and Rendy Cheng, U.S. Army Aeroflightdynamics Directorate, Ames Research Center.

CONTROL OF SYSTEMS WITH PERIODIC COEFFICIENTS, WITH APPLICATION TO ACTIVE ROTOR CONTROL

Contract Number DAAD19-01-1-0415
Project Number 41569-EG

FINAL REPORT

submitted by:

Roberto Celi
Department of Aerospace Engineering
University of Maryland, College Park

and

Marco Lovera
Patrizio Colaneri
Sergio Bittanti
Dipartimento di Elettronica e Informazione
Politecnico di Milano, Milano, Italy

June 30, 2004

Contents

List of Figures

Notation

A, B	State and control matrices
$A(t)$	Open loop stability matrix
A_0	Stability matrix (constant approximation)
$\mathcal{A}, \mathcal{B}$	A and B matrices in Fourier reformulation
$\bar{A}(t)$	Closed loop stability matrix
B	Number of blocks in the Harmonic Transfer Function
$B(t)$	Input (control) matrix
B_0	Input (control) matrix (constant approximation)
C, D	Output and feedthrough matrix
$C(t)$	Output (measurement) matrix
C_0	Output (measurement) matrix (constant approximation)
C_T	Rotor thrust coefficient
$\mathcal{C}, \mathcal{D}$	C and D matrices in Fourier reformulation
$D(s)$	Denominator of the system transfer function
$D(t)$	Direct input/output matrix
D_0	Direct Input/Output matrix (constant approximation)
E_k	Feedthrough matrix of time-lifted reformulation
F_k	State matrix of time-lifted reformulation
$G(\sigma, k)$	Input-output transfer function
G_k	Control matrix of time-lifted reformulation
$G(s)$	System transfer function
$H(s)$	IBC compensator's transfer function
H_k	Output matrix of time-lifted reformulation
$H_i(z, s)$	Sampled transfer function

m	Number of control inputs
M	Monodromy matrix
k	Sample number, $k = \ell T + s$, and discrete-time variable associated with T (1/rev dynamics)
K	Gain of HHC controller
ℓ	Number of periods required to reach k
$M_i(k)$	Periodic Markov coefficients
N	Number of rotor blades
n	Number of measured outputs
n	System order
n_s	System order
n_s	Number of acceleration (output) samples per revolution, $n_s = T/P$
$N(s)$	Numerator of the system transfer function
p	Number of measured outputs
P	Acceleration (output) sampling interval, $P = T/n_s$
r	Relative degree
r	Tuning parameter in HHC performance index
R	Zero dynamics
R	Control weighting matrix in HHC performance index
s	Sample number within a period
T	Number of samples in one period, also, period of one rotor revolution
T_C	HHC gain matrix
t	Time
$\mathbf{u}$	Control (or input) vector
$\mathbf{u}_{FCS}$	Pilot or flight control system input
$\mathbf{u}_{HHC}$	HHC input

$\mathbf{v}(k), \mathbf{V}(\sigma)$	Generic signal and its z-transform
$w, \dot{w}$	Heave velocity and acceleration of the CG
$\tilde{W}(\sigma)$	Frequency-lifted transfer function
W	Output weighting matrix in HHC performance index
$\mathbf{x}$	State vector
$\mathbf{y}$	Output (measurement) vector
$\mathbf{y}^i_{Nc}$, $\mathbf{y}^i_{Ns}$	N/rev cosine and sine harmonic of i-th acceleration measurement (output)
z	Time shift operator (by T samples)
β	Blade flapping angle
Γ	Instantaneous interaction matrix
η	Discrete-time variable associated with P (acceleration sampling)
θ_0	Collective pitch
θ_{1c}, θ_{1s}	Lateral and longitudinal cyclic pitch
θ_{kc}, θ_{ks}	k/rev cosine and sine harmonic of pitch control input
μ	Advance ratio
ϕ	Complex number, $\phi = \exp(j2\pi/T)$
Φ	Transition matrix
$\Phi_A(t, \tau)$	Transition matrix from τ to t
ψ	Azimuth angle of reference blade, $\psi = \Omega t$
$\Psi_A(0)$	Transition matrix at the end of one period
σ	Rotor solidity
σ	Time shift operator (by one sample)
ω_{L1}	Fundamental rotor lag frequency
Ω	Rotor angular velocity

Subscripts and superscripts

$(\ )_C$	Quantity in the controller model

$(\ )_F$	Quantity in the harmonic analyzer model
$(\ )_H$	Quantity in the helicopter dynamic model
$(\ )_{lift}$	Time-lifted quantity
$(\ )_Z$	Quantity in the zero-order-hold model
$(\tilde{\ })$	Discrete-time counterpart of continuous-time signal

Abbreviations

CG	Center of mass of the helicopter
EMP	Exponentially Modulated Periodic
HHC	Higher Harmonic Control
HTF	Harmonic Transfer Function
IBC	Individual Blade Control
LTI	Linear Time Invariant (or constant-coefficient) model
LTP	Linear Time Periodic (or periodic-coefficient) model
MCT	Multiblade Coordinate Transformation
MIMO	Multi-Input Multi-Output
NMP	Nonminimum phase
PHHC	Periodic Higher Harmonic Control
RHP	Right-Half-Plane
SISO	Single-Input Single-Output
/rev	Per rotor revolution (frequency)

Chapter 1

Summary

This Final Report begins with a summary of key accomplishments for the entire project. They include: (i) the first systematic study of the effect of zeros in rotorcraft aeromechanics, (ii) the first study of the effects of closed-loop HHC/IBC on the aeroelastic stability of a helicopter rotor, (iii) a presentation to the rotorcraft community of techniques for the analysis of systems with periodic coefficients developed in other areas of engineering, and (iv) the first study of the effects of closed-loop HHC/IBC on the aeroelastic stability of a helicopter, considered as a discrete system. Each of the accomplishments and their significance are briefly discussed.

The next chapter, Chapter 3, describes the role of the zeros of input-output models for coupled rotor-fuselage systems, modeled as linear systems with constant or periodic coefficients. The zeros do not affect open loop stability, but they can affect closed loop stability, and may trigger closed-loop instabilities with high feedback gains. The constant coefficient approximations obtained through a multiblade coordinate transformation usually give accurate pole predictions for advance ratios of up to $\mu = 0.3 - 0.35$, but the zeros are reasonably accurate only up to about $\mu = 0.2$. The calculation of the zeros can have much worse numerical properties than that of the poles because of large ratios between largest and smallest zeros. Therefore the techniques normally used in Floquet stability analysis often prove inadequate. The study also shows that the lag poles are not canceled by corresponding zeros, therefore the heave response to collective is affected by rotor lag dynamics, especially

at higher thrust, and for stiff-in-plane configurations. This transfer function has several zeros close to the imaginary axis or with positive real parts. Their number and location depend on the configuration, but at least one nonminimum phase zeros is present, and at every speed. This limits the benefits achievable from active control systems.

The following chapter, Chapter 4, describes the development of a state space formulation for a Multi-Input Multi-Output (MIMO) Higher Harmonic Control (HHC) system. The development starts with a simple state space derivation for the continuous time form of a Single-Input Single-Output (SISO) HHC compensator with input and output at the same rotor harmonic; then the same approach is extended to the case of different harmonics in input and output, which result in a periodic SISO HHC compensator; finally, that result is generalized for the derivation of the state space form for a MIMO HHC controller. The chapter contains results of a numerical investigation into the performance and stability properties of a closed loop HHC system, implemented in the rotating system, based on a simulation study of the coupled rotor-fuselage dynamics of a four bladed hingeless rotor helicopter.

The results show that the HHC controller is very effective in reducing the 4/rev accelerations at the center of gravity. The percentage reductions obtained in the simulations are in excess of 80-90%. The vibration attenuation occurs within 5-7 seconds after the HHC system is turned on. This is equivalent to a frequency of around 1 rad/sec, which is a frequency at which flight control systems and human pilots tend to operate. Therefore, the interactions and potential adverse effects on the stability and control characteristics of the helicopter should be explored. The HHC problem is intrinsically time-periodic if the HHC inputs include frequencies other than the frequency one wishes to attenuate. This is true even if the rest of the model is assumed to be time-invariant. In these cases, the closed-loop stability results obtained using a constant coefficient approximations may be incorrect even at lower values of the advance ratio μ, where constant coefficient approximations of the open-loop dynamics are accurate.

Chapter 5 describes in great detail some basic concepts in the treatment of discrete systems with periodic coefficients. In particular, the chapter describes the derivation of transfer functions for such systems, which are the foundation for the methods to convert systems with periodic coefficients into equivalent systems with constant coefficients.

The following chapter, Chapter 6, describes how to convert the periodic coefficient representation of a discrete linear system into a constant coefficient model that has the same stability characteristics and is equivalent from the input-output point of view. This is the key ingredient for the stability analysis of a helicopter with a closed-loop higher harmonic control (HHC) system. In fact, typical HHC implementation contain discrete elements and multiple sample/update rates. The extraction of a linearized discrete model from the continuous one is described. The Floquet characteristic multipliers and characteristic exponents are the same for the discrete and continuous systems, and therefore the open loop stability characteristics of the two systems are exactly the same. Time-lifting converts a system with periodic coefficients into a larger system, but with constant coefficients. Time-lifting is based on two properties of discrete periodic systems, namely: (i) the response of the periodic system can be modeled as the combination of the responses of multiple constant-coefficient systems, one per sample, and (ii) using shifting operators, it is possible to "move" all the system inputs at the same sample in multiple periods to that sample in a single period. Other discrete, constant coefficient reformulations are available, both in the time- and in the frequency-domain. These reformulations can be useful for theoretical studies and practical applications. Numerical examples for a simple helicopter blade model are provided for transfer functions and time-lifted reformulations.

The last chapter, Chapter 7, presents an aeromechanical closed loop stability and response analysis of a hingeless rotor helicopter with a Higher Harmonic Control (HHC) system for vibration reduction. The analysis includes the rigid body dynamics of the helicopter and blade flexibility. The gain matrix is assumed to be fixed and computed off-line. The discrete

elements of the HHC control loop are rigorously modeled, including the presence of two different time scales in the loop. By also formulating the coupled rotor-fuselage dynamics in discrete form, the entire coupled helicopter-HHC system could be rigorously modeled as a discrete system. The effect of the periodicity of the equations of motion is rigorously taken into account by converting the system into an equivalent system with constant coefficients and identical stability properties using a time lifting technique.

The most important conclusion of the study is that the discrete elements in the HHC loop must be modeled in any HHC analysis. Not doing so is unconservative. For the helicopter configuration and HHC structure used in this study, an approximate continuous modeling of the HHC system indicates that the closed loop, coupled helicopter-HHC system is always stable, whereas the more rigorous discrete analysis shows that closed loop instabilities can occur. The HHC gains must be reduced to account for the loss of gain margin brought about by the discrete elements. Other conclusions of the study are: (i) the HHC is effective in quickly reducing vibrations, at least at its design condition; (ii) a linearized model of helicopter dynamics is adequate for HHC design, as long as the periodicity of the system is correctly taken into account, i.e., periodicity is more important than nonlinearity, at least for the mathematical model used in this study; and (iii) when discrete and continuous systems are both stable, the predicted HHC control harmonics are in good agreement, although the initial transient behavior can be considerably different.

Chapter 2

Key accomplishments

2.1 Research accomplishments

The key accomplishments of the project are briefly summarized below:

1. *First systematic study of the effect of zeros in rotorcraft aeromechanics.* The "zeros" of a dynamic system play a key role in the closed-loop behavior of the system. For example, if one or more of the zeros have positive real parts, a control system designed to stabilize the system could instead make it unstable. The rotorcraft dynamics community had been able to mostly neglect the issue because rotor systems were not actively controlled. As rotor active controls become technologically feasible and desirable, the calculation and study of zeros must become a routine step of rotor design.

2. *First study of the effects of closed-loop HHC/IBC on the aeroelastic stability of a helicopter rotor.* Despite over three decades of research in HHC/IBC, no information was available on how an HHC/IBC system would affect, for example, the in-plane damping of a helicopter rotor. No results showing the effects of HHC/IBC on stability eigenvalues or Floquet characteristic exponents for rotor and/or fuselage modes had ever been presented. This is clearly a vital piece of information for the future use of active rotor controls in configurations with inherently low inplane damping such as hingeless and bearingless rotors.

3. *Presentation to the rotorcraft community of techniques for the analysis of systems with periodic coefficients developed in other areas of engineering.* Several time- and frequency-domain techniques, developed in the last two decades primarily in the signal processing and control engineering communities, have been introduced to the rotorcraft community through relevant, helicopter-oriented application examples.

4. *First study of the effects of closed-loop HHC/IBC on the aeroelastic stability of a helicopter, considered as a discrete system.* A typical model of a helicopter with HHC or IBC contains continuous portions (e.g., rotor and fuselage dynamics) and discrete portions (e.g., harmonic analysis to extract vibratory components, HHC inputs updated once per revolution, etc.). The stability study mentioned as item 3. above was carried out by approximately modeling some discrete elements as continuous and simply neglecting the rest. Subsequently, we have modeled the entire system as discrete. As a consequence, we have developed *the first rigorous solution of the aeroelastic stability problem for a helicopter with HHC or IBC, including the effects of the discrete elements, and of different sampling and update rates in the system.* Also, this was essentially the first solution of the aeroelastic equations as discrete systems (a previous example in the literature was much more limited in scope).

In all the accomplishments just listed, the mathematical model of the helicopter was of realistic complexity, and not an idealized, simplified representation. In most cases, the model contained more than 35 degrees of freedom, including finite element-based rotor blade coupled flag-lag-torsional dynamics, full six degree-of-freedom rigid body dynamics, and inflow dynamics.

Finally, Dr. Rendy Cheng, as part of his Ph.D. dissertation at the University of Maryland (with Dr. Celi as academic advisor), and in collaboration with Dr. Mark Tischler of the U. S. Army Aeroflightdynamics Directorate, Ames Research Center, developed a model for the

closed-loop analysis of a UH-60 with an IBC system. This work, intended to support the RADICL project at Ames, was not directly part of the ARO sponsored research. However, the results of the ARO research helped clarify the results of Dr. Cheng's research from a theoretical point of view.

2.2 Publications

The research performed in this project resulted in the following conference and journal publications:

2.2.1 Conference publications

1. Lovera, M., Colaneri, P., Celi, R., and Bittanti, S., "On the Role of Zeros in Rotorcraft Aeromechanics," *Proceedings of the 58th Annual Forum of the American Helicopter Society*, Montréal, Canada, June 2002.

2. Lovera, M., Colaneri, P., and Celi, R., "Periodic Control Issues in the Higher Harmonic Control of Helicopter Rotors," *Proceedings of the 2003 American Control Conference*, Denver, USA, June 2003.

3. Lovera, M., Colaneri, P., Malpica, C., and Celi, R., "Closed-Loop Aeromechanical Stability Analysis for a Hingeless Rotor Helicopter With HHC or IBC," *Proceedings of the 29th European Rotorcraft Forum*, Friedrichshafen, Germany, September 2003.

4. Colaneri, P., Celi, R., and Bittanti, S., "Constant-Coefficient Representations of Periodic-Coefficient Discrete Linear Systems," *Proceedings of the AHS 4th Decennium Specialist Conference on Aeromechanics*, San Francisco, CA, January 2004.

5. Lovera, M., Colaneri, P., Malpica, C., and Celi, R., "Discrete-Time, Closed-Loop Aeromechanical Stability Analysis of Helicopters With Higher Harmonic Control," *Pro-*

ceedings of the 60th Annual Forum of the American Helicopter Society, Baltimore, MD, June 2004.

2.2.2 Journal publications

1. Lovera, M., Colaneri, P., and Celi, R., "On the Role of Zeros in Rotorcraft Aeromechanics," to appear in the October 2004 issue of the *Journal of the American Helicopter Society*.

2. Lovera, M., Colaneri, P., Malpica, C., and Celi, R.,"Closed-Loop Aeromechanical Stability of a Hingeless Rotor Helicopter with Higher Harmonic Control," accepted for publication in the *Journal of Guidance, Control, and Dynamics*.

3. Colaneri, P., Celi, R., and Bittanti, S., "Constant-Coefficient Representations of Periodic-Coefficient Discrete Linear Systems," to be submitted for publication in the *Journal of the American Helicopter Society*.

4. Lovera, M., Colaneri, P., Malpica, C., and Celi, R., "Discrete-Time, Closed-Loop Aeromechanical Stability Analysis of Helicopters With Higher Harmonic Control," to be submitted for publication in the *Journal of Guidance, Control, and Dynamics*.

Chapter 3

On the Role of Zeros in Rotorcraft Aeromechanics

3.1 Introduction and Problem Statement

Various types of active control of a helicopter rotor have been proposed as a means to improve main rotor performance, and reduce vibratory loads and noise (see e.g.,[20, 37]). The rotor controls would be based on nonrotating actuators mounted in the fuselage or on rotating actuators, either mounted on the rotating portion of the swashplate and replacing the conventional rigid pitch links, or on the rotor blades themselves in the form of trailing edge flaps, spoilers, elevons, or active tips.

Traditionally, the dynamics community has been primarily interested in the *open loop* behavior of the rotor. For example, the behavior of the stability eigenvalues (or of the Floquet characteristic exponents, if the periodicity of the rotor equations of motion is taken into account) has been studied extensively, and it is now well known how they are influenced by flight condition and rotor configuration [19, 10]. Stability eigenvalues and Floquet characteristic exponents can be seen as the *poles* of the system.

When a feedback loop is closed around the rotor, not only the poles, but also the *zeros* of the system become significant. For example, zeros in the right-half-plane (RHP), or nonminimum phase (NMP) zeros, can limit the performance achievable through feedback control, and more or less precise pole-zero cancellation can increase or decrease intermodal coupling. For a single-input single-output (SISO) system, high values of the feedback gains are desirable for good tracking of the desired response, and to reduce the sensitivity to

actuator noise, modeling uncertainties, and changes in operating conditions. As the gains increase, the zeros of the system tend to "attract" some of the closed-loop poles of the systems, and if the system has unstable, or NMP, zeros, closed-loop instabilities can result. Many of these concepts carry over to the multi-input, multi-output (MIMO) case.

Clearly, a fundamental understanding of coupled rotor-fuselage zeros is a key ingredient for the success of closed-loop, active rotor control. Yet, with the partial exception of Refs. [24] and [5], no systematic study on this topic has appeared in the literature. Ref. [5] used a relatively simple, isolated rotor model, and showed that NMP zeros can indeed be present, both in hover and in forward flight.

A rigorous study of the aeroelastic stability of a rotor system in forward flight should include the effects of periodic coefficients in the governing equations. A simpler, constant coefficient approximation can be obtained by performing a Multiblade Coordinate Transformation (MCT) and neglecting the residual periodicity of the equations: the poles, or stability eigenvalues, of this approximate model are typically accurate up to an advance ratio of $\mu = 0.3 - 0.35$. No studies have been published on whether such approximations are also accurate for the *zeros*, and, if this is the case, up to what advance ratio.

In the literature related to the analysis of systems with periodic coefficients the problem of defining and computing system zeros has been studied only in recent years. The first contributions were devoted to the case of discrete time systems (see [7], [23] and [15]). On the other hand, the case of continuous time systems has been investigated for the first time in Ref. [16]. In this paper, a system theoretic definition for the zeros of a continuous time linear system with periodic coefficients is given.

In light of the preceding discussion, the objectives of the present chapter are:

1. To summarize the main properties of the zeros of linear systems with periodic coefficients, especially as they apply to a helicopter rotor system, and their implication on

rotor design;

2. To present methods for the calculation of the zeros, both for governing equations with constant and with periodic coefficients, and to discuss the accuracy of approximate, constant coefficient models; and

3. To present results for realistic hingeless rotor configurations, both in hover and forward flight.

A fundamental difference between the calculation of poles and of zeros is that the former is only based on the homogeneous system, whereas specific outputs and controls need to be defined for the latter. Therefore, any matrix of test cases is multidimensional and potentially very large. The results of this chapter will be limited to rotating swashplate inputs, and the output will be limited to fuselage and rotor states. Other possible outputs, such as hub loads or fuselage vibrations at points other than the center of gravity, will not be considered.

3.2 Helicopter simulation model

The baseline simulation model used in this chapter is a nonreal-time, blade element type, coupled rotor-fuselage simulation model [38]. The fuselage is assumed to be rigid and dynamically coupled with the rotor. A total of nine states describe fuselage motion through nonlinear Euler equations. Fuselage and blade aerodynamics are described through tables of aerodynamic coefficients, and no small angle assumption is required. A coupled flap-lag-torsion elastic rotor model is used. Blades are modeled as Bernoulli-Euler beams. The rotor is discretized using finite elements, with a modal coordinate transformation to reduce the number of degrees of freedom. The elastic deflections are not required to be small. Blade element theory is used to obtain the aerodynamic characteristics on each blade section. Quasi-steady aerodynamics is used, with a 3-state dynamic inflow model.

The trim procedure is the same as in Ref. [8]. The rotor equations of motion are transformed into a system of nonlinear algebraic equations using a Galerkin method. The algebraic equations enforcing force and moment equilibrium, the Euler kinematic equations, the inflow equations and the rotor equations are combined in a single coupled system. The solution yields the harmonics of a Fourier expansion of the rotor degrees of freedom, the pitch control settings, trim attitudes and rates of the entire helicopter, and main and tail rotor inflow. Linearized models are extracted numerically, by perturbing rotor, fuselage, and inflow states about a trimmed equilibrium position.

3.3 Zeros of linear time-periodic systems

Consider the continuous-time multivariable linear periodic system

$$\begin{aligned} \dot{x}(t) &= A(t)x(t) + B(t)u(t) \\ y(t) &= C(t)x(t) + D(t)u(t) \end{aligned} \tag{3.1}$$

where all the matrices have a common fundamental period T, such that it is, for example $A(t) = A(t+T)$, and the state vector $x(t)$, the control vector $u(t)$, and the output vector $y(t)$, have dimension n, m, and p, respectively.

Introduce then the class of *Exponentially Modulated Periodic* (EMP) signals [41]. The (complex) signal $u(t)$ is said to be EMP of period T and modulation s if

$$u(t) = \sum_{n=0,\pm1,\pm2,\ldots} u_n e^{s_n t} = e^{st} \sum_{n=0,\pm1,\pm2,\ldots} u_n e^{jn\Omega t} \tag{3.2}$$

where $t \geq 0$, $s_n = s + jn\Omega$, and s is a complex scalar.

The class of EMP signals is a generalization of the class of T-periodic signals (i.e., signals with period T) in the sense that $u(t)$ can be written as $u(t) = \bar{u}(t)e^{st}$ where $\bar{u}(t)$ is a T-periodic signal. Consequently, an EMP signal with $s = 0$ is just an ordinary time-periodic signal. In much the same way as a time invariant system subject to a (complex) exponential input has an exponential steady-state response, a periodic system subject to an EMP input

has an EMP steady-state response. In such a response, all signals of interest (x, $\dot{x}$, y) can be expanded as EMP signals. By deriving Fourier expansions for $A(t)$, $B(t)$, $C(t)$ and $D(t)$, it is possible to prove that the EMP steady-state response of the system can be expressed as an infinite dimensional matrix equation with *constant* elements (see Ref. [41] for details).

This chapter will focus on periodic systems with equal number of inputs and outputs, i.e., *square systems* ($m = p$). Moreover, the assumption will be made that the given system is reachable and observable (a formal definition of the structural properties of periodic systems can be found in Ref. [2]). With this last assumption it is not necessary to distinguish between transmission and invariant zeros, and therefore it is possible to refer simply to the" zeros of a periodic system" without any additional specification. A complex number z is said to be a zero of the system of Eq. (3.1) if there exist two T-periodic vectors $\bar{x}(t)$ and $\bar{u}(t)$ (not both identically zero) such that

$$\begin{bmatrix} (\sigma + z)I - A(t) & -B(t) \\ C(t) & D(t) \end{bmatrix} \begin{bmatrix} \bar{x}(t) \\ \bar{u}(t) \end{bmatrix} = 0 \tag{3.3}$$

where σ is the derivative operator d/dt. Equation (3.3) can be rewritten in terms of the so-called *blocking property* condition. Precisely, the complex number z is a zero of the system of Eq. (3.1) if and only if there exist an exponentially modulated periodic signal $u(t) = \sum_{n=0,\pm1,\pm2,\ldots} u_n e^{s_n t}$ and an initial state $x(0)$ such that the corresponding output $y(t)$ is identically zero.

The above definition of periodic zeros, based on the blocking property, is not the most appropriate one when dealing with the problem of *computing* zeros. Therefore, a different definition that leads to a viable computational approach will be discussed next.

First, introduce the operator

$$L_A h(t) = h(t)A(t) + \frac{d}{dt}h(t) \tag{3.4}$$

where $A(t)$ is a square $n \times n$ matrix, and $h(t)$ is a vector function of compatible dimensions.

Then, with reference to the system of Eq. (3.1) consider the following definition of "relative degree $r(t)$" [16].

For $i = 1, \ldots, p$, suppose that there exists an integer valued function $r_i = r_i(t)$, $1 \leq r_i(t) \leq n$ such that, indicating by $c_i(t)$ the i-th row of the matrix $C(t)$:

1. $c_i(\tau)B(\tau) = L_A c_i(\tau)B(\tau) = \ldots = L_A^{r_i-2} c_i(\tau)B(\tau) = 0$ for all τ in a neighborhood of t.

2. in every neighborhood of t there exists τ such that $L_A^{r_i-1} c_i(\tau)B(\tau) \neq 0$.

Then, the system is said to have *relative degree* $r(t) = [r_1(t) \ldots r_p(t)]$ at time t.

The above definition of relative degree is the natural extension to time-periodic systems of the same concept for time-invariant systems. Indeed, for a SISO LTI system of order n described by a transfer function

$$G(s) = \frac{N(s)}{D(s)} = \frac{n_0 s^m + n_1 s^{m-1} + \ldots + n_m}{s^n + d_1 s^{n-1} + \ldots + d_n} \tag{3.5}$$

with $n_0 \neq 0$, the relative degree r_{LTI}, defined as

$$r_{LTI} = n - m \tag{3.6}$$

(i.e., equal to the difference between the degree of the polynomial at the denominator of the transfer function and that at the numerator or, equivalently, to the difference between the number of poles and the number of zeros) can be given a state space interpretation which coincides with the given definition. The transfer function $G(s)$, Eq. (3.5), can be written as

$$\begin{aligned} G(s) &= \frac{N(s)}{D(s)} = C(sI - A)^{-1}B + D \\ &= \frac{\bar{N}(s)}{D(s)} + D \end{aligned} \tag{3.7}$$

where $\bar{N}(s)/D(s) \stackrel{def}{=} C(sI - A)^{-1}B$, and $\bar{N}(s)$ and $D(s)$ are, respectively, polynomials in s of degree n and $n-1$. If the D matrix (in the SISO case, a 1 by 1 matrix) is not equal

to zero, then $N(s) = \bar{N}(s) + D(s)D$ is a polynomial of degree n, and the relative degree is $r = 0$. If $D = 0$ but $CB \neq 0$ it can be shown (see, for example, Ref. [34]) that the relative degree is $r = 1$. If $D = 0$ and $CB = 0$, but $CAB \neq 0$, the relative degree is $r = 2$, and so on. For a MIMO system the relative degree becomes a vector, each element of which gives the relative degree of each output channel.

In principle, for a generic periodic system the relative degree is a function of time. This means that in general the number of zeros of the system might be itself a function of time. However, in most practical problems the number of zeros is fixed, the relative degree r is independent from t, and r can be calculated using the same tests on A, B, C, and D previously mentioned; the only condition is that if any of A, B, C, D becomes equal to zero, it does so only for isolated instants in time, and not time intervals (see Ref. [16] for a more mathematically rigorous discussion). This leads to the notion of *uniform* relative degree.

Assuming first that the system of Eq. (3.1) has relative degree $r(t)$, one can define an *instantaneous interaction matrix* $\Gamma(t)$ of the system as

$$\Gamma(t) = \begin{bmatrix} L_A^{r_1(t)-1} c_1(t)B(t) \\ \vdots \\ L_A^{r_p(t)-1} c_p(t)B(t) \end{bmatrix} \tag{3.8}$$

Then the system of Eq. (3.1) is said to have *uniform relative degree* $r = [r_1 \dots r_p]$ if $r(t) = r$, $1 \leq r_i \leq n$, $i = 1, \dots, p$, the rank of the matrix $\Gamma(t)$ is equal to p for every value of t, and $\Gamma(t)$ has a bounded inverse. It can be shown (see Ref. [16]) that, for such a system, the zeros coincide with $n - r$ periodic poles of the system

$$\dot{x}(t) = R(t)x(t) \tag{3.9}$$

where the matrix $R(t)$ is defined as

$$R(t) = A(t) - B(t)\Gamma(t)^{-1}Q(t) \tag{3.10}$$

and the p by n matrix $Q(t)$ is given by

$$Q(t) = \begin{bmatrix} L_A^{r_1(t)} c_1(t) \\ \vdots \\ L_A^{r_p-1} c_p(t) \end{bmatrix}, \tag{3.11}$$

the remaining r poles being zero. As in the case of the definition of periodic poles, periodic zeros can be described both in terms of characteristic multipliers and characteristic exponents.

The previously introduced definitions related to periodic zeros hold for a generic *square* continuous time linear periodic system, i.e., a system with equal number of inputs and outputs. The extension of the above definition to nonsquare periodic systems is presently a subject of research.

3.4 Closed loop zeros of periodic systems

Another interesting issue in the study of periodic zeros is their role in determining the closed loop behavior of control systems in high gain situations. It turns out that *periodic zeros have the same property of their time-invariant counterpart of attracting closed loop poles for high gain.* In fact, it can be shown that a finite zero of a square periodic system can be seen as the limit of a closed loop pole as the gain matrix goes to infinity.

This result plays a fundamental role in explaining why the closed loop behavior of an "almost time invariant" LTP system can turn out to be completely different from the one of its LTI approximation. To illustrate this fact, consider the following simple example: a linear time periodic system is given, which is described by the matrices

$$A(t) = \begin{bmatrix} -1 + \sin(t) & 0 \\ 1 - \cos(t) & -3 \end{bmatrix}, B(t) = \begin{bmatrix} -1 - \cos(t) \\ 2 - \sin(t) \end{bmatrix} \tag{3.12}$$

$$C(t) = \begin{bmatrix} 0 & 1 \end{bmatrix}, D(t) = 0. \tag{3.13}$$

As $A(t)$ is lower triangular, it is easy to see that the poles (characteristic exponents) of the periodic system are given by -1 and -3 and coincide with the poles of the corresponding time-invariant approximation of the system.

Consider now the closed loop system

$$\begin{aligned} \bar{A}(t) &= A(t) + kB(t)C(t) \\ &= \begin{bmatrix} -1+\sin(t) & -k-k\cos(t) \\ 1-\cos(t) & -3+2k-k\sin(t) \end{bmatrix} \end{aligned} \tag{3.14}$$

and its time-invariant approximation

$$\bar{A}_0 = \begin{bmatrix} -1 & -k \\ 1 & -3+2k \end{bmatrix}. \tag{3.15}$$

The constant coefficient $\bar{A}_0$ is asymptotically stable for $k < 2$, however the time-periodic $\bar{A}(t)$ is asymptotically stable only for $k < 1.6$, so in this case the closed loop stability analysis based on the LTI approximation can be misleading, even if the open loop periodic poles coincide with the time-invariant ones. As the two systems have the same poles, the discrepancy in the closed loop behavior can only be interpreted by looking at the zeros. The LTI system has relative degree equal to 1 (transfer function with two poles and one zero or, equivalently, $D_0 = 0$ and $C_0B_0 \neq 0$), and the same holds for the time-periodic one, as the product $C(t)B(t)$ is generically nonzero, as required by the definition of relative degree $r(t)$ previously introduced. The zero of the time invariant system $[A_0, B_0, C_0, D_0]$ is given by $z_{LTI} = -0.5$, while the zero of the time periodic system $[A(t), B(t), C(t), D(t)]$, computed according to the definitions in the previous Section, is given by $z_{LTP} = -0.69$.

Clearly, the different behavior of the closed loop system in the two cases is due to the different structure of the zero dynamics, so in this example a correct analysis of the closed loop behavior of the system can be carried out only by taking into account the periodicity of the dynamics. To this purpose, the following Section will show how to compute periodic zeros for the case of rotor-fuselage models.

3.5 Calculation of coupled rotor-fuselage zeros

The linearized coupled rotor-fuselage system can be modeled as a continuous-time linear periodic system of the type of Eq. (3.1), where the matrices $[A(t), B(t), C(t), D(t)]$ have a common fundamental period T, equal to $1/N$ rotor revolutions. While, for a given flight condition and helicopter configuration, the matrix $A(t)$ is fixed, matrices $B(t), C(t), D(t)$ vary according to the input-output configuration one wants to study. For simplicity, this chapter will concentrate on the analysis of SISO rotor fuselage models, however the extension of the results presented here to the more general case of a (square) MIMO model does not pose any theoretical or computational problems.

As described in the previous Section, the simplest way to compute the zeros of a periodic system is to cast the problem into that of computing of the characteristic exponents of an associated periodic matrix $R(t)$. While the general form of $R(t)$ given in equation (3.10) is a complicated one, the problem is considerably simpler if one considers the particular cases of systems with uniform relative degree $r = 0$ ($D(t)$ generically non singular) and $r = 1$ ($D(t) = 0$ for all t, and $C(t)B(t)$ generically non singular).

If $D(t)$ is invertible for each t, then the zeros of the system coincide with the characteristic exponents of the inverse system, i.e., of matrix

$$R(t) = A(t) - B(t)D(t)^{-1}C(t) \tag{3.16}$$

If the system has a singular $D(t)$ ($D(t) = 0$ in the SISO case) and $C(t)B(t)$ is generically non singular ($C(t)B(t) \neq 0$ for all t in the SISO case), then the zeros of the system coincide with the characteristic exponents of

$$R(t) = A(t) - B(t)[C(t)B(t)]^{-1}\left[\frac{dC(t)}{dt} + C(t)A(t)\right] \tag{3.17}$$

except for one at the origin. For the determination of r, it has been assumed that the relative

degree of the periodic models coincides with the one of the corresponding LTI approximations, which can be computed very easily.

The problem of computing the characteristic multipliers of a linear periodic system has been extensively studied in the literature, and a number of approaches have been proposed. In particular, four classes of computational methods can be defined (see Ref. [30] for a detailed overview):

- Direct integration methods (single or multiple shooting [24]).
- Frequency domain methods [41, 43].
- Symbolic methods [36].
- Linear algebra methods (periodic Schur decomposition [6, 31]).

From a practical viewpoint, as the helicopter model used in this chapter has 53 state variables, the use of the symbolic and frequency response methods is probably not a viable option. Therefore, only the direct integration approach and the method based on the periodic Schur decomposition have been used. The main difference between the two approaches can be best understood by looking at the operations needed to determine the characteristic multipliers. The multipliers are defined as the eigenvalues of the monodromy matrix (i.e., the Floquet transition matrix at the end of one period) of the periodic system under investigation. Therefore, the conventional (direct integration) approach to the problem consists of the following steps:

1. Solving the initial value problem

$$\begin{aligned} \dot{\Phi}_R(t,0) &= R(t)\Phi_R(t,0) \\ \Phi_R(0,0) &= I_n \end{aligned} \tag{3.18}$$

over the interval from 0 to T, to compute the monodromy matrix $M = \Phi_R(T,0)$. Any numerical integration algorithm can be used to this purpose.

2. Computing the characteristic multipliers as the eigenvalues of M.

This scheme has been successfully used for the computation of *poles* of rotorcraft dynamics, as the open loop dynamics do not give rise to any major numerical problems in the solution of Eq. (3.18) (the coupled rotor-fuselage dynamics is at most only mildly unstable and not particularly stiff). Unfortunately, the situation can be considerably different when dealing with the problem of computing *zeros*. In fact, zeros that are very large and positive can often occur. In this case the zero dynamics will be strongly nonminimum phase (i.e., unstable) and stiff, leading to potentially severe numerical problems in the solution of Eq. (3.18). For example, if the real part of one or more nonminimum phase zeros is sufficiently large, the integration required to compute the monodromy matrix will fail because of numerical overflow before reaching the end of the period. Also, the monodromy matrix associated with the zero dynamics can be poorly scaled. These problems do not necessarily occur in every single zero calculation, but they can easily occur in otherwise well behaved, practical problems. As a consequence, it is desirable to use a computational scheme that can deal with these situations, should they occur. The so-called "periodic" Schur decomposition is one such scheme, based on the idea of avoiding the explicit calculation of the monodromy matrix M. The main idea behind this approach is the following.

Consider a sequence of time instants $t_k, k = 1, \ldots, K$, with $t_0 = 0$, $t_{k+1} > t_k$, and $t_K = T$, and let

$$M_k \stackrel{def}{=} \Phi_R(t_k, t_{k-1}) \qquad k = 1, \ldots, K \tag{3.19}$$

Then clearly one has

$$M = M_K M_{K-1} \ldots M_1 \tag{3.20}$$

If each of the M_k matrices is diagonal or lower (upper) triangular, then the characteristic multipliers are given by the product of the eigenvalues of the M_k matrices. Because in

general this is not the case, the periodic Schur decomposition algorithm can be used to apply a suitable sequence of *unitary* operations to the M_k matrices in order to transform each of them to upper triangular form (except one which can be in quasi upper triangular form). It can be proved (see Refs.[6, 31, 21] for details) that this decomposition of the M_k matrices corresponds to an implicit Schur decomposition for M, from which the characteristic multipliers can be easily be computed. Therefore, the overall numerical scheme for the computation of the characteristic multipliers proceeds as follows:

1. Select K and the time instants t_k (usually equally spaced) and compute the K transition matrices from t_{k-1} to t_k. Note that if K is chosen sufficiently large, then the assumption that $R(t)$ is approximately constant over each interval can be introduced and each of the M_k can be computed as

$$M_k \approx e^{R(t_{k-1})[t_k - t_{k-1}]} \tag{3.21}$$

2. Use the periodic Schur decomposition algorithm to determine the upper triangular (or quasi upper triangular) form of each of the M_k matrices in the appropriate order.

3. Compute the eigenvalues of the monodromy matrix M from the triangular form of the matrices M_k.

This computational scheme has two major advantages over the direct integration method: firstly, it does not require the numerical integration of the dynamics, which can be a critical step when dealing with zero dynamics (stiffness); secondly, it avoids the explicit formation of M and applies (almost) only *unitary* operations to the data, thus minimizing the propagation of numerical errors. The results presented in the following Section have been obtained using this computational method, in particular by resorting to the implementation of the periodic Schur algorithm described in [31].

3.6 Results

All the results presented in this section refer to a hingeless rotor configuration similar to the Eurocopter BO-105. The linearized system has 53 states: 9 for the rigid body motion; 40 to model five elastic coupled modes, for each of the four rotor blades; 3 for the main rotor dynamic inflow model; and one for the tail rotor dynamic inflow model. In this chapter, an analysis of the complex plane representations of the poles and zeros of the SISO transfer function from collective input to the acceleration $\dot{w}$ of the center of gravity of the helicopter is presented. This is one of the open loop transfer functions that would have to be taken into account in the implementation of IBC for vibration reduction.

Three configurations will be analyzed, namely:

1. A baseline configuration, with value of the thrust coefficient $C_T/\sigma = 0.07$ and the basic soft-in-plane rotor with a fundamental rotating lag frequency of approximately 0.7 /rev;

2. A heavier configuration, with $C_T/\sigma = 0.10$, and the same soft-in-plane rotor; and

3. A stiff-in-plane configuration, with the baseline value of $C_T/\sigma = 0.07$ and a fundamental rotating lag frequency of approximately 1.4/rev. This configuration has often been used in rotary-wing aeroelasticity studies because it becomes unstable at high advance ratios [18].

The results will cover a speed range from hover to up to 150 kts, depending on the configuration. The upper speed limit is determined in each case by the maximum speed at which a converged trim solution can be achieved. Because a value of $\mu = 0.1$ corresponds to a speed of about 42 kts, the maximum advance ratio considered in the results is just above $\mu = 0.35$.

All the states are defined in a nonrotating coordinate system. The multiblade coordinate transformation is used to convert the rotor states from the rotating to the fixed coordinate

system. The controls are defined in a rotating coordinate system. The state matrix A and the control matrix B are computed using numerical perturbations at 9 equidistant azimuth steps over one quarter of a revolution, corresponding to 36 samples over one revolution, and are expressed in the form of a Fourier series. For the time-periodic case, the entire Fourier series is used; for the time-invariant case, only the constant term of the series is retained. Because the four rotor blades are assumed to be identical, the Fourier series only contains harmonics that are integer multiples of four. In this chapter, the harmonics retained are 4/, 8/ and 12/rev.

3.6.1 Baseline configuration

Figures 3.1 shows the real parts of the poles of the first lag mode as a function of μ, computed using the constant coefficient approximation (solid lines) and the rigorous periodic model (dashed lines). In all the results presented in this section, the word "pole" means "stability eigenvalue" for the constant coefficient, or LTI, cases, and "characteristic exponent" for the periodic, or LTP, cases. Also, all the periodic coefficient results are obtained using the periodic Schur method. The figure confirms the well known behavior of soft-in-plane rotor stability, namely, that the low frequency lag mode is the least damped. This mode is traditionally called "regressive" although, strictly speaking, both the highest and lowest frequency lag modes in this case are progressive modes (for example, see [24] for further details). Also, hover is the least damped flight condition, and the lag damping increases with advance ratio. Finally, as expected, for the case of very small values of the advance ratio, the poles computed on the basis of Floquet theory coincide with the poles of time-invariant systems, while the difference increases slightly with the advance ratio.

Root locus plots of the poles and zeros of the first lag mode with advance ratio μ as the parameter are shown in Figures 3.2 and 3.3 for the LTI and LTP cases respectively. It should be noted that the zeros, besides being dependent on the specific choice of input and output,

cannot be associated with normal modes in the same sense that the poles can. The four zeros in the figures are those that are closest to the four poles of the first lag mode, and are given the same name as the specific pole to which they are closest. A combination of pole and zero is often called a "dipole". If pole and zero are coincident, then the dynamics associated with that pole are canceled by the zero, and therefore they do not appear in the transfer function. For example, in Figure 3.2, poles and zeros of the progressive and regressive lag modes almost exactly cancel one another in hover. As a consequence, the heave acceleration response to collective is almost unaffected by the progressive lag mode, and it would be legitimate to remove the progressive lag mode to obtain a simplified model of this response. Similarly for the regressive lag mode. In other words, pole-zero cancellation for a certain mode decouples that mode from the input-output dynamics being considered. Conversely, as the distance between pole and zero of a dipole increases, the corresponding mode plays an increasing role. Therefore, the pole-zero distance can be seen as a measure of coupling.

Figure 3.2 shows that, in general, pole-zero cancellation does not occur, and that the lag dynamics cannot be neglected *a priori* in computing the heave acceleration response to collective (the extent of the effect of lag dynamics will depend on the range of input-output frequencies). The figure also shows that the zeros of one of the collective modes and of the progressive mode become less damped than the respective poles, although they remain minimum phase (i.e., with negative real part). Because the zeros tend to "attract" the poles as the gains of a feedback loop are increased, this implies that the closed loop system may have a lower lag stability.

Figure 3.3 shows the same type of information as Fig. 3.2, except that the effect of periodic coefficients is fully taken into account, and therefore the "poles" are the characteristic exponents of the system. The same general considerations as for Fig. 3.2 apply. Comparing Fig. 3.3 and Fig. 3.2, one can see only small differences between the behavior of the time-invariant and of the time-periodic zeros. This indicates that the constant coefficient

approximation is generally as accurate for zeros as it is for poles.

Figure 3.4 compares the real parts of the LTI and LTP zeros nearest to the lag poles (each zero is given the name of the closest pole). As is the case for the poles, in hover the LTI and LTP zeros essentially coincide; in fact, in hover the only periodicity is caused by the small amount of cyclic pitch required to balance the tail rotor forces and moments. The regressive lag zero has a substantially smaller real part than the corresponding pole, indicating a potential reduction of inplane damping in closed loop operation.

Figure 3.5 shows a comparison between the set of all the zeros closest to the imaginary axis for the LTI and LTP transfer functions. The flight speeds range from hover to 150 kts, corresponding to values of advance ratio μ from 0 to 0.35. Similarly to the time-periodic poles, the imaginary parts of time-periodic zeros are defined within a multiple of the period. Therefore the numerical values of the imaginary parts resulting from the calculations are not necessarily the correct ones. Again, similarly to the time-periodic poles, each time-periodic zero can be identified by continuation, i.e., by starting at hover, where the periodicity is small, and time-invariant and time-periodic poles are essentially the same, and following the evolution of the zero as μ increases. This procedure was not followed for the time-periodic zeros shown in Fig. 3.5, and therefore the imaginary parts of those zeros are not necessarily meaningful. On the other hand, the real parts are meaningful, and therefore the figure shows the presence of lowly damped or nonminimum phase zeros. Several very lowly damped and one nonminimum phase zeros are clearly visible.

This may have important analysis and design implications from a control engineering point of view. In general, the higher the frequency of a stable zero near the imaginary axis, the higher the performance limitations; the reverse is true for NMP zeros, i.e., the performance limitations are higher if the frequency of the zero is lower.

3.6.2 High thrust configuration

Figures 3.6 through 3.10 show results for the same soft-in-plane configuration, but at a higher thrust condition, i.e., with a value of $c_T/\sigma = 0.1$.

Figure 3.6 shows the real parts of the poles (stability eigenvalues for the time-invariant case, and characteristic exponents for the time-periodic case) of the first lag mode as a function of advance ratio. Compared with the baseline case, Figure 3.1, the overall damping of the mode is higher: this is a well known result, which depends on the higher aerodynamic damping generated by the higher thrust.

The same poles and the four zeros closest to them are plotted on the complex plane in Fig. 3.7 for the constant coefficient approximation, and as a function of speed. From the point of view of pole-zero cancellation, the same general pattern as in the baseline case, Fig. 3.7, is visible. One of the two pole-zero pairs corresponding to the collective mode cancels out almost exactly at all speeds. The regressive mode pair also nearly cancels out. Significant separations can be seen for the progressive and the other collective mode dipole. The zero of the collective dipole remains very close to the imaginary axis.

The same type of information is shown in Fig. 3.8 for the time-periodic case. Comparing Figs. 3.7 and 3.8 shows that the constant coefficient approximation is about as accurate for the zeros as it is for the poles. The only exception is the damping of the progressive lag zero at $V = 150$ kts and $\mu \approx 0.35$, which is substantially underestimated by the constant coefficient approximation. This is also evident from Fig. 3.9, which shows the real part of the same zeros as a function of the advance ratio μ. Finally, Fig. 3.10 compares LTP and LTI predictions for the zeros closest to the imaginary axis and in the right-half plane. As in Fig. 3.5, the ambiguity in the imaginary parts of the periodic zeros have not been resolved, and therefore only the real parts are always correct. The same general arrangement as in the baseline case, Fig. 3.5, can be seen, with several very lowly damped and one nonminimum

phase zero. Therefore, the effect of thrust on the character of the zeros does not appear to be significant.

3.6.3 Stiff-in-plane configuration

Figures 3.11 and 3.12 refer to a stiff-in-plane configuration obtained by modifying the lag stiffness of the baseline configuration so as to obtain a lag frequency in hover of approximately 1.4/rev. Figure 3.11 shows the real part of the LTI and LTP poles of the lag modes as a function of the advance ratio μ. As typical for stiff-in-plane hingeless rotor configurations, the lag degree of freedom is stable in hover, but its stability decreases dramatically at high speed, and the rotor becomes unstable at $\mu \approx 0.35$. There are some small differences between LTI and LTP predictions at hover: these are caused by the periodicity introduced by the cyclic pitch required to balance the effects of the tail rotor.

Figure 3.12 shows the real parts of the zeros closest to the four lag poles, as a function of μ. The corresponding figures for the soft-in-plane case, Figs. 3.4 and 3.9, showed four zeros, whereas Fig. 3.12 only shows three. In fact, for the stiff-in-plane case, only three zeros are so close to corresponding poles that they can be clearly identified as being part of a dipole. While other zeros are in the general vicinity of the fourth lag pole, none can be associated with it unambiguously. Therefore, because there is not even an approximate pole-zero cancellation for this lag pole, the lag mode is likely to participate in a noticeable way to the heave acceleration response to collective pitch. For the stiff-in-plane case too the accuracy of constant coefficient approximation begins to deteriorate for lower values of μ for the zeros than for the poles. This is shown by the differences between the exact LTP poles and the approximate LTI poles, clearly visible in Fig. 3.12, which become noticeable for as low as $\mu = 0.2$. Finally, the figure shows that a nonminimum phase zero exists at hover.

3.7 Summary and Conclusions

This chapter presented a methodology for the calculation of the zeros of transfer functions associated with coupled rotor-fuselage systems, considering governing equations with constant and periodic coefficients. Only the single-input single-output case, and the specific transfer function from collective pitch to CG heave accelerations were considered: this should be kept in mind when generalizing the conclusions of this study. The baseline helicopter configuration was similar to the Eurocopter BO-105. A flight condition with higher rotor thrust and a stiff-in-plane configuration were also studied.

The main conclusions of this chapter are:

1. The zeros of a coupled rotor-fuselage system do not affect its open loop stability, and therefore can be ignored if no active control system is present. On the other hand, if an active control system is present, the location of zeros can affect the closed loop stability characteristics, and may trigger closed-loop instabilities if the feedback gain is sufficiently high. The presence of zeros with positive real parts (nonminimum phase zeros) is particularly critical in determining performance limitations of the control system.

2. Whereas the constant coefficient approximations obtained through a multiblade coordinate transformation usually give accurate predictions of the stability eigenvalues for advance ratios of up to $\mu = 0.3 - 0.35$, the predictions of the zeros are reasonably accurate only up to an advance ratio of about $\mu = 0.2$, and occasionally lower. Therefore, beyond this value the effects of periodic coefficients must be explicitly taken into account.

3. The zeros of a system with periodic coefficients can be computed using Floquet theory, however, in practice, the calculation of the zeros can have much worse numerical

properties because of large ratios between the largest and the smallest zeros (stiffness). Therefore the conventional shooting techniques normally used in Floquet stability analysis often prove inadequate and more accurate computational tools must be used. These large zeros cannot simply be moved to infinity, and therefore neglected, because this can cause inaccurate predictions of the zeros near the imaginary axis, which in turn are important for the closed-loop stability of the coupled rotor-fuselage system.

4. The heave acceleration response to collective pitch is affected by the rotor lag dynamics. This is shown by the fact that the poles of the lag dynamics are not canceled by corresponding zeros. This coupling with rotor dynamics is stronger at higher c_T/σ, and even more for stiff-in-plane configurations.

5. The transfer function from collective pitch to heave acceleration exhibits several zeros close to the imaginary axis or with positive real parts. The number and location of these zeros depend on the configuration and flight condition, but at least one nonminimum phase zeros is present for each configuration, and at every speed. These zeros can intrinsically limit the benefits achievable from active control systems, and therefore it is very important to identify them as part of the design of any such control system.

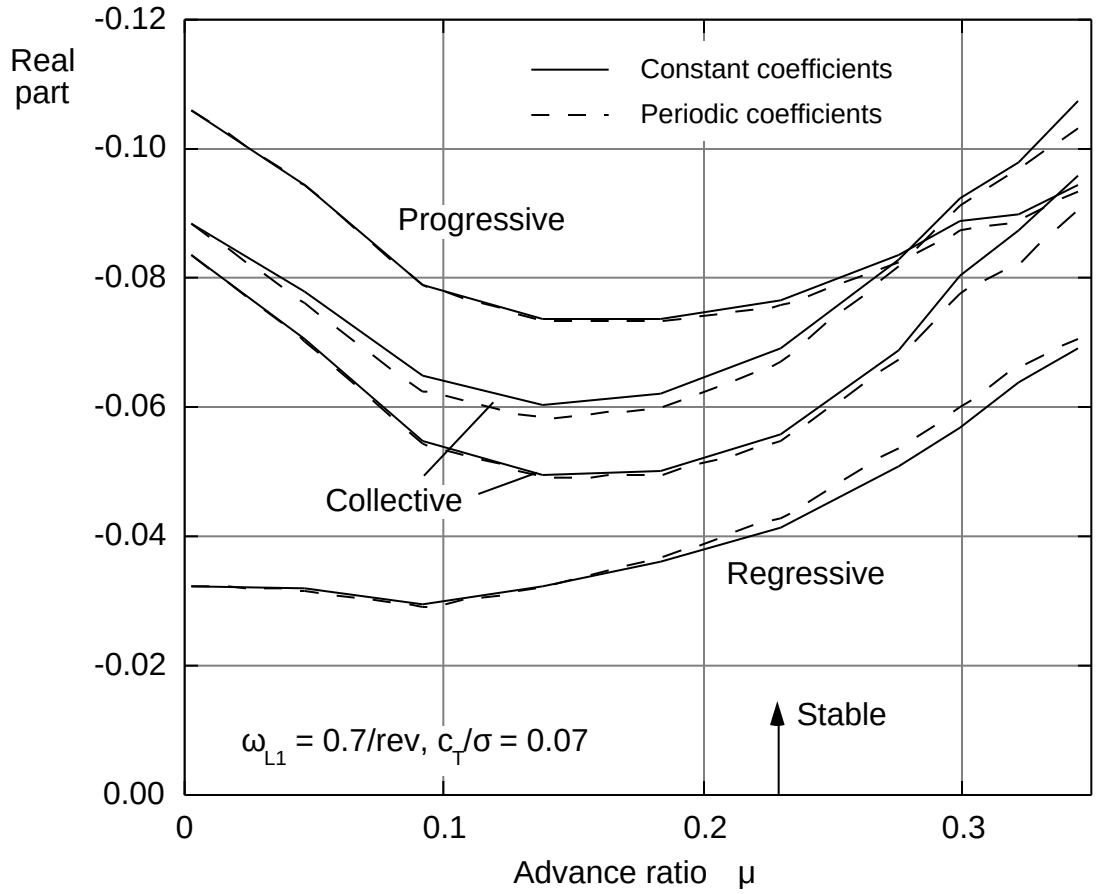

Figure 3.1: Real part of the poles of the first lag mode as a function of μ; baseline configuration.

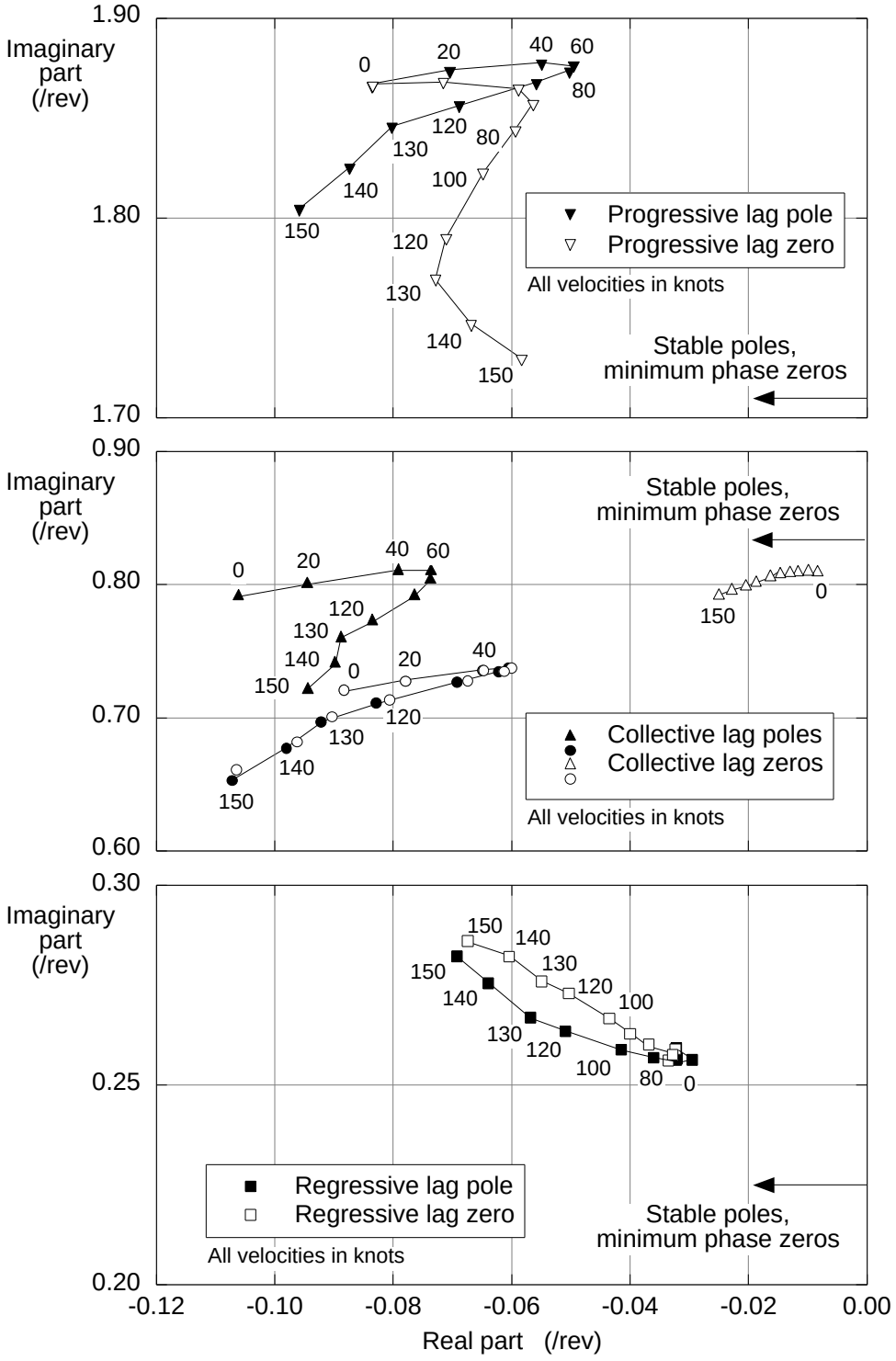

Figure 3.2: LTI lag poles and zeros as a function of μ.

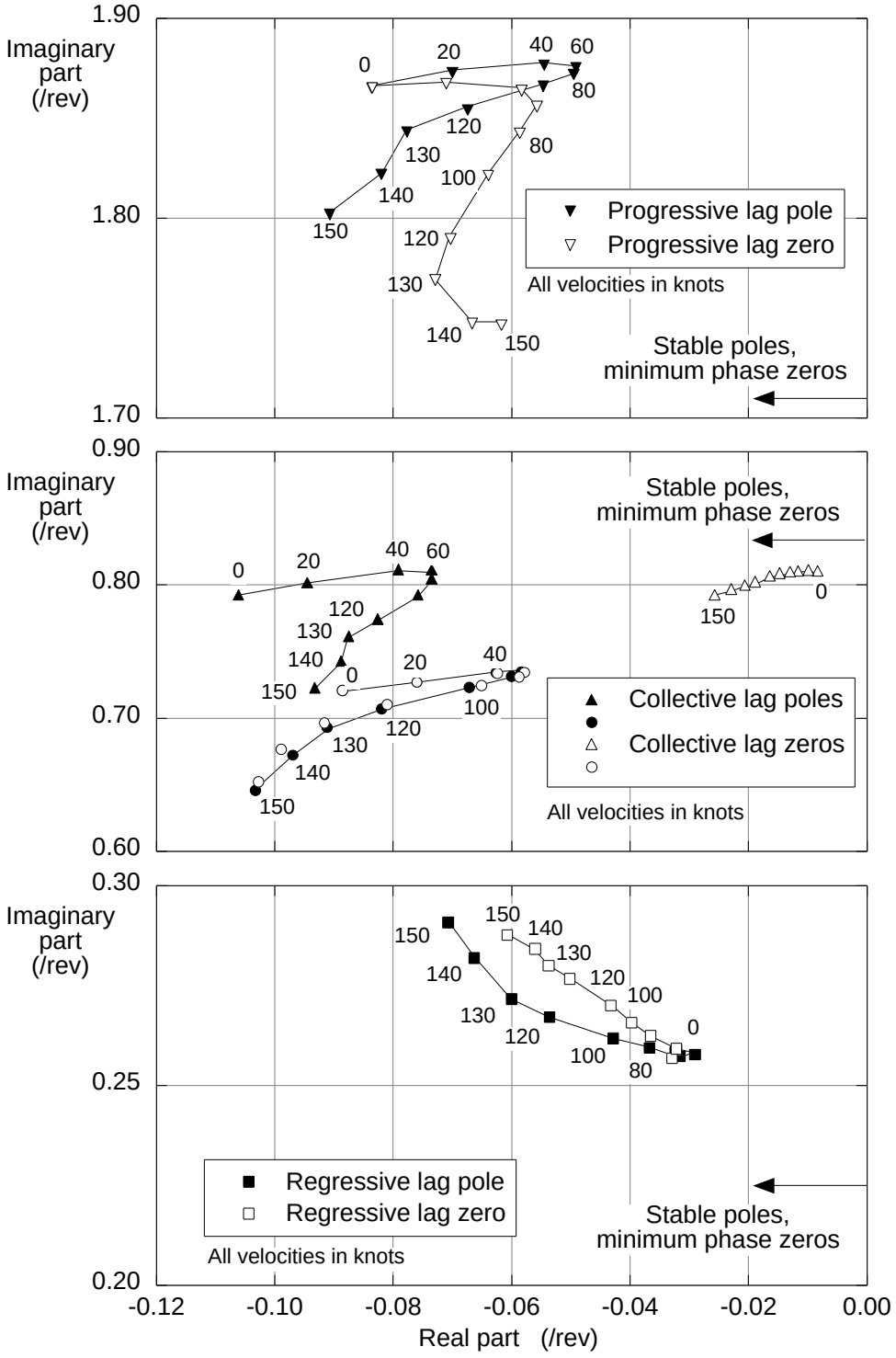

Figure 3.3: LTP lag poles and zeros as a function of μ.

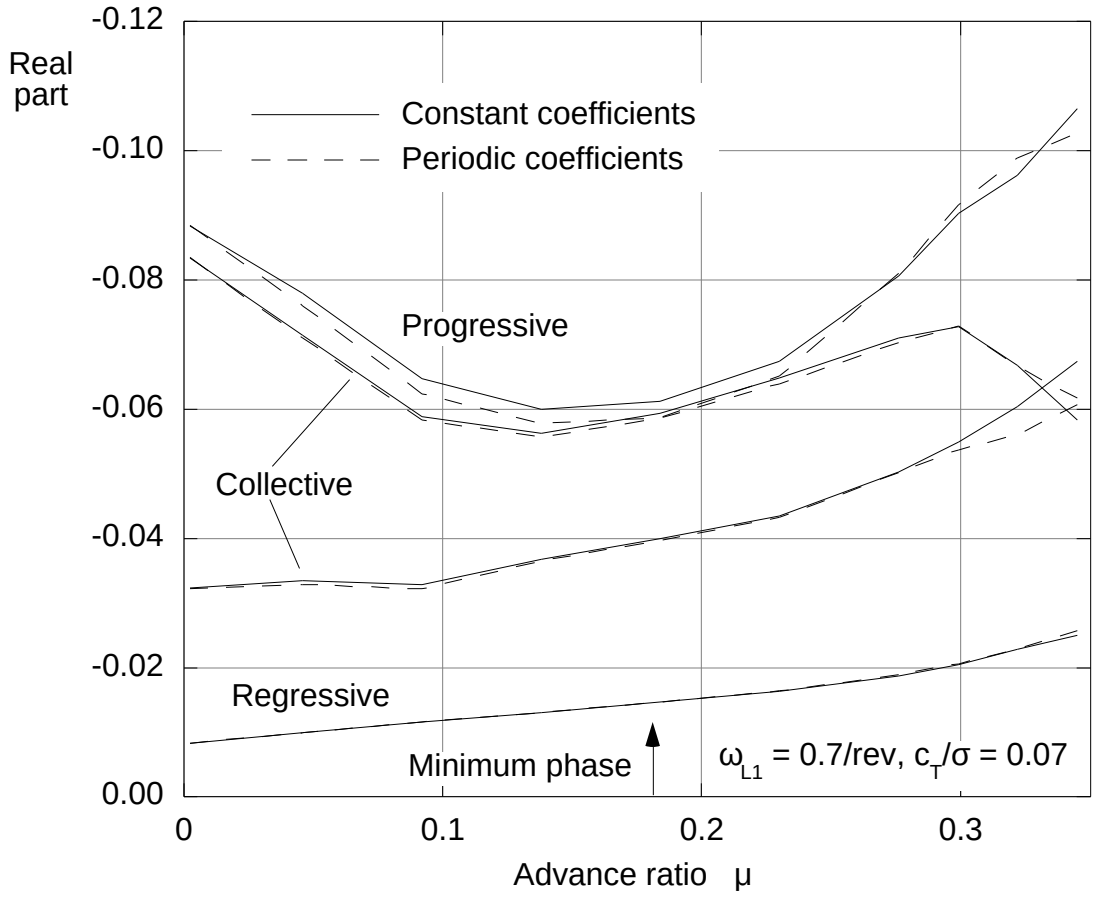

Figure 3.4: Real part of LTI and LTP lag zeros as a function of μ.

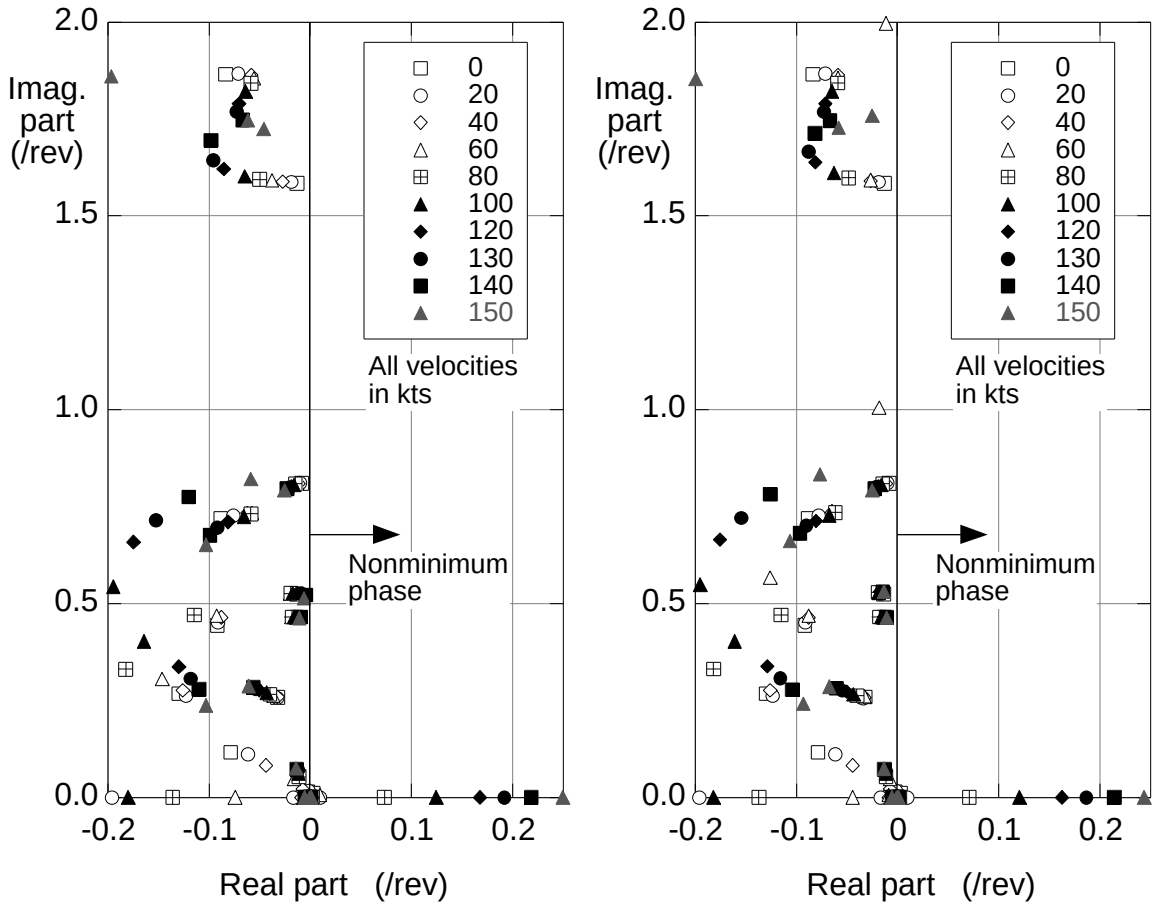

Figure 3.5: Comparison of LTP (left) and LTI (right) zeros as a function of μ.

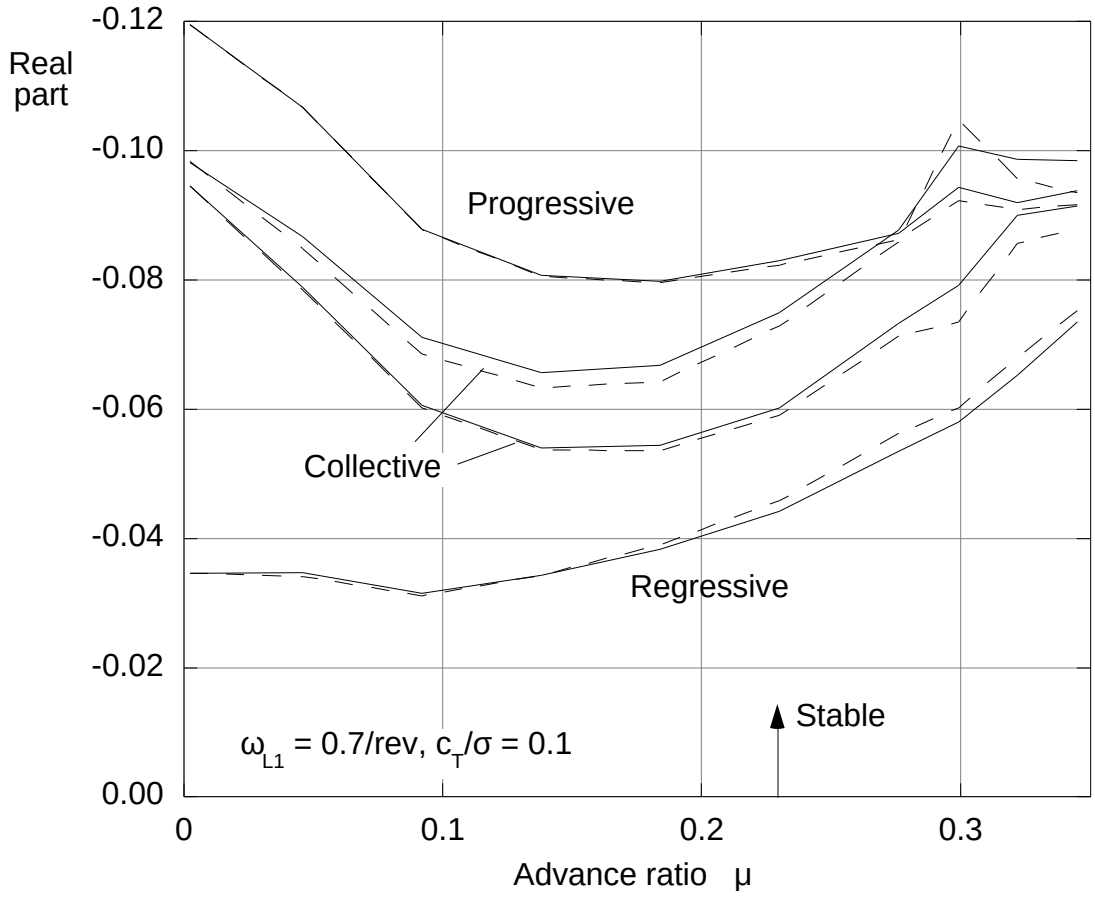

Figure 3.6: Real part of LTI and LTP lag poles as a function of μ, high thrust case.

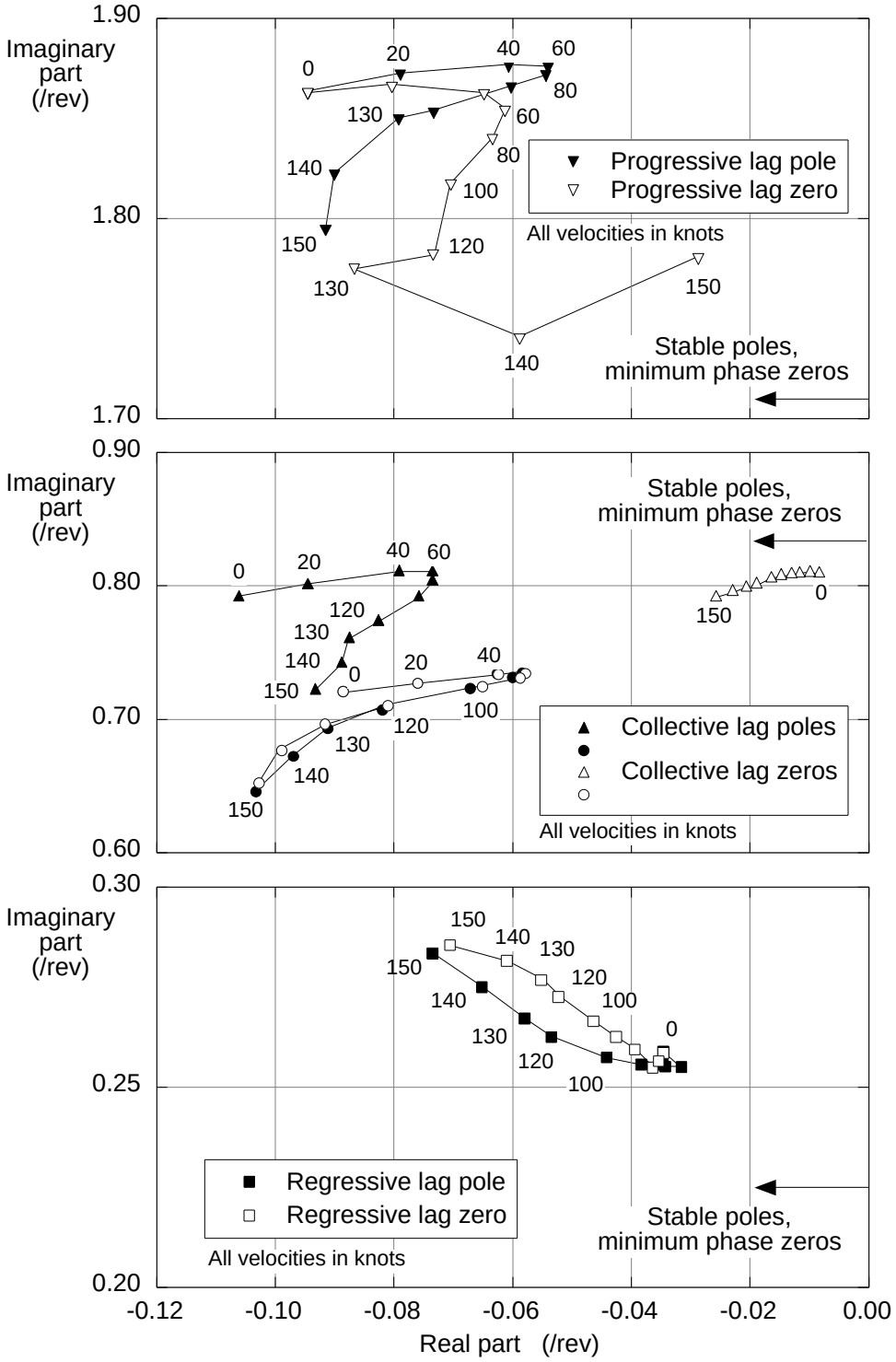

Figure 3.7: LTI lag poles and zeros as a function of μ, high thrust case.

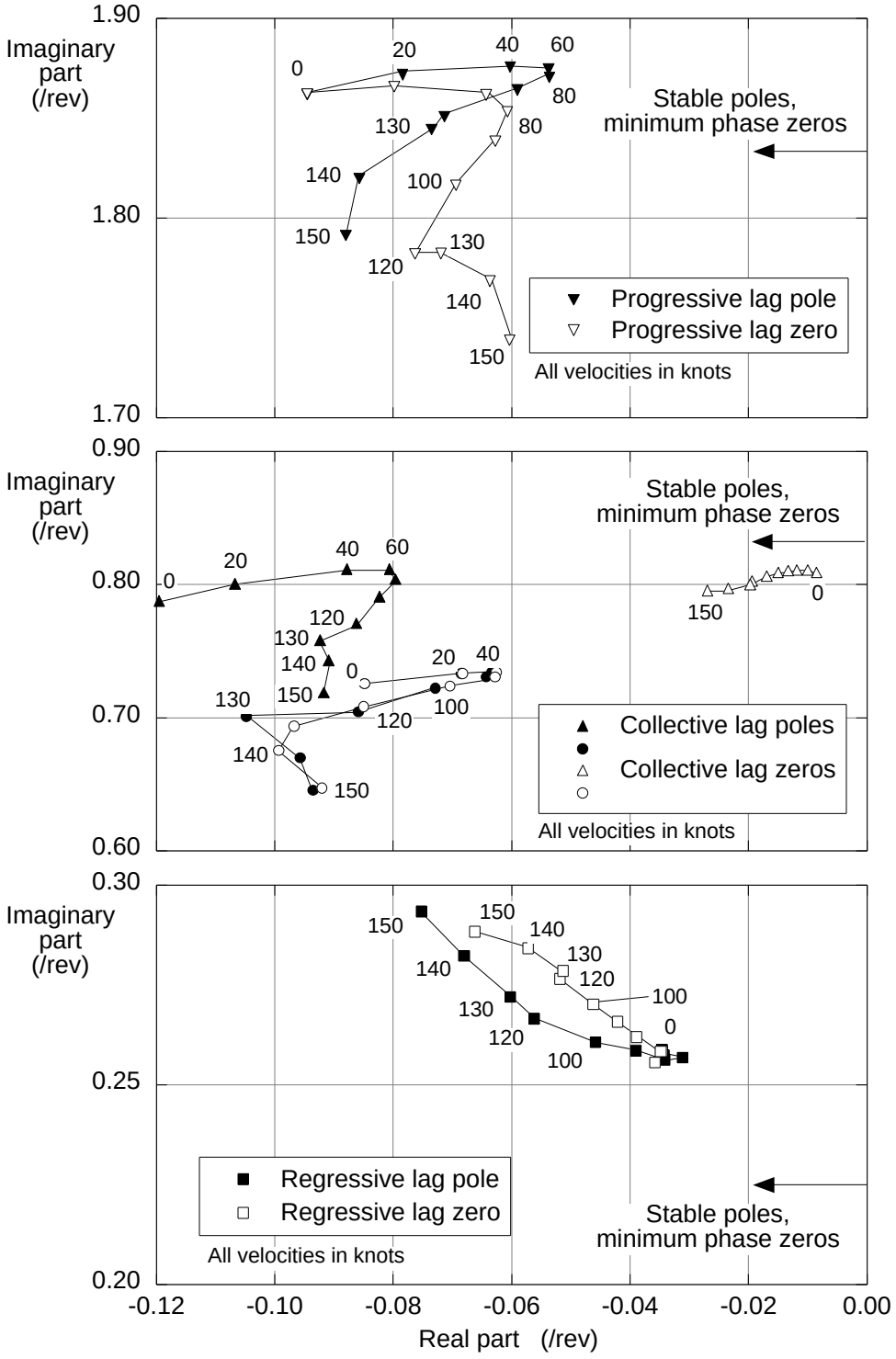

Figure 3.8: LTP lag poles and zeros as a function of μ, high thrust case.

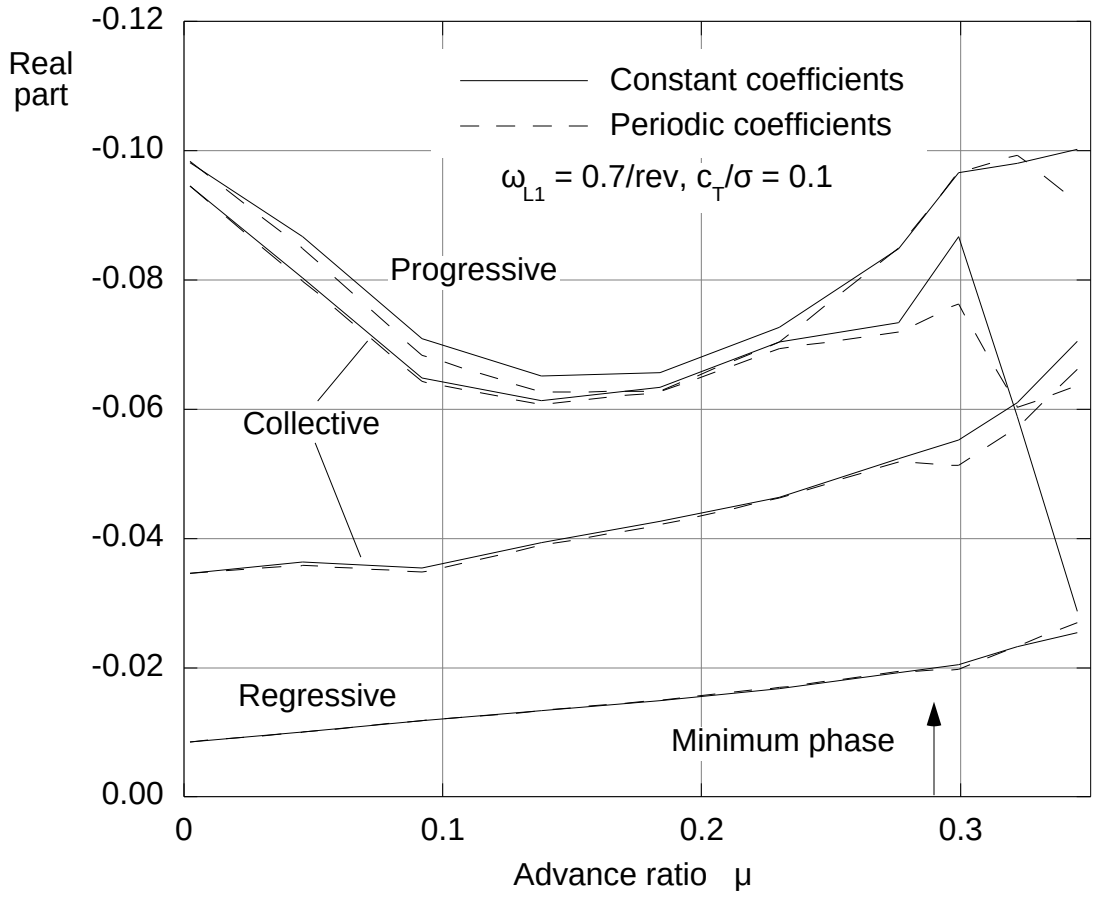

Figure 3.9: Real part of LTI and LTP lag zeros as a function of μ, high thrust case.

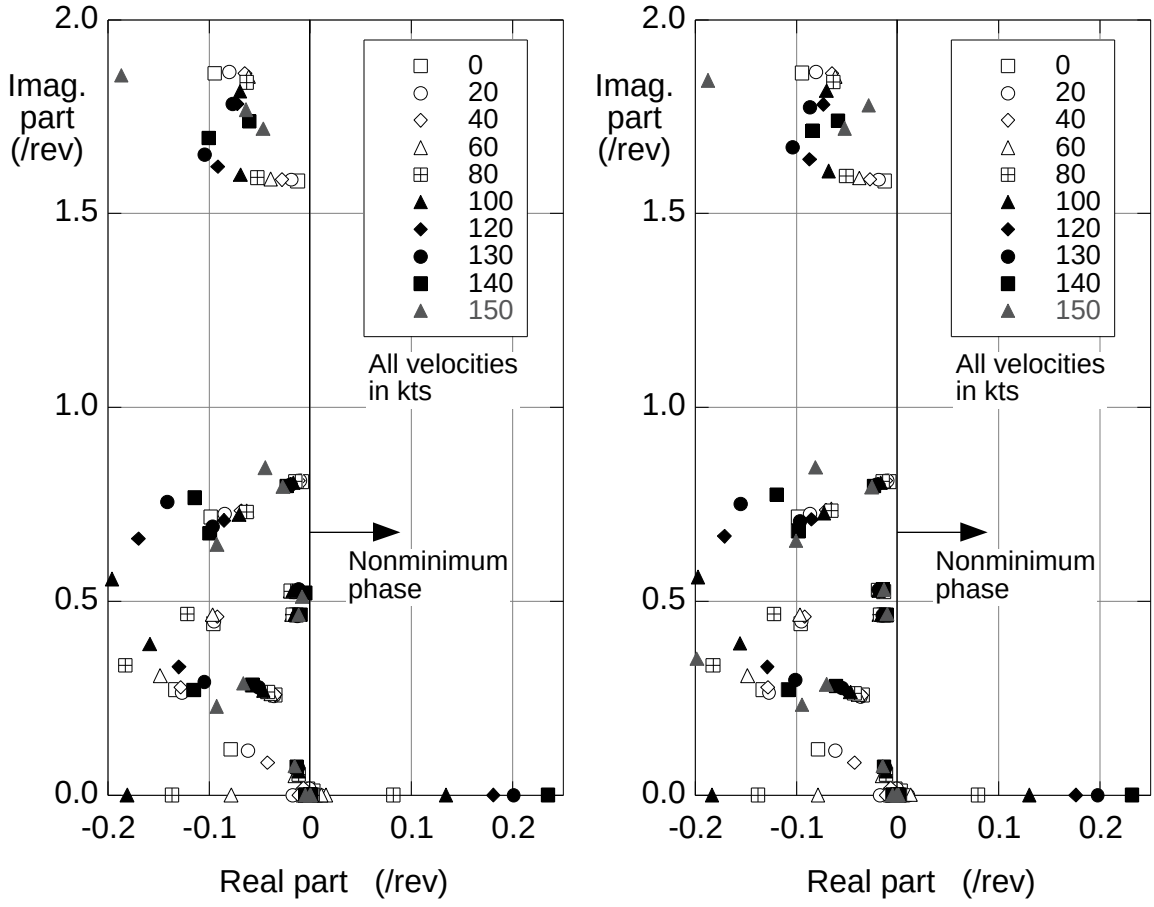

Figure 3.10: Comparison of LTP (left) and LTI (right) zeros as a function of μ, high thrust case.

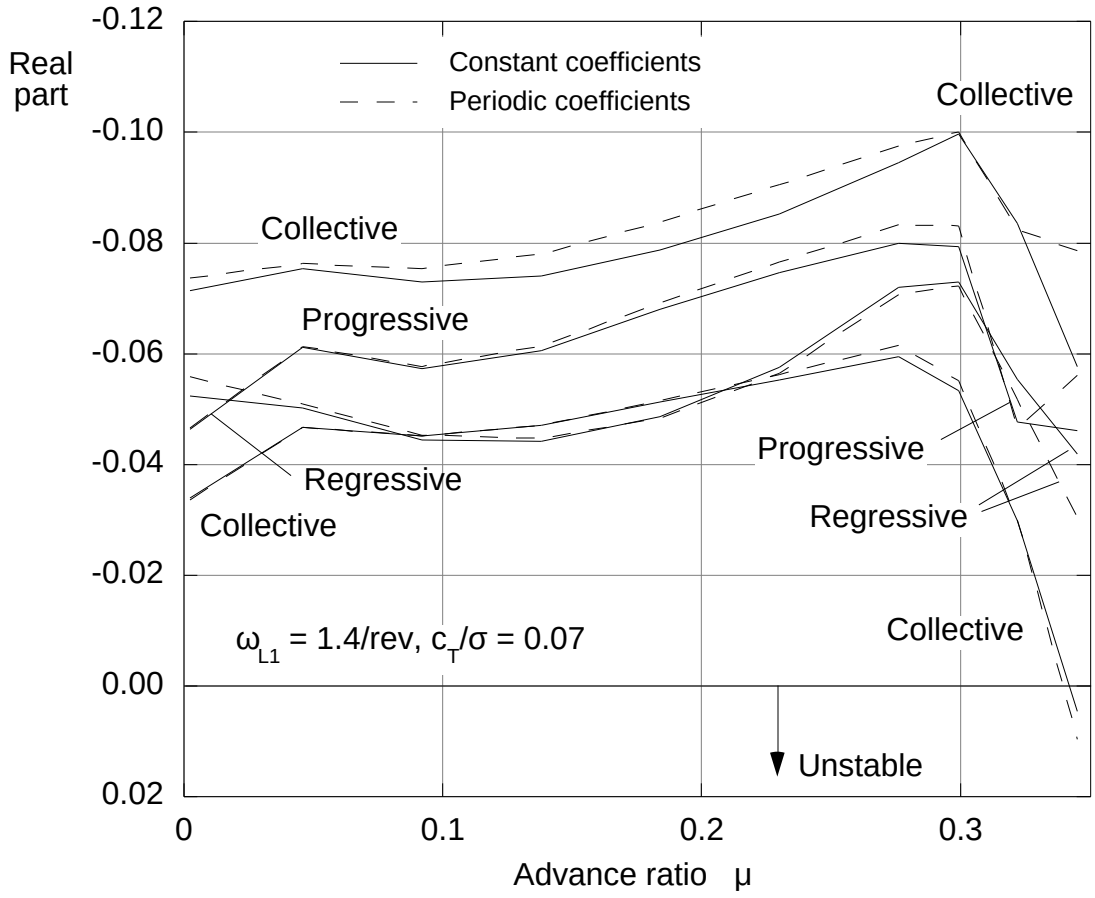

Figure 3.11: Real part of LTI and LTP lag poles as a function of μ, stiff-in-plane case.

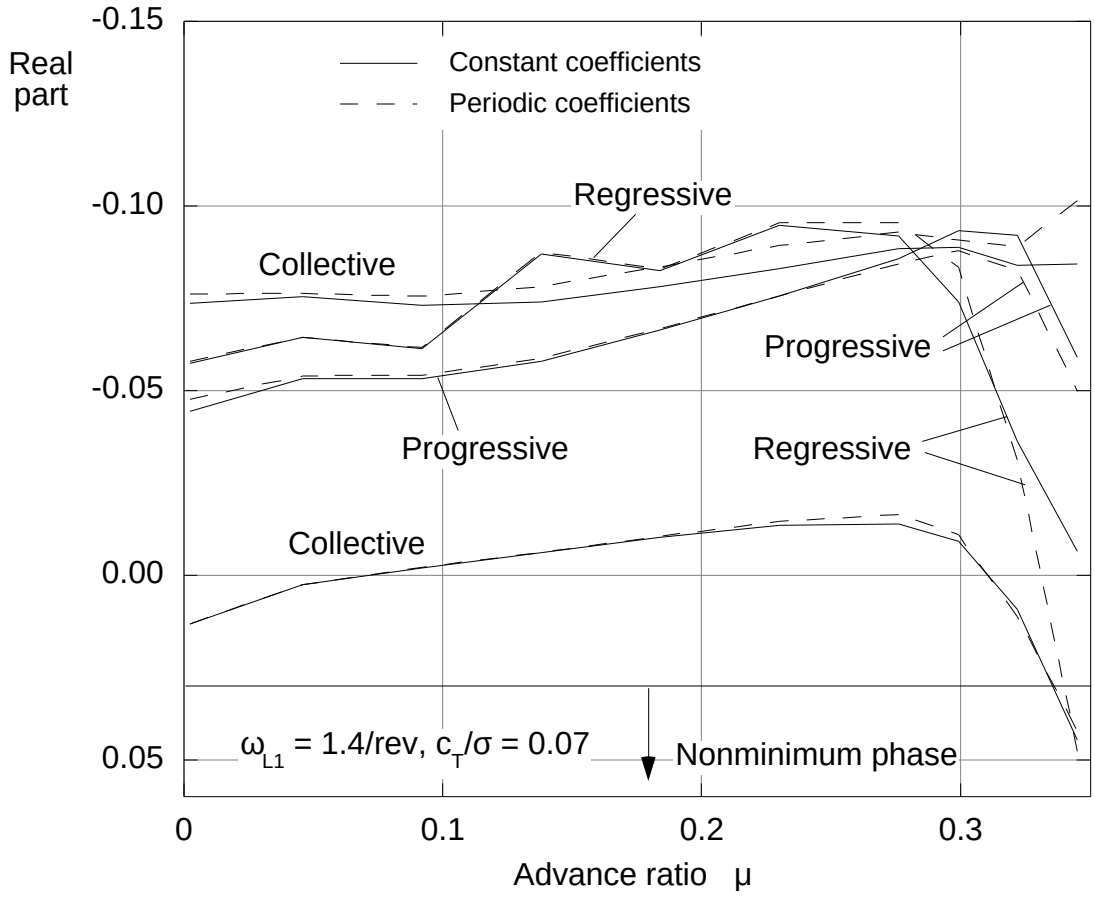

Figure 3.12: Real part of LTI and LTP lag zeros as a function of μ, stiff-in-plane case.

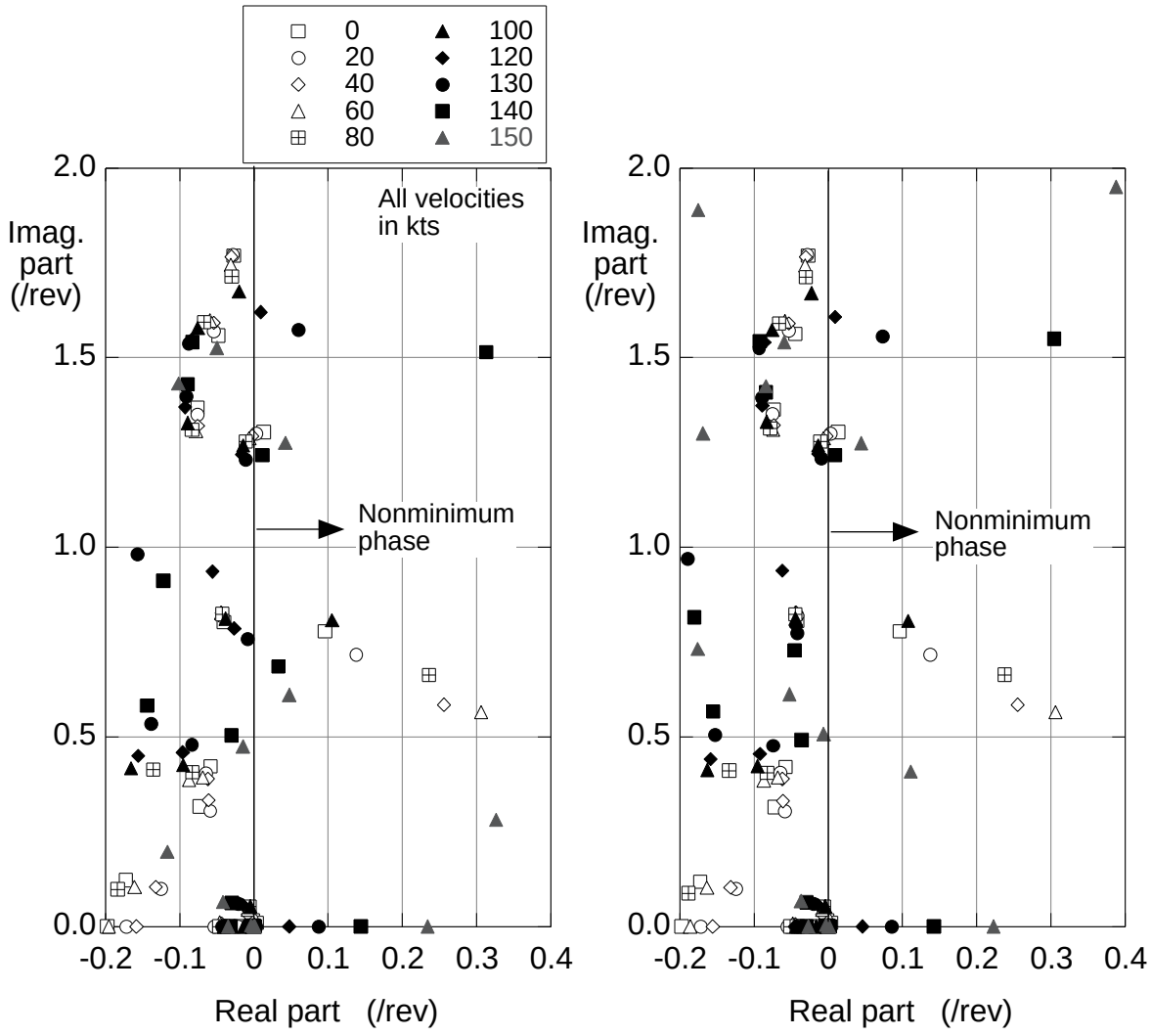

Figure 3.13: Comparison of LTP (left) and LTI (right) zeros as a function of μ, stiff-in-plane case.

Chapter 4

Closed-Loop Aeromechanical Stability of Hingeless Rotor Helicopters with Higher Harmonic Control

4.1 Introduction

Higher Harmonic Control (HHC) and Individual Blade Control (IBC) have been considered for many years as a viable approach for the design and the implementation of active rotor control laws aiming at the attenuation of helicopter vibrations (see, e.g., the recent survey papers [20, 37]). The main idea of HHC and IBC is to try to attenuate N/rev vibratory components in the fuselage accelerations (N being the number of rotor blades) or in the rotor hub loads by adding suitably phased N/rev and other components to the rotor controls, either in the fixed (HHC) or rotating (IBC) frame. A number of studies have been carried out to determine the feasibility of active vibration control both from the theoretical and the experimental point of view; in particular, as far as the analysis of the dynamic behavior of the single-input single-output (SISO) HHC is concerned, a fundamental result was given in [40] where a continuous time analysis of HHC was carried out for the first time and it was shown that, to first approximation, the classical T-matrix HHC algorithm (see [35]) can be written as a linear time invariant dynamic compensator. More recently, however, it has been proposed to try to exploit the *interharmonic coupling* due to the periodicity of rotor dynamics in forward flight to achieve the attenuation of N/rev vibrations by means of lower frequency inputs, such as, e.g., 2/rev or 3/rev for a 4 bladed rotor. To this purpose, a generalization of the T-matrix algorithm has been proposed in the literature (see [32]), but

no detailed theoretical analysis of that approach has been carried out so far. As the above mentioned generalization of the T-matrix algorithm turns out to be a linear time-periodic compensator, we will refer to it as the Periodic HHC (PHHC) algorithm. Therefore, both the HHC and the PHHC algorithms call for the use of periodic systems theory ([1]) for closed loop stability and performance analysis. However, a very limited attention has been devoted so far in the literature to the dynamic analysis of vibration attenuation schemes; in particular, the existing contributions to the study of closed loop stability issues (see for example [17]) deal only with time-invariant dynamic models of helicopter dynamics, and the assessment of the role of periodicity in determining the actual closed loop dynamics still has to be fully assessed. More recently, Cheng *et al.* [9] have presented a methodology for the derivation of approximate linearized, time-invariant, state-space models of helicopters and have examined the interaction between HHC and FCS.

In the light of the above remarks, the objectives of this chapter are the following:

1. to provide a simple state space derivation for the continuous time form of the SISO HHC compensator (input and output at the same rotor harmonic), first introduced in [40];

2. to demonstrate how the same approach can be used to work out a state space representation for the SISO PHHC compensator (input and output at different rotor harmonics), which is suitable for closed-loop stability and robustness analysis;

3. to generalize the above results to get to a general approach for the derivation of the state space form for a MIMO HHC controller (any combinations of harmonics for inputs and outputs); and

4. to present the results of a numerical investigation into the closed-loop stability properties of Higher Harmonic Control, based on a simulation study of the coupled rotor-

fuselage dynamics of a four bladed hingeless rotor helicopter.

(Note that some preliminary results have been presented in [27]).

The main significance of this work is that it addresses the question of whether the presence of a closed-loop HHC will affect the aeroelastic stability of a coupled rotor-fuselage system. Although some partial answers could obviously be extracted from the analysis of transient time histories, no suitable methodology to answer this question directly is available in the published literature.

4.2 Helicopter simulation model

The baseline simulation model used in this chapter is a nonreal-time, blade element type, coupled rotor-fuselage simulation model (see [38] for details). The fuselage is assumed to be rigid and dynamically coupled with the rotor. A total of nine states describe fuselage motion through the nonlinear Euler equations. Fuselage and blade aerodynamics are described through tables of aerodynamic coefficients, and no small angle assumption is required. A coupled flap-lag-torsion elastic rotor model is used. Blades are modeled as Bernoulli-Euler beams. The rotor is discretized using finite elements, with a modal coordinate transformation to reduce the number of degrees of freedom. The elastic deflections are not required to be small. Blade element theory is used to obtain the aerodynamic characteristics on each blade section. Quasi-steady aerodynamics is used, with a 3-state dynamic inflow model. Linearized models are extracted numerically, by perturbing rotor, fuselage, and inflow states about a trimmed equilibrium position. Because the equations of the coupled rotor/fuselage dynamics are written in the fixed frame of reference, the linearized models turn out to be time-periodic with period T/N, where N is the number of blades and T is the period of one rotor revolution. Note that in the following the azimuth angle $\psi = \Omega t$ will be used as independent variable.

The matrices of the linearized model are generated as Fourier series. For example, the

state matrix $A(\psi)$ is given as:

$$A(\psi) = A_0 + \sum_{k=1}^{K} \left[A_{kc} \cos(kN\psi) + A_{ks} \sin(kN\psi) \right] \tag{4.1}$$

where the matrices A_0, A_{kc}, and A_{ks} are constant, and only A_0 is retained for constant coefficient approximations.

Similarly, the control matrix $B(\psi)$ is obtained assuming for the pitch control of each blade the form

$$\theta_i(\psi) = \theta_0 + \sum_{k=1}^{K} \left[\theta_{kc} \cos\left(\psi + \frac{2\pi}{N} i\right) + \theta_{ks} \sin\left(\psi + \frac{2\pi}{N} i\right) \right] \qquad i = 0, \ldots, N-1 \tag{4.2}$$

where i is the blade number, and K is the total number of input harmonics. The rotor input vector $\mathbf{u}$ used in this chapter is

$$\mathbf{u} = \begin{bmatrix} \theta_0 & \theta_{1c} & \theta_{1s} & \theta_{3c} & \theta_{3s} & \theta_{4c} & \theta_{4s} & \theta_{5c} & \theta_{5s} \end{bmatrix}^T \tag{4.3}$$

therefore, for the 4-bladed rotor considered in this chapter, the higher harmonic input is composed of the N-1/rev, N/rev, and N+1/rev harmonics. For simplicity, the tail rotor collective input θ_{0t} is omitted from all the equations of this chapter, but it is obviously included in the actual mathematical model.

As Eq. (4.2) shows, the higher harmonic control is applied in the *rotating* system. Therefore, although the control is identical for all blades at the same azimuth angle, this arrangement is what is often defined as Individual Blade Control (IBC). However, it should be pointed out that while HHC and IBC represent significantly different technologies from the implementation point of view (e.g., choice of actuators and sensors), they are completely equivalent from the control theoretic point of view.

Finally, the trim procedure is the same as in Ref. [8]. The rotor equations of motion are transformed into a system of nonlinear algebraic equations using a Galerkin method. The algebraic equations enforcing force and moment equilibrium, the Euler kinematic equations,

the inflow equations and the rotor equations are combined in a single coupled system. The solution yields the harmonics of a Fourier expansion of the rotor degrees of freedom, the pitch control settings, trim attitudes and rates of the entire helicopter, and main and tail rotor inflow. During the trim calculations the HHC system is turned off.

4.3 State space formulation of higher harmonic controllers

This section presents the derivation of the state space formulation of a MIMO HHC controller in which inputs and outputs can be at arbitrary multiples of the fundamental rotor frequency. This is done by building state space formulations of HHC controllers of increasing complexity. After some background on the T-matrix algorithm, a continuous-time, state space analysis is presented for the case of a SISO HHC system in which input and output are at the same harmonic (in this case, N/rev). Next, the analysis is extended to the case in which input and output are at different harmonics. Finally, the case of the MIMO HHC system with inputs and outputs at arbitrary harmonics is considered, by combining the results of the two previous cases. More precisely the following three cases, corresponding to three different selections for the control input vector $\mathbf{u}$, will be considered:

- Control input given by a single harmonic at the blade passing frequency N/rev:

$$\mathbf{u} = \mathbf{u}_N = \begin{bmatrix} \theta_{Nc} & \theta_{Ns} \end{bmatrix}^T$$

- Control input given by a single harmonic at a frequency M/rev different from N/rev:

$$\mathbf{u} = \mathbf{u}_M = \begin{bmatrix} \theta_{Mc} & \theta_{Ms} \end{bmatrix}^T$$

- Control input given by the superposition of a number of different harmonics, such as, for example:

$$u = \begin{bmatrix} \theta_{(N-1)c} \; \theta_{(N-1)s} \; \theta_{Nc} \; \theta_{Ns} \; \theta_{(N+1)c} \; \theta_{(N+1)s} \end{bmatrix}^T \tag{4.4}$$

For the purpose of the present chapter, only *fixed parameters* HHC will be considered, i.e., the T-matrix will be fixed and not adaptive. Also, the stability analysis will be carried out in continuous time: the role of digital implementation on the stability and performance of the HHC loops will be investigated in future work [29].

4.3.1 Basic T-matrix algorithm

A typical non-adaptive HHC system is based on a discrete time mathematical model describing the response of the helicopter to higher harmonic inputs, of the general form

$$\mathbf{y}_N(k) = T_{N,N}\mathbf{u}_N(k) + \mathbf{y}_{0N}(k) \tag{4.5}$$

where k is the rotor revolution index, $\mathbf{y}_N$ is a vector of N/rev harmonics of measured outputs (e.g., hub loads or accelerations at some point of the fuselage), $\mathbf{u}_N$ is a vector of control inputs, and $T_{N,N}$ is a 2 by 2 constant matrix. The vector $\mathbf{y}_N(k)$ is defined as

$$\mathbf{y}_N(k) \;=\; \begin{bmatrix}\mathbf{y}_{Nc}(k)\\ \mathbf{y}_{Ns}(k)\end{bmatrix} = \begin{bmatrix} \dfrac{1}{\pi}\displaystyle\int_{k\pi}^{(k+1)\pi} \mathbf{y}(\psi)\cos(N\psi)\,d\psi \\ \\ \dfrac{1}{\pi}\displaystyle\int_{k\pi}^{(k+1)\pi} \mathbf{y}(\psi)\sin(N\psi)\,d\psi \end{bmatrix} \tag{4.6}$$

The vector $\mathbf{y}_{0N}$ contains the N/rev harmonics of the "baseline" vibrations, i.e., the vibrations in the absence of HHC. In practical applications, $\mathbf{y}_N$ is typically the output of a digital or analog harmonic analyzer. The control input vector is similarly defined as:

$$\mathbf{u}_N = \begin{bmatrix}\theta_{Nc}\\ \theta_{Ns}\end{bmatrix} \tag{4.7}$$

where θ_{Nc} and θ_{Ns} are, respectively, the cosine and sine components of the N/rev pitch control input, applied in the rotating system.

The HHC inputs are generally updated at discrete time intervals, for example, once per rotor revolution. The conventional HHC control law is derived by minimizing at each discrete time step k the cost function

$$J(k) = \mathbf{y}_N(k)^T Q y_N(k) + \Delta\mathbf{u}_N(k)^T R \Delta\mathbf{u}_N(k) \tag{4.8}$$

where $Q = Q^T \geq 0$, $R > 0$ and $\Delta \mathbf{u}_N(k)$ is the increment of the control variable at time k, i.e.

$$\Delta u_N(k) = u_N(k) - u_N(k-1) \tag{4.9}$$

Differentiating Eq. (4.8) with respect to $\Delta \mathbf{u}_N(k)$ yields the control law

$$\mathbf{u}_N(k+1) = \mathbf{u}_N(k) - K_{N,N}\mathbf{y}_N(k) \tag{4.10}$$

where $K_{N,N} = (T_{N,N}^T Q T_{N,N} + R)^{-1} T_{N,N}^T Q$. Equation (4.10) is well known in the literature as the "T-matrix" algorithm. It can be seen from Eqs. (4.5) and (4.10) that this control algorithm introduces a discrete time integral action which ensures that $y_N \to 0$ as $k \to \infty$. Actually, with $Q = I_{2,2}$ and $R = 0$ deadbeat control (i.e., the output goes to zero after one discrete-time step) could in principle be achieved if exact knowledge of the $T_{N,N}$ matrix was available, and if the static model, Eq. (4.5), was an accurate representation of rotor dynamics. However, these two assumptions are generally not satisfied, as $T_{N,N}$ can only be estimated and Eq. (4.5) clearly does not hold if the helicopter is not operating in steady state. Note, also, that if in the cost function, Eq. (4.8), one chooses $R = 0$ and Q proportional to the identity matrix, then the control law, Eq. (4.10) reduces to

$$\mathbf{u}_N(k+1) = \mathbf{u}_N(k) - T_{N,N}^{-1}\mathbf{y}_N(k) \tag{4.11}$$

which can be given a minimum variance interpretation, in the sense that this control law guarantees at each time step the closed loop minimization of the cost function

$$J(k) = \mathbf{y}_N(k)^T \mathbf{y}_N(k) \tag{4.12}$$

Neglecting the effects of the sample and hold scheme of the digital implementation in the T-matrix algorithm, the overall control algorithm can be represented by the block diagram given in Figure 4.1.

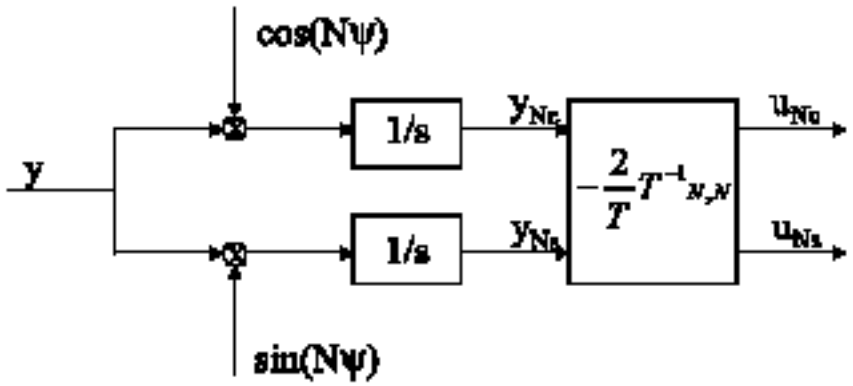

Figure 4.1: Block diagram of the continuous time SISO HHC algorithm.

4.3.2 SISO HHC with input and output at the same frequency

Following Ref. [40], choose y_{Nc} and y_{Ns} as state variables for the controller in Fig. 4.1. Then, the following state space model for the HHC compensator is obtained:

$$\dot{\mathbf{y}}_N = A_c \mathbf{y}_N + B_c(\psi)\mathbf{y} \tag{4.13}$$

$$u = C_c \mathbf{y}_N \tag{4.14}$$

where

$$A_c = \begin{bmatrix} 0 & 0 \\ 0 & 0 \end{bmatrix} \tag{4.15}$$

$$B_c(\psi) = K_{N,N} \begin{bmatrix} \cos(N\psi) \\ \sin(N\psi) \end{bmatrix} \tag{4.16}$$

$$C_c = -\frac{2}{T} I_{2,2}$$

4.3.3 SISO HHC with input and output at different frequencies

The HHC input in the rotating system is usually not limited to the same N/rev frequency of the vibrations to be attenuated. Typically, inputs at N-1/rev and N+1/rev are also applied (recall that N/rev inputs of collective, longitudinal, and lateral cyclic pitch in the fixed system result in N-1, N, and N+1/rev pitch inputs in the rotating system).

In this case, the steady state model relating the N/rev harmonic of the output $y(t)$ to the M/rev harmonic of the pitch input $u(t)$, with $M \neq N$, can be written in the form

$$\mathbf{y}_N(k) = T_{N,M}\mathbf{u}_M(k) + \mathbf{y}_{0N}(k) \tag{4.17}$$

where $\mathbf{u}_M$ is defined as in Eq. (4.7), but for an M/rev harmonic, and where the (constant) matrix $T_{N,M}$ relates the amplitude of the M/rev control input u to the corresponding steady state amplitude of the N/rev component of the output y. The control scheme for the attenuation of N/rev vibrations using an M/rev input can then be derived along the lines of the previous case, and is represented by the equation

$$\mathbf{u}_M(k+1) = \mathbf{u}_M(k) - K_{N,M}\mathbf{y}_N(k) \tag{4.18}$$

where $K_{N,M} = (T_{N,M}^T Q T_{N,M} + R)^{-1} T_{N,M}^T Q$. As shown in the following section, the matrix $T_{N,M}$ can be related to the Harmonic Transfer Function (HTF) of the controlled system, which is an extension to periodic systems of the frequency response function of a time-invariant system [41, 14]. In addition, as in the case of HHC with input and output at the same frequency N/rev, the discrete control law, Eq. (4.18) guarantees that $y_N \to 0$ as $k \to \infty$, provided that the system can be modeled as in Eq. (4.17).

Similarly to the $M = N$ case, the state space model for the case $N \neq M$ is given by

$$\dot{\mathbf{y}}_N = A_c\mathbf{y}_N + B_c(\psi)\mathbf{y} \tag{4.19}$$

$$u = C_c\mathbf{y}_N \tag{4.20}$$

where

$$A_c = \begin{bmatrix} 0 & 0 \\ 0 & 0 \end{bmatrix} \tag{4.21}$$

$$B_c(\psi) = K_{N,M}\begin{bmatrix} \cos(N\psi) \\ \sin(N\psi) \end{bmatrix} \tag{4.22}$$

$$C_c = -\frac{2}{T}I_{2,2} \tag{4.23}$$

This discussion shows that a coupled rotor-fuselage system with even a simple SISO HHC controller is intrinsically a system with periodic coefficients if the HHC output and the vibration to be attenuated are at two different multiples of the rotor frequency. This happens even if the rotor-fuselage system is modeled as a system with constant coefficients. Therefore, rigorous stability, performance and robustness analyses of an HHC system can only be carried out using the tools of periodic systems theory.

4.3.4 MIMO with input and output at arbitrary harmonics

In typical implementations of HHC, multi-harmonic signals are frequently used to attenuate several components of the vibratory loads. For example, inputs at N-1/, N/ and N+1/rev, sine and cosine (for a total of 6 inputs), could be used simultaneously to control six components of the N/rev vibratory hub forces and moments. Therefore, this section extends the previous SISO discussion to a MIMO HHC system. We will consider a general configuration in which output measurements of N/rev vibration are available at n different locations, while a number m of harmonics at frequencies N_i, $i = 1, \ldots, m$ is applied on the control input $\mathbf{u}$. In this case, the measurement vector has $2n$ elements and is defined as:

$$\mathbf{y}_N^T = \begin{bmatrix} y_{Nc}^1 & \ldots & y_{Nc}^n & \ldots & y_{Ns}^1 & \ldots & y_{Ns}^n \end{bmatrix} \tag{4.24}$$

where y_{Nc}^i and y_{Ns}^i, $i = 1, \ldots, n$ are, respectively, the cosine and sine components of the i-th N/rev output, which can be, for example, a force or moment component, or a component of a linear or angular acceleration at one or more points of the fuselage.

The HHC input vector $\mathbf{u}$ has $2m$ elements and is defined as

$$\mathbf{u}^T = [u_{N_1c} \;\; u_{N_1s} \ldots u_{N_2c} \;\; u_{N_2s} \ldots u_{N_mc} \;\; u_{N_ms}] \tag{4.25}$$

where u_{N_ic}, $i = 1, \ldots, m$ and u_{N_is}, $i = 1, \ldots, m$ are the cosine and sine component of the HHC input, at desired harmonics not necessarily equal to N/rev.

Assume now, as in the SISO case, that input and output harmonics are related by the linear equation

$$\mathbf{y}_N(k) = T\mathbf{u}(k) + \mathbf{y}_{0N}(k) \tag{4.26}$$

where T is a $2n \times 2m$ constant coefficient matrix, which is again related to the HTF of the time periodic linearized model of the helicopter. Then, the "T-matrix algorithm" is given by

$$\mathbf{u}(k+1) = \mathbf{u}(k) - K\mathbf{y}_N(k) \tag{4.27}$$

where $K = (T^T Q T + R)^{-1} T^T Q$, where $Q = Q^T \geq 0$ and $R = R^T > 0$ are cost weighting matrices of suitable dimensions.

In the MIMO case, the operation of the HHC control law differs considerably depending on the relationship between the number of control inputs and measured variables which are available. To illustrate this difference, the formulation of the "T-matrix algorithm" in the MIMO case with $Q = I_{n,n}$ and $R = 0$, will be presented separately for the cases of $n = m$ and of $n > m$. (The case $n < m$, i.e., with more controls than vibration outputs to be attenuated, is not likely to be important in practice.)

In the case of a "square" control problem, i.e., when $n = m$, the SISO algorithm can be readily extended to

$$\mathbf{u}(k+1) = \mathbf{u}(k) - T^{-1}\mathbf{y}_N(k) \tag{4.28}$$

On the other hand, if $n > m$ the matrix T is no longer square and the discrete time control algorithm must be written as

$$\mathbf{u}(k+1) = \mathbf{u}(k) - T^{\dagger}\mathbf{y}_N(k) \tag{4.29}$$

where $T^{\dagger} = (T^T T)^{-1} T^T$ is the pseudoinverse of T. In particular, the minimum of the cost function equals zero only in the $n = m$ case, i.e., unless one considers (at least) the square

case, it is not possible to guarantee that the vibratory disturbance will be zeroed on all output channels.

The equivalent continuous time formulation for the MIMO HHC compensator, described in discrete form by Eq. (4.27), can be obtained by applying the previously described SISO results. Therefore, considering first the case of a control system with as many inputs as outputs, the state-space formulation is given by the order $2n$ system:

$$\dot{\mathbf{y}}_N = A_c \mathbf{y}_N + B_c(\psi)\mathbf{y} \tag{4.30}$$

$$u = C_c \mathbf{y}_N \tag{4.31}$$

where A_c is the $2n \times 2n$ matrix

$$A_c = \begin{bmatrix} 0 & 0 & \dots & 0 \\ 0 & 0 & \dots & 0 \\ \vdots & \vdots & & \vdots \\ 0 & 0 & \dots & 0 \end{bmatrix} \tag{4.32}$$

$B_c(\psi)$ is the $2n \times n$ matrix

$$B_c(\psi) = K \begin{bmatrix} \cos(N\psi) I_{n,n} \\ \sin(N\psi) I_{n,n} \end{bmatrix} \tag{4.33}$$

and

$$C_c = -\frac{2}{T} I_{2n \times 2n} \tag{4.34}$$

For example, consider the case of a control system relying on the application of N-1/, N/, and N+1/rev inputs in the rotating frame to attenuate one component of the accelerations in $n = 3$ different locations in the fuselage, so that $m = 3$, $N_1 = N - 1$, $N_2 = N$ and $N_3 = N + 1$ and

$$u^T = \left[\theta_{(N-1)c}\, \theta_{(N-1)s}\, \theta_{Nc}\, \theta_{Ns}\, \theta_{(N+1)c}\, \theta_{(N+1)s}\right] \tag{4.35}$$

$$y^T = [y_1\ y_2\ y_3] \tag{4.36}$$

Then, the state space model for the controller is given by

$$A_c = 0_{6\times 6} \tag{4.37}$$

$$B_c(\psi) = K \begin{bmatrix} \cos(N\psi) & 0 & 0 \\ 0 & \cos(N\psi) & 0 \\ 0 & 0 & \cos(N\psi) \\ \sin(N\psi) & 0 & 0 \\ 0 & \sin(N\psi) & 0 \\ 0 & 0 & \sin(N\psi) \end{bmatrix} \tag{4.38}$$

As in the SISO case, because the control inputs are directly given by the higher harmonics of θ, there is no need for a "modulation" term in matrix C_c which therefore turns out to be constant:

$$C_c = -\frac{2}{T} I_{6\times 6} \tag{4.39}$$

Similar expressions can be worked out in the case of a control system with more outputs than inputs.

4.4 Definition of the T matrix in terms of the helicopter models

The control laws discussed in the previous section call for the availability of input/output models for the helicopter response to higher harmonic control inputs. This section provides some background on the frequency response of time-periodic systems and uses such analytical tools to derive explicit expressions for the T matrix.

4.4.1 Development of the Harmonic Transfer Function

This section summarizes the main aspects of the development of the Harmonic Transfer Function (HTF) [41]. Consider a continuous-time linear periodic system:

$$\begin{aligned} \dot{\mathbf{x}}(t) &= A(t)\mathbf{x}(t) + B(t)\mathbf{u}(t) \\ \mathbf{y}(t) &= C(t)\mathbf{x}(t) + D(t)\mathbf{u}(t) \end{aligned} \tag{4.40}$$

Each matrix can be expanded in a complex Fourier series

$$A(t) = \sum_{m=-\infty}^{\infty} A_m e^{jm\Omega t} \tag{4.41}$$

and similarly for $B(t)$, $C(t)$ and $D(t)$. The system can be analyzed in the frequency domain as follows. Introduce the class of *Exponentially Modulated Periodic* (EMP) signals [41]. The (complex) signal $u(t)$ is said to be EMP of period T and modulation s if

$$u(t) = \sum_{k=-\infty}^{\infty} u_k e^{s_k t} = e^{st} \sum_{k=-\infty}^{\infty} u_k e^{jk\Omega t} \tag{4.42}$$

where $t \geq 0$, $s_k = s + jk\Omega$, and s is a complex scalar.

The class of EMP signals is a generalization of the class of T-periodic signals, i.e., of signals with period T: in fact, an EMP signal with $s = 0$ is just an ordinary time-periodic signal.

In much the same way as a time invariant system subject to a (complex) exponential input has an exponential steady-state response, a periodic system subject to an EMP input has an EMP steady-state response. In such a response, all signals of interest (x, $\dot{x}$, y) can be expanded as EMP signals. By deriving Fourier expansions for $A(t)$, $B(t)$, $C(t)$ and $D(t)$, it is possible to prove that the EMP steady-state response of the system can be expressed as the infinite dimensional matrix equation with *constant* elements [41]

$$\begin{array}{rcl} s\mathcal{X} & = & (\mathcal{A} - \mathcal{N})\mathcal{X} + \mathcal{B}\mathcal{U} \\ \mathcal{Y} & = & \mathcal{C}\mathcal{X} + \mathcal{D}\mathcal{U} \end{array} \tag{4.43}$$

where $\mathcal{X}$, $\mathcal{U}$ and $\mathcal{Y}$ are doubly infinite vectors formed with the harmonics of $\mathbf{x}$, $\mathbf{u}$ and $\mathbf{y}$ respectively, organized in the following fashion:

$$\mathcal{X}^T = \left[\cdots \;\; \mathbf{x}_{-2}^T \;\; \mathbf{x}_{-1}^T \;\; \mathbf{x}_0^T \;\; \mathbf{x}_1^T \;\; \mathbf{x}_2^T \;\; \cdots\right] \tag{4.44}$$

and similarly for $\mathcal{U}$ and $\mathcal{Y}$. $\mathcal{A}$, $\mathcal{B}$, $\mathcal{C}$ and $\mathcal{D}$ are doubly infinite Toeplitz matrices formed with

the harmonics of $A(\cdot)$, $B(\cdot)$, $C(\cdot)$ and $D(\cdot)$ respectively as follows

$$\mathcal{A} = \begin{bmatrix} \ddots & \vdots & \vdots & \vdots & \vdots & \vdots & \\ \cdots & A_0 & A_{-1} & A_{-2} & A_{-3} & A_{-4} & \cdots \\ \cdots & A_1 & A_0 & A_{-1} & A_{-2} & A_{-3} & \cdots \\ \cdots & A_2 & A_1 & A_0 & A_{-1} & A_{-2} & \cdots \\ \cdots & A_3 & A_2 & A_1 & A_0 & A_{-1} & \cdots \\ \cdots & A_4 & A_3 & A_2 & A_1 & A_0 & \cdots \\ & \vdots & \vdots & \vdots & \vdots & \vdots & \ddots \end{bmatrix} \tag{4.45}$$

(and similarly for $\mathcal{B}$, $\mathcal{C}$ and $\mathcal{D}$), where the submatrices A_n in Eq. (4.45) are the coefficients of the Fourier expansion of matrix $A(t)$, given in Eq. (4.41). To relate these coefficients to those of the Fourier series expansion in trigonometric form, Eq. (4.1), recall that the Fourier series expansion of a scalar function can be rewritten in complex exponential form, i.e., $a(t) = a_0 + \sum_{k=1}^{\infty} (a_{nc} \cos n\omega t + a_{ns} \sin n\omega t) = \sum_{k=-\infty}^{\infty} a_k e^{jk\omega t}$, with $a_k = (a_{kc} - j a_{ks})/2$, and $a_{-k} = (a_{kc} + j a_{ks})/2, k = 1, 2, \ldots$. Therefore, the coefficients of Eqs. (4.41) and (4.1) are related by:

$$\begin{array}{l} A_k = \frac{1}{2}(A_{kc} - jA_{ks}) \\ \\ A_{-k} = \frac{1}{2}(A_{kc} + jA_{ks}) \end{array} \qquad k = 1, 2, \ldots \tag{4.46}$$

with A_0 identical in both Eq. (4.41) and Eq. (4.1). Similar relations hold for the harmonics of B, C, and D.

Matrix $\mathcal{N}$ is a block diagonal complex-valued matrix given by

$$\mathcal{N} \;=\; \text{blkdiag}\,\{jn\Omega I\} = j\Omega \begin{bmatrix} \ddots & \vdots & \vdots & \vdots & \vdots & \vdots & \\ \cdots & -2I & 0 & 0 & 0 & 0 & \cdots \\ \cdots & 0 & -I & 0 & 0 & 0 & \cdots \\ \cdots & 0 & 0 & 0 & 0 & 0 & \cdots \\ \cdots & 0 & 0 & 0 & I & 0 & \cdots \\ \cdots & 0 & 0 & 0 & 0 & 2I & \cdots \\ & \vdots & \vdots & \vdots & \vdots & \vdots & \ddots \end{bmatrix} \tag{4.47}$$

where I is the identity matrix, of size equal to the number of states.

From Eq. (4.43), one can define the HTF $\mathcal{G}(s)$ as the operator:

$$\mathcal{G}(s) \stackrel{def}{=} \mathcal{C}[s\mathcal{I} - (\mathcal{A} - \mathcal{N})]^{-1}\mathcal{B} + \mathcal{D} \tag{4.48}$$

which relates the input harmonics and the output harmonics (contained in the infinite vectors $\mathcal{U}$ and $\mathcal{Y}$ respectively). Equation (4.48) is the extension to the case of periodic systems of the corresponding constant coefficient expression for the transfer function

$$G(s) = C\left[sI - A\right]^{-1} B + D \tag{4.49}$$

In particular, if $s = 0$, which, in the helicopter case, corresponds to the steady-state response of the system to a periodic input of basic frequency N/rev, the appropriate input/output operator for periodic systems becomes

$$\mathcal{G}(0) = \mathcal{C}[\mathcal{N} - \mathcal{A}]^{-1}\mathcal{B} + \mathcal{D} \tag{4.50}$$

4.4.2 Definition of the T matrix

The $T_{N,N}$, $T_{N,M}$ and T matrices used in the formulation of the HHC and PHHC algorithms can be related to the elements of the HTF of the linearized helicopter model, as follows.

First of all, note that according to the definition of the control input vector $\mathbf{u}$ which has been adopted, the rotor will be subject to a proper, steady state higher harmonic control input whenever the control vector $\mathbf{u}$ is *constant*. This implies that to define the T matrix for the helicopter we only have to study the response of the periodic helicopter models to a EMP input with $s = 0$, i.e., we only have to compute the input/output operator $\hat{\mathcal{G}}(0)$. For example, consider the linear time-periodic system, Eq. (4.40), and the constant input $\mathbf{u}(t) = \mathbf{u}_0$. The vector $\mathcal{U}$ corresponding to $\mathbf{u}(t) = \mathbf{u}_0$ is given by

$$\mathcal{U}^T = \begin{bmatrix} \cdots & 0 & 0 & \mathbf{u}_0^T & 0 & 0 & \cdots \end{bmatrix} \tag{4.51}$$

and the steady state response $\mathcal{Y}$ of the periodic system is given by

$$\mathcal{Y} = \mathcal{G}(0)\mathcal{U} \tag{4.52}$$

which can be equivalently written as

$$\begin{bmatrix} \vdots \\ y_{-2N} \\ y_{-N} \\ y_0 \\ y_N \\ y_{2N} \\ \vdots \end{bmatrix} = \begin{bmatrix} \ddots & \vdots & \vdots & \vdots & \vdots & \vdots & \\ \cdots & G_{-2N,-2N} & G_{-2N,-N} & G_{-2N,0} & G_{-2N,N} & G_{-2N,2N} & \cdots \\ \cdots & G_{-N,-2N} & G_{-N,-N} & G_{-N,0} & G_{-N,N} & G_{-N,2N} & \cdots \\ \cdots & G_{0,-2N} & G_{0,-N} & G_{0,0} & G_{0,N} & G_{0,2N} & \cdots \\ \cdots & G_{N,-2N} & G_{N,-N} & G_{N,0} & G_{N,N} & G_{N,2N} & \cdots \\ \cdots & G_{2N,-2N} & G_{2N,-N} & G_{2N,0} & G_{2N,N} & G_{2N,2N} & \cdots \\ \ddots & \vdots & \vdots & \vdots & \vdots & \vdots & \ddots \end{bmatrix} \begin{bmatrix} \vdots \\ 0 \\ 0 \\ u_0 \\ 0 \\ 0 \\ \vdots \end{bmatrix} \tag{4.53}$$

From Eq. (4.53) we have that

$$\begin{bmatrix} y_{-N} \\ y_N \end{bmatrix} = \begin{bmatrix} G_{-N,0} \\ G_{N,0} \end{bmatrix} u_0 \tag{4.54}$$

and converting the N/rev harmonics of the output from exponential to trigonometric form we have that

$$\begin{bmatrix} y_{Nc} \\ y_{Ns} \end{bmatrix} = 2 \begin{bmatrix} \text{Real}[G_{N,0}] \\ \text{Imag}[G_{N,0}] \end{bmatrix} u_0, \tag{4.55}$$

(note that $G_{-N,0}$ and $G_{N,0}$ are complex conjugate) so that the T matrix is given by

$$T = 2 \begin{bmatrix} \text{Real}[G_{N,0}] \\ \text{Imag}[G_{N,0}] \end{bmatrix} \tag{4.56}$$

4.4.3 Construction of the T matrix

From a practical point of view, the above theoretical analysis of the frequency response of periodic system, and the corresponding definitions for the T-matrix relating selected input-output frequencies only, rely on the use of infinite dimensional matrices. When it comes to the numerical construction of the T-matrix, however, one has to resort to finite dimensional approximations of the system matrices $\mathcal{A}$, $\mathcal{B}$, $\mathcal{C}$, and $\mathcal{D}$. Consider, for example, the problem of constructing the T-matrix, as defined in Eq. (4.56) for a periodic system of the form of Eq. (4.40) with n outputs, m inputs and n_s states. First of all, one chooses the dimension of the expansions $\mathcal{A}$, $\mathcal{B}$, $\mathcal{C}$, and $\mathcal{D}$ for the state space matrices A, B, C, and D, in terms of the number of block rows one wants to take into account in $\mathcal{A}$. For example, if we choose

to include a number $n_B = 5$ of blocks in each row of the expansion of the system matrices, then $\mathcal{A}$ has dimension $n_s n_B \times n_s n_B$ and is given by

$$\mathcal{A} = \begin{bmatrix} A_0 & A_{-1} & A_{-2} & A_{-3} & A_{-4} \\ A_1 & A_0 & A_{-1} & A_{-2} & A_{-3} \\ A_2 & A_1 & A_0 & A_{-1} & A_{-2} \\ A_3 & A_2 & A_1 & A_0 & A_{-1} \\ A_4 & A_3 & A_2 & A_1 & A_0 \end{bmatrix} \tag{4.57}$$

and similarly for $\mathcal{B}$, $\mathcal{C}$, and $\mathcal{D}$. Therefore, the HTF is given by the $2nn_B \times mn_B$ matrix, as follows

$$\begin{bmatrix} y_{-2N} \\ y_{-N} \\ y_0 \\ y_N \\ y_{2N} \end{bmatrix} = \mathcal{G}(0)\,\mathcal{U} = \begin{bmatrix} G_{-2N,-2N} & G_{-2N,-N} & G_{-2N,0} & G_{-2N,N} & G_{-2N,2N} \\ G_{-N,-2N} & G_{-N,-N} & G_{-N,0} & G_{-N,N} & G_{-N,2N} \\ G_{0,-2N} & G_{0,-N} & G_{0,0} & G_{0,N} & G_{0,2N} \\ G_{N,-2N} & G_{N,-N} & G_{N,0} & G_{N,N} & G_{N,2N} \\ G_{2N,-2N} & G_{2N,-N} & G_{2N,0} & G_{2N,N} & G_{2N,2N} \end{bmatrix} \begin{bmatrix} 0 \\ 0 \\ u_0 \\ 0 \\ 0 \end{bmatrix} \tag{4.58}$$

The blocks $G_{-N,0}$, $G_{N,0}$ can be extracted from $\mathcal{G}(0)$ as the submatrices $\mathcal{G}_{ij}(0), i = 2n + 1, \ldots, 3n$ and $j = 2m + 1, \ldots, 3m$, and $\mathcal{G}_{ij}(0), i = 4n + 1, \ldots, 5n$ and $j = 2m + 1, \ldots, 3m$ respectively. Clearly, the choice of the number of block rows n_B will affect the accuracy of the numerical construction (see Ref. [42] for an analysis of the effect of truncation in the study of frequency response operators), so as a general rule, n_B should be chosen sufficiently large to ensure that the T-matrix constructed from the truncated HTF gives a good approximation to the actual T-matrix.

4.5 Formulation of the coupled helicopter/HHC model

The compensator will be designed along the lines of Ref. [41]. Denote with $A(\psi)$, $B(\psi)$, $C(\psi)$, and $D(\psi)$ the matrices for the LTP state space model of the helicopter, for the selected input/output pair. Similarly, denote with $A_c(\psi)$, $B_c(\psi)$, $C_c(\psi)$ the compensator's state space model. Then the closed-loop LTP state matrix $A_e(\psi)$ is given by

$$A_e(\psi) = \begin{bmatrix} A(\psi) & B(\psi)C_c(\psi) \\ B_c(\psi)C(\psi) & A_c(\psi) + B_c(\psi)D(\psi)C_c(\psi) \end{bmatrix} \tag{4.59}$$

The closed-loop stability of the helicopter with HHC is then given by the characteristic exponents of $A_e(\psi)$, and will be studied as a function of the design parameters Q and R.

4.6 Results

This section presents closed-loop stability and response results for a coupled helicopter-HHC system. The stability results are obtained from the linearized model of Eq. (4.59) or its constant coefficient approximation. The closed-loop response results are obtained from the full nonlinear simulation of the coupled helicopter-HHC system.

The helicopter configuration used for the present chapter is similar to the Eurocopter B0-105, with a thrust coefficient $C_T/\sigma = 0.071$. Three blade modes are used in the modal coordinate transformation, namely, the fundamental flap, lag, and torsion modes, with natural frequencies of 1.12/rev, 0.7/rev, and 3.4/rev, respectively. Because the aerodynamic model consists of a simple linear inflow with quasi-steady aerodynamics, vibratory loads and CG accelerations, and consequently also HHC inputs, tend to be underestimated. Therefore, their absolute values can be considered representative only in a qualitative sense. However, the overall simulation model is likely reasonable for stability studies, and for a general assessment of the design and closed-loop analysis methodology.

For all the vibratory response results, the helicopter is first trimmed in steady, straight flight at the desired velocity with the HHC system turned off. Then, the nonlinear simulation begins, with the pilot controls held fixed at their trim values and the HHC system turned on at time $t = 0$. The Q and R matrices in Eq. (4.8) have been defined as $Q = I_{6,6}$ and $R = rI_{6,6}$, respectively, where $I_{6,6}$ is an identity matrix with six rows and columns, and r is a parameter that varies from r=0 (no restriction on control effort) to r=1000.

4.6.1 Results for V=80 kts

Figure 4.2 shows the peak-to-peak magnitude of the 4/rev component of the vertical (i.e., along the z-body axis) acceleration at the CG, for a speed $V = 80$ kts, corresponding to $\mu = 0.19$. The figure shows four curves, one each for values of r=0, 10, 100, and 1000, corresponding to increasing restrictions on the control effort. The high-frequency oscillations

visible in the curves of this, and of many subsequent figures, are largely an artifact of the numerical procedure used to extract the 4/rev magnitude and phase from the time histories of the accelerations. Clearly, the HHC system is very effective, and reduces the 4/rev vertical acceleration to a small fraction of its trim value in just a few seconds. The vibration attenuation is also very clear for the CG roll acceleration $\dot{p}$ and pitch acceleration $\dot{q}$: the magnitudes of the 4/rev components are shown in Fig. 4.3. Both $\dot{p}$ and $\dot{q}$ are reduced to 5% or less of their trim values in no more than 6-7 seconds.

Figure 4.4 shows the magnitude of the 3/, 4/, and 5/rev components of the HHC input for the cases $r = 0$ and $r = 1000$. Figure 4.5 shows the corresponding phase angles. Comparing the two sets of results, it can be seen that the controls reach their steady-state values much more quickly for the case $r = 0$ than for $r = 1000$. In the latter case, the steady-state values of θ_3 and θ_5 have not yet been reached at the end of 7 sec of simulation.

It is interesting to note that the action of the HHC system, and the consequent vibration reduction, occurs within times of the order of 5-7 sec or, equivalently, of about 1 rad/sec. These are also typical time scales for flight control systems, and also overlap typical piloting frequencies. Therefore, the results previously shown indicate the possibility of interaction with the stability and control characteristics of the helicopter.

It is also interesting to consider the closed-loop eigenvalues of the system. The computation of the closed-loop state matrix A_e, Eq. (4.59), was carried out by linearizing the augmented nonlinear set of equations. Figure 4.6 shows a root locus plot of just the controller eigenvalues for increasing values of r, using a constant coefficient approximation to A_e. The system displays a mildly unstable complex conjugate pair at 80 knots, but there is no trace of the instability in the closed-loop simulations using the full nonlinear system, previously shown. The instability is probably due to the errors made in modeling the periodic system with a constant coefficient approximation. In fact, when the periodicity is fully taken into account, the instability disappears. This can be seen in Fig. 4.7, which shows the real parts

of both the stability eigenvalues of the LTI system and the Floquet characteristic exponents of the LTP system, for the least damped modes. None of the characteristic exponents, which include controller, rotor, and rigid body modes, becomes unstable for any of the values of r considered. This confirms that, whenever the HHC input includes harmonics that are different from the harmonic that one is trying to attenuate, the closed-loop problem is intrinsically time-periodic. Constant coefficient approximations may not yield correct correct closed-loop stability results, as in this case, even at lower advance ratios, where constant coefficient approximations give acceptable results for the open-loop system. Apart from the heading eigenvalue at the origin, the modes with the lowest amount of damping are those of the controller.

Finally, the position of the eigenvalues appears to be linked to the vibration reduction performance. In general, for the highest control effort (tuning parameter $r = 0$) controller eigenvalues tend to be farther away from the origin, and as r increases they come closer to it.

4.6.2 Results for V=140 and 170 kts

Figures 4.8 and 4.9 show the 4/rev CG acceleration components at a speed of V=140 kts, corresponding to an advance ratio $\mu = 0.33$. The magnitude of the vertical acceleration is shown in Fig. 4.8. The HHC is extremely effective, and reduces the magnitude of the 4/rev accelerations to almost zero within about 7 seconds. Near-perfect attenuation of the roll acceleration $\dot{p}$ can be seen in Fig. 4.9. The figure also shows that the pitch acceleration $\dot{q}$ is also very well attenuated by the HHC system.

The magnitudes of the corresponding values of the 3/, 4/, and 5/rev inputs are shown in Fig. 4.10 for the cases $r = 0$ and $r = 1000$. The steady-state values of each control are reached in about 7 seconds, therefore the time scale of action of the controller is approximately the same as in the 80 kts case. Differently from the 80 kts case, the control time histories for

$r = 0$ and $r = 1000$ are very similar.

The LTI, closed-loop eigenvalues for V=140 kts are shown in Fig. 4.11. At this speed, all the eigenvalues are stable, with the partial exception of a complex controller eigenvalue, which is unstable but extremely close to the origin. The real parts of both the stability eigenvalues of the LTI system and the Floquet characteristic exponents of the LTP system, for the least damped modes, are shown in Fig. 4.12. All the characteristic exponents are stable. As in the V=80 kts case, the modes with the lowest amount of damping are those of the controller.

Finally, Figure 4.13 shows one result for the case V=170 kts, corresponding to $\mu = 0.4$. Note that the simulation cannot determine a trim state at this speed. Therefore, the drag of the fuselage was arbitrarily reduced until a trimmed state could be achieved. Figure 4.13 shows baseline and HHC-on magnitudes of the 4/rev component of the vertical acceleration. Again, the HHC is very effective at attenuating vibrations, and the attenuation occurs on the same time scales as for the speeds previously shown. Additional results were obtained for this speed, but are not presented here for reasons of space. However, the overall trends are the same as seen for the V=80 kts and V=140 kts cases, except that the closed-loop LTI system is stable.

4.7 Conclusions

The chapter presented the development of a state space formulation for a Multi-Input Multi-Output (MIMO) Higher Harmonic Control (HHC) system. The development started with a simple state space derivation for the continuous time form of a Single-Input Single-Output HHC compensator with input and output at the same rotor harmonic; then the same approach was extended to the case of different harmonics in input and output, which resulted in a periodic SISO HHC compensator; finally, that result was generalized for the derivation of the state space form for a MIMO HHC controller. The chapter also presented results of a

numerical investigation into the performance and stability properties of a closed loop HHC system, implemented in the rotating system, based on a simulation study of the coupled rotor-fuselage dynamics of a four bladed hingeless rotor helicopter.

The results of the simulation study indicate that:

1. The HHC controller is very effective in reducing the desired components of the 4/rev accelerations at the center of gravity. Because the aerodynamic model used leads to underestimating these vibratory components, the absolute values of the reduction and of the control inputs may not be fully reliable. However, the percentage reductions indicated by the simulations are in excess of 80-90%.

2. The vibration attenuation occurs within 5-7 seconds after the HHC system is turned on. This is equivalent to a frequency of around 1 rad/sec, which is within the frequency band in which flight control systems and human pilots tend to operate. Therefore, the interactions and potential adverse effects on the stability and control characteristics of the helicopter should be explored.

3. The HHC problem is intrinsically time-periodic if the HHC inputs include frequencies other than the frequency one wishes to attenuate. This is true even if the rest of the model is assumed to be time-invariant. In these cases, the closed-loop stability results obtained using a constant coefficient approximations may be incorrect even at lower values of the advance ratio μ, where constant coefficient approximation of the open-loop dynamics are accurate.

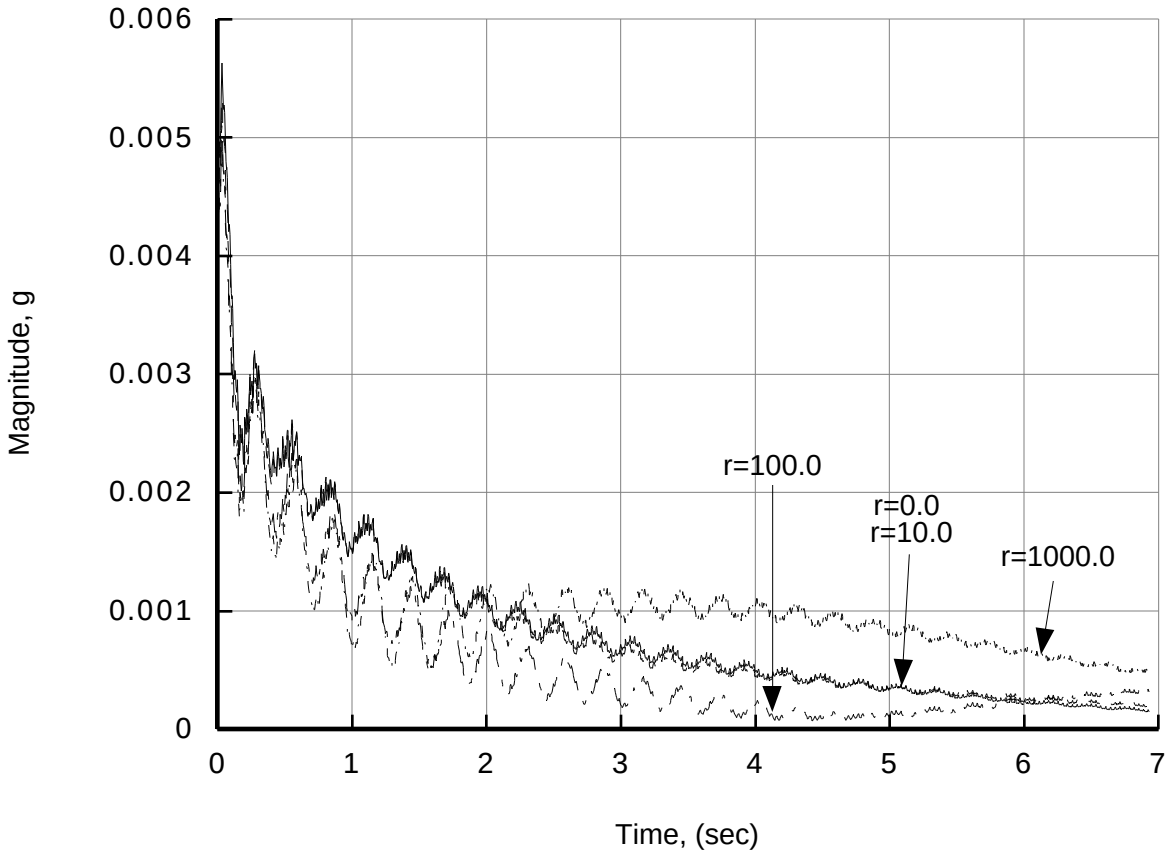

Figure 4.2: Peak-to-peak 4/rev vertical accelerations at the helicopter center of mass for V=80 kts ($\mu = 0.188$).

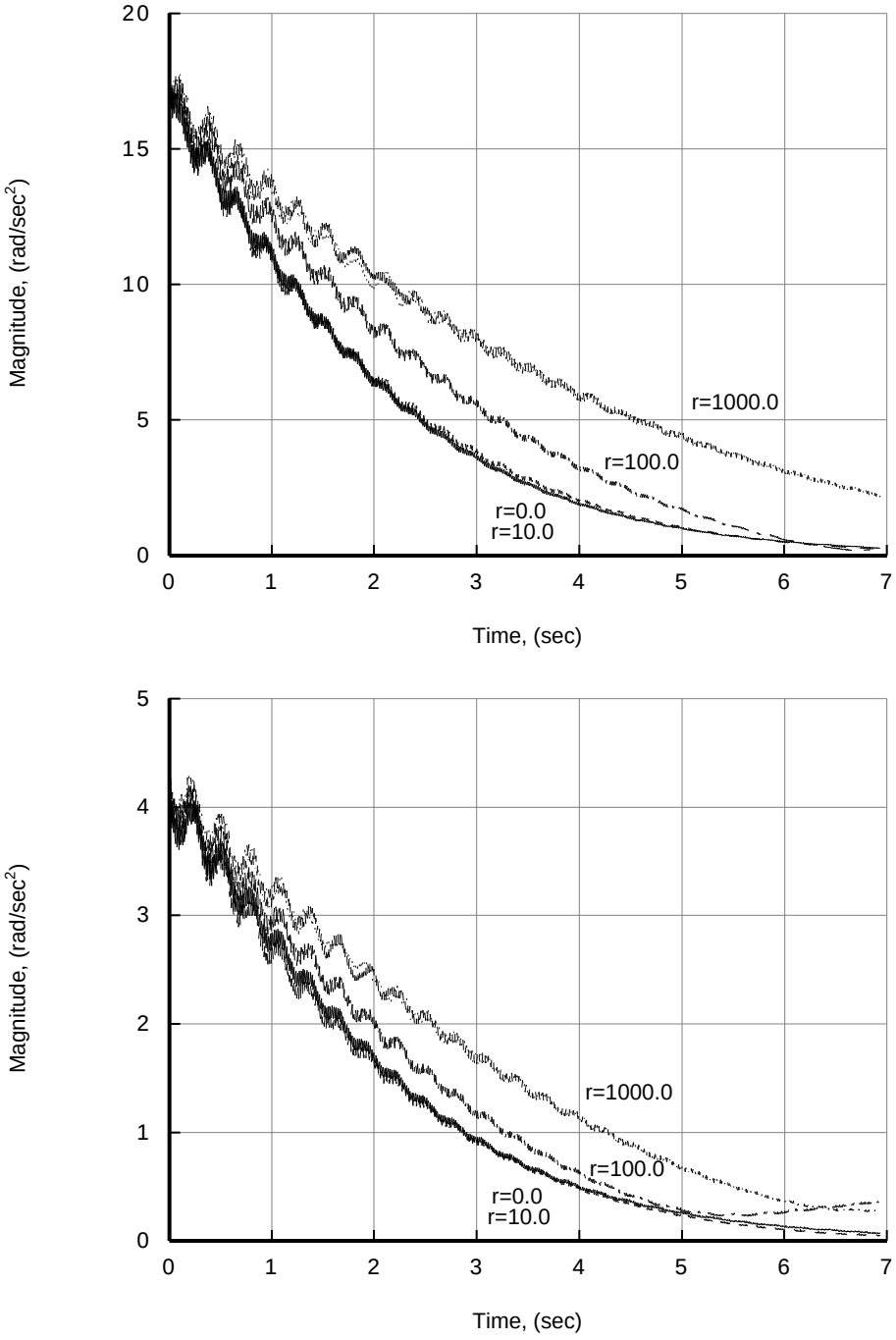

Figure 4.3: Peak-to-peak 4/rev roll (top) and pitch (bottom) accelerations at the helicopter center of mass for V=80 kts ($\mu = 0.188$).

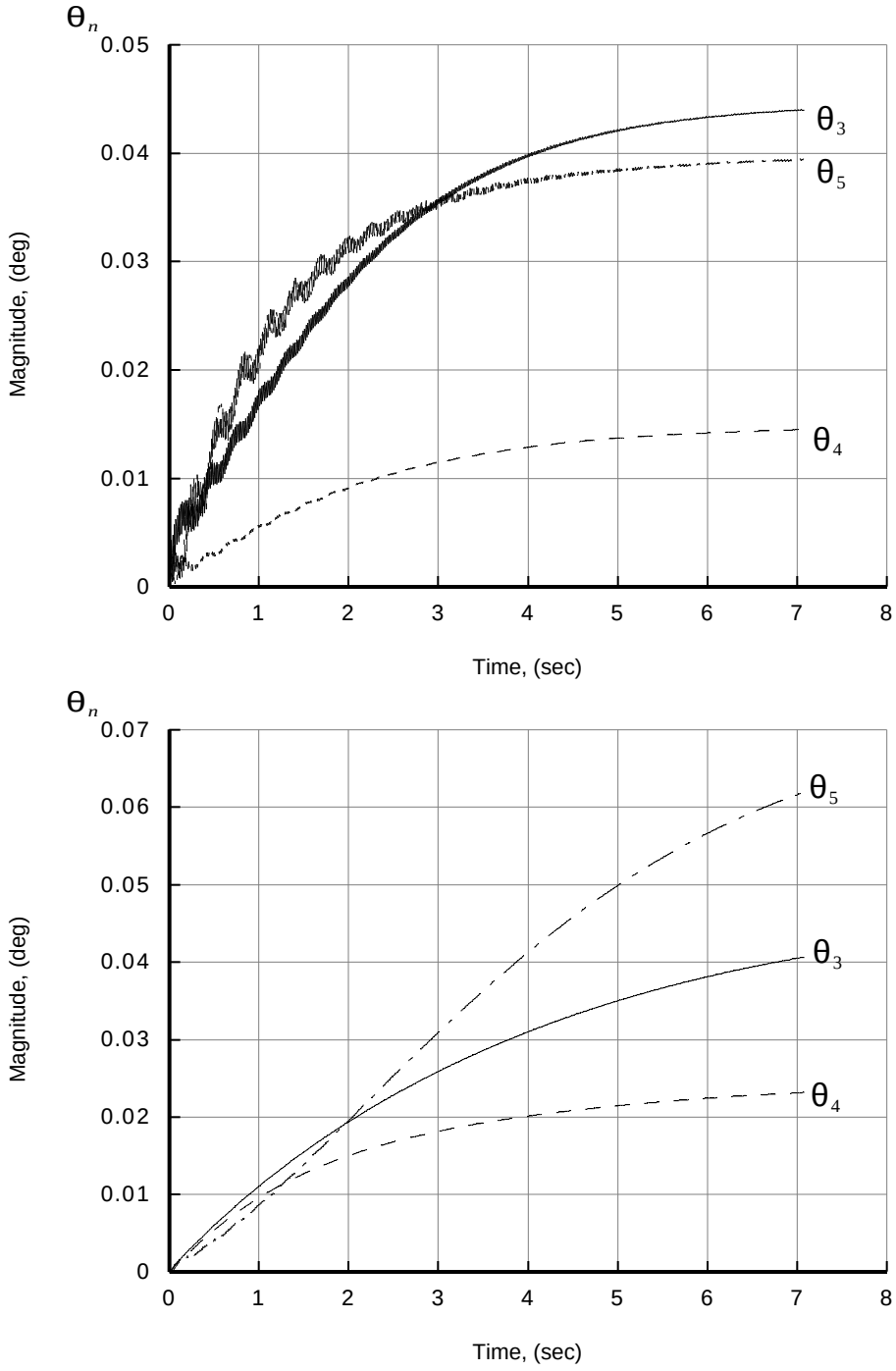

Figure 4.4: HHC control input amplitude in degrees, V=80 kts ($\mu \approx 0.189$) for r = 0 (top) and r=1000 (bottom).

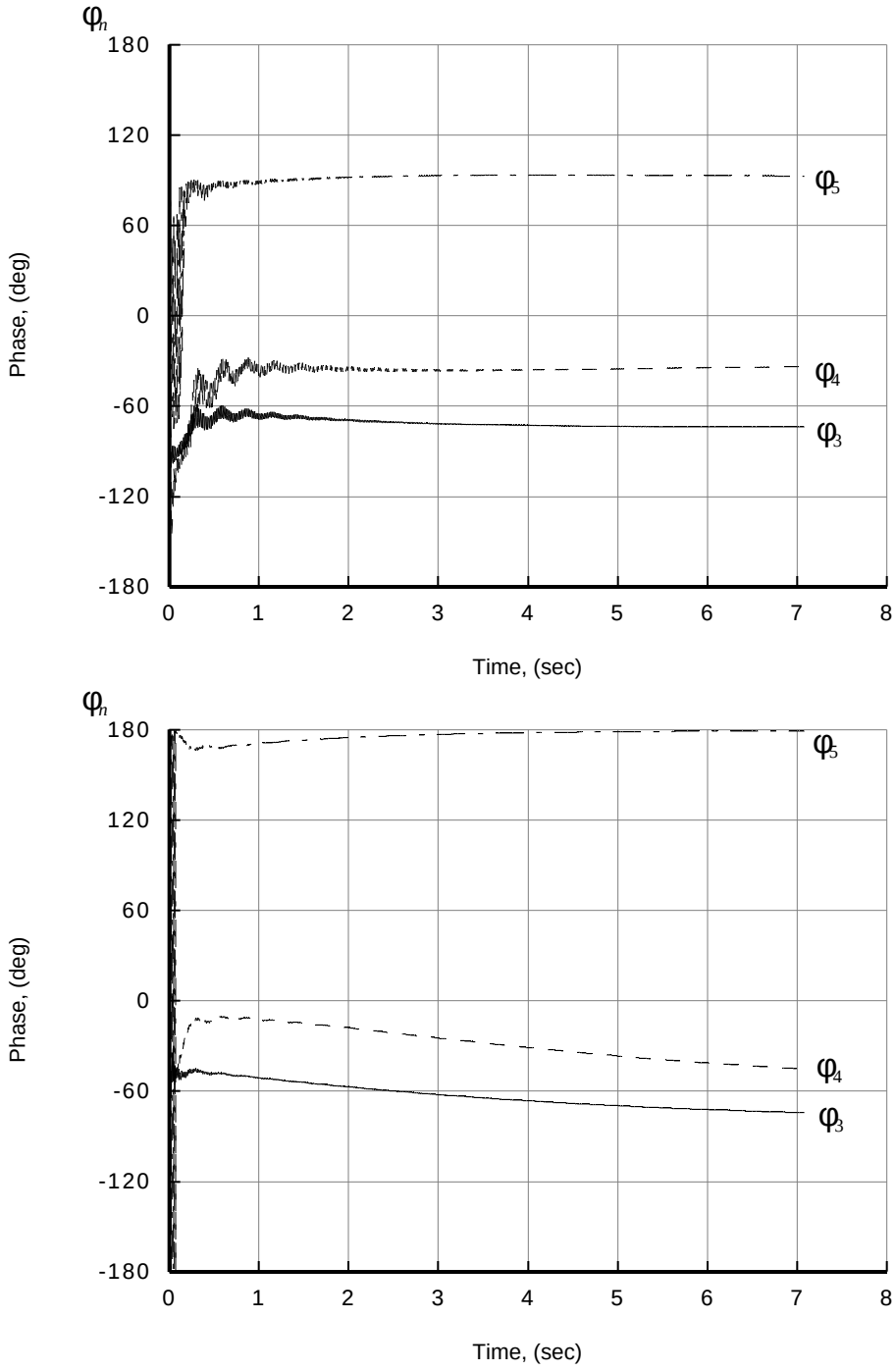

Figure 4.5: HHC control input phase in degrees, V=80 kts ($\mu \approx 0.189$) for r=0 (top) and r=1000 (bottom).

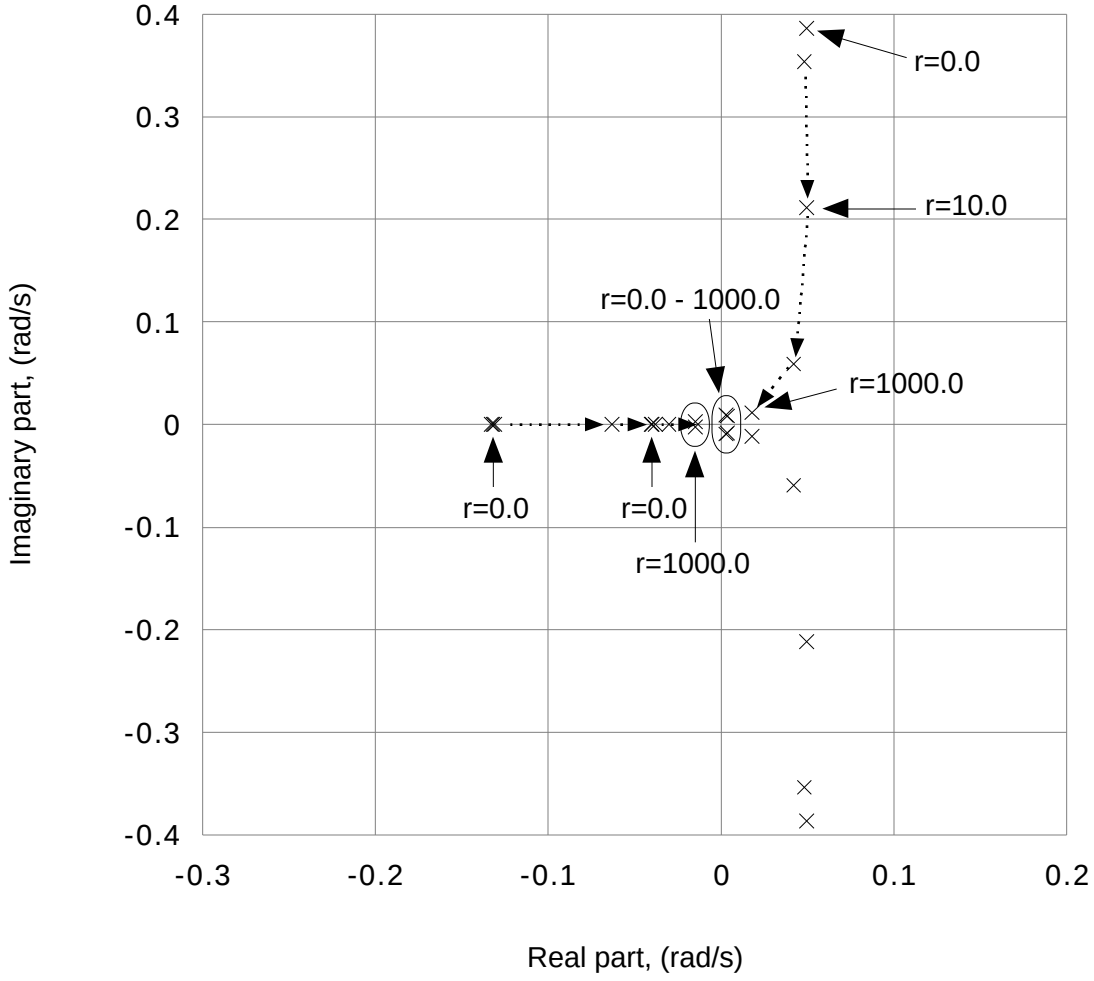

Figure 4.6: Root-locus of controller eigenvalues of LTI closed-loop system, V=80 kts.

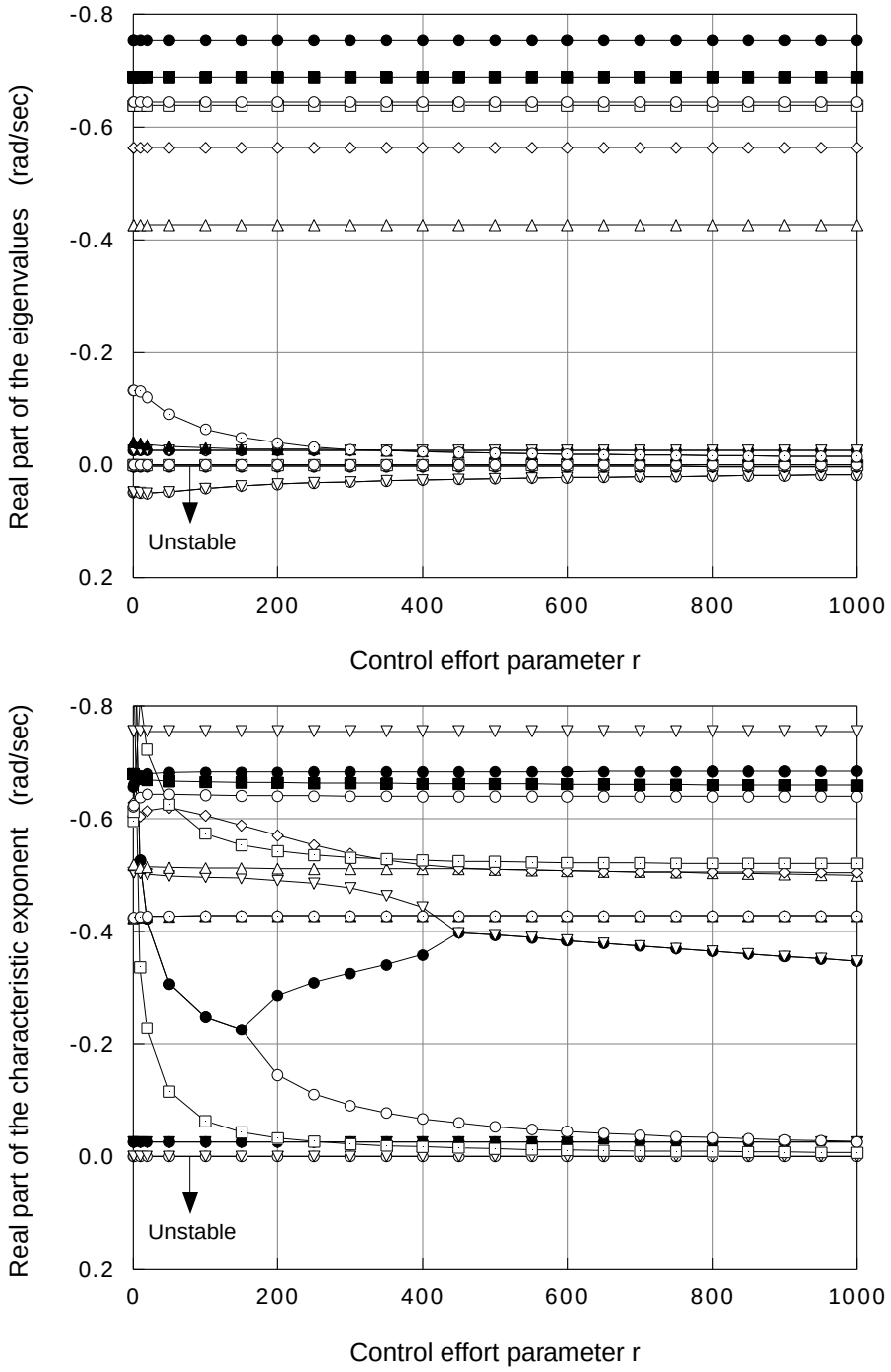

Figure 4.7: Real parts of eigenvalues (top) and characteristic exponents (bottom) of the least damped modes, V=80 kts.

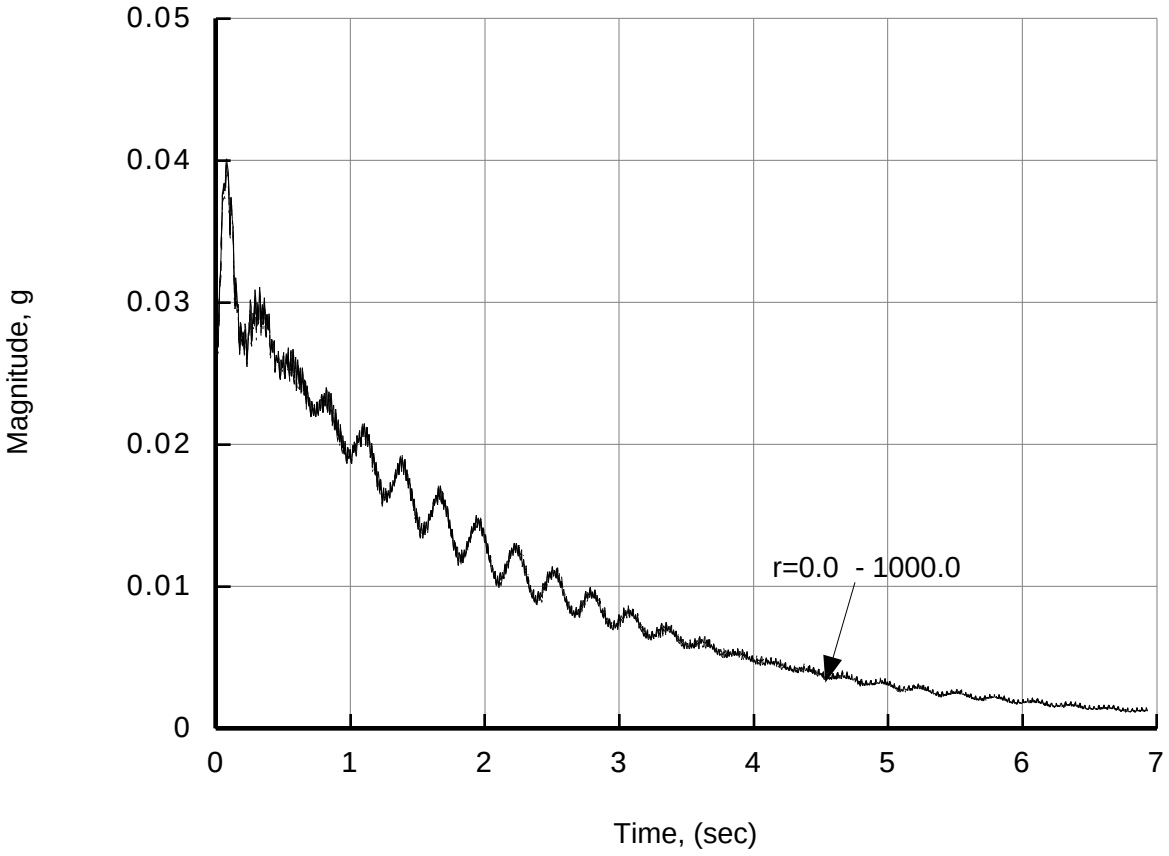

Figure 4.8: Peak-to-peak 4/rev vertical accelerations at the helicopter center of mass for V=140 kts ($\mu = 0.330$).

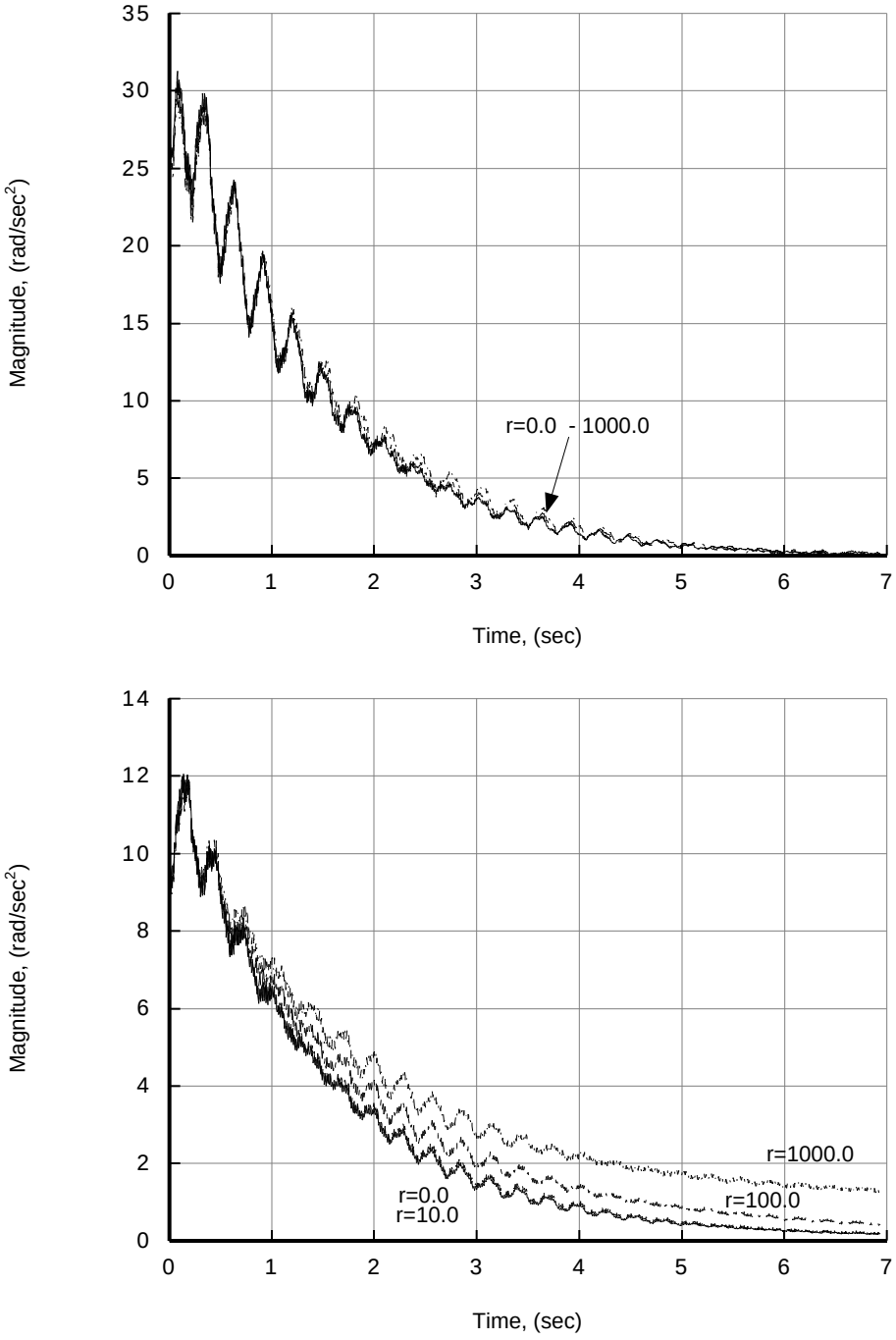

Figure 4.9: Peak-to-peak 4/rev roll (top) and pitch (bottom) accelerations at the helicopter center of mass for V=140 kts ($\mu = 0.330$).

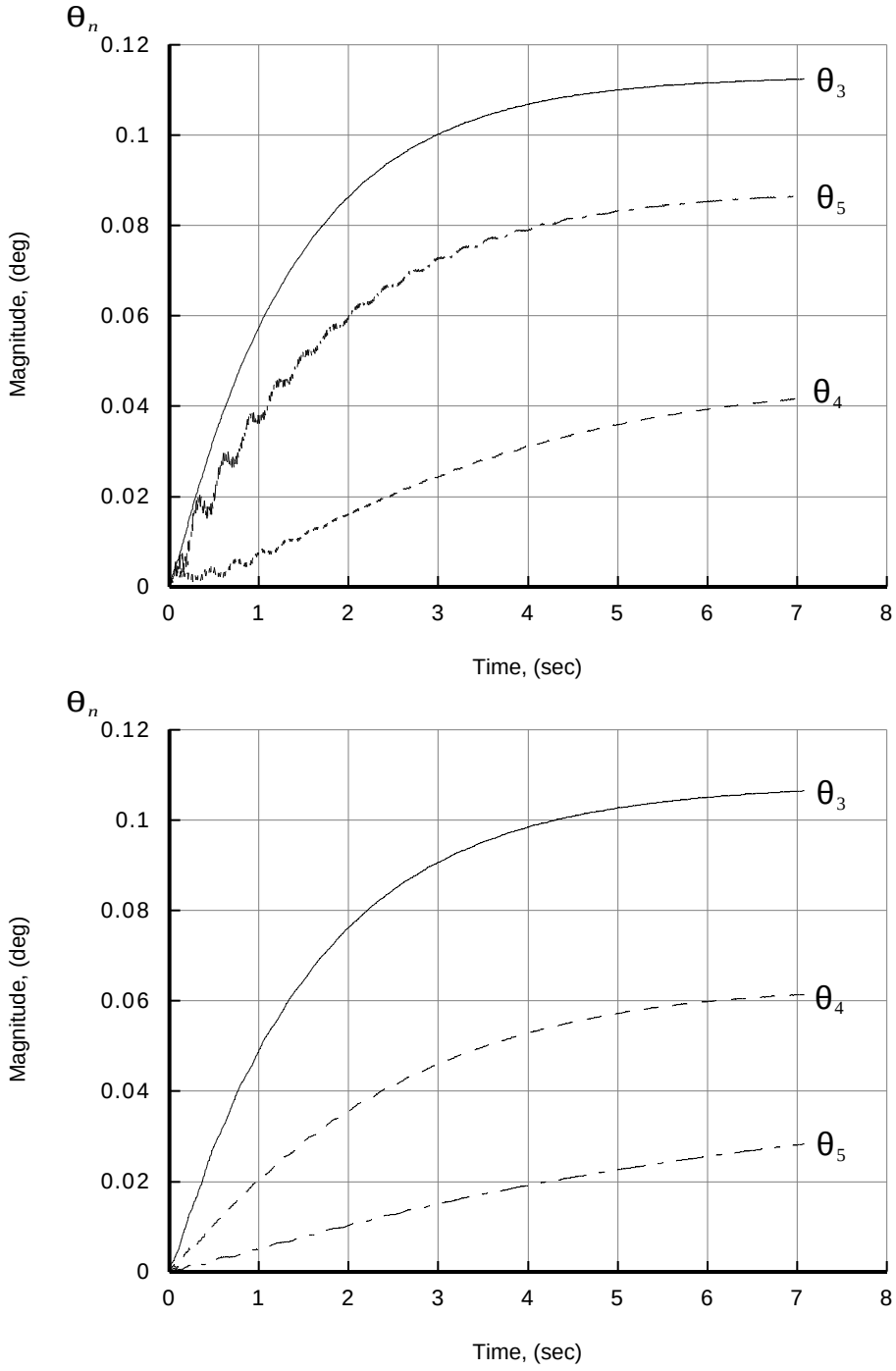

Figure 4.10: HHC control input amplitude in degrees, V=140 kts ($\mu \approx 0.33$) for r=0 (top) and r=1000 (bottom).

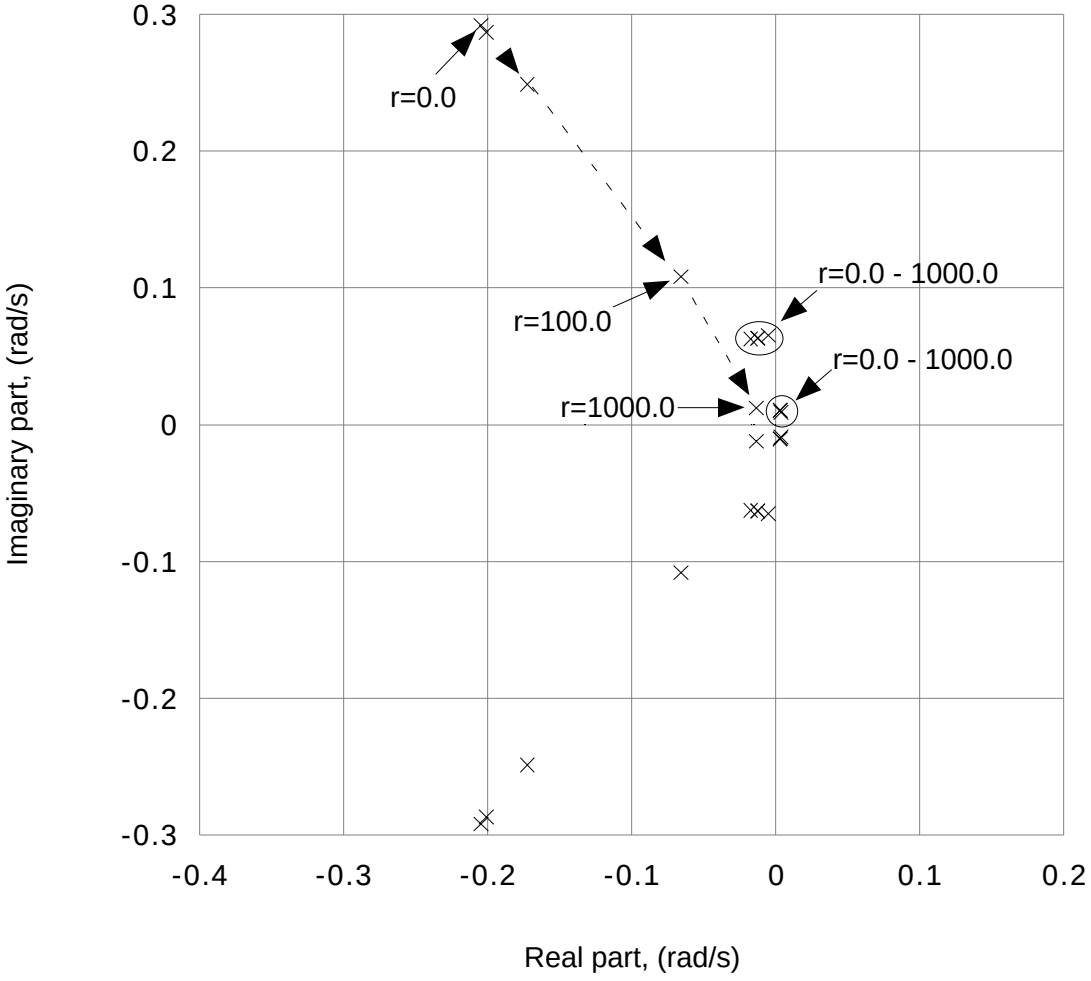

Figure 4.11: Root-locus of controller eigenvalues of LTI closed-loop system, V=140 kts.

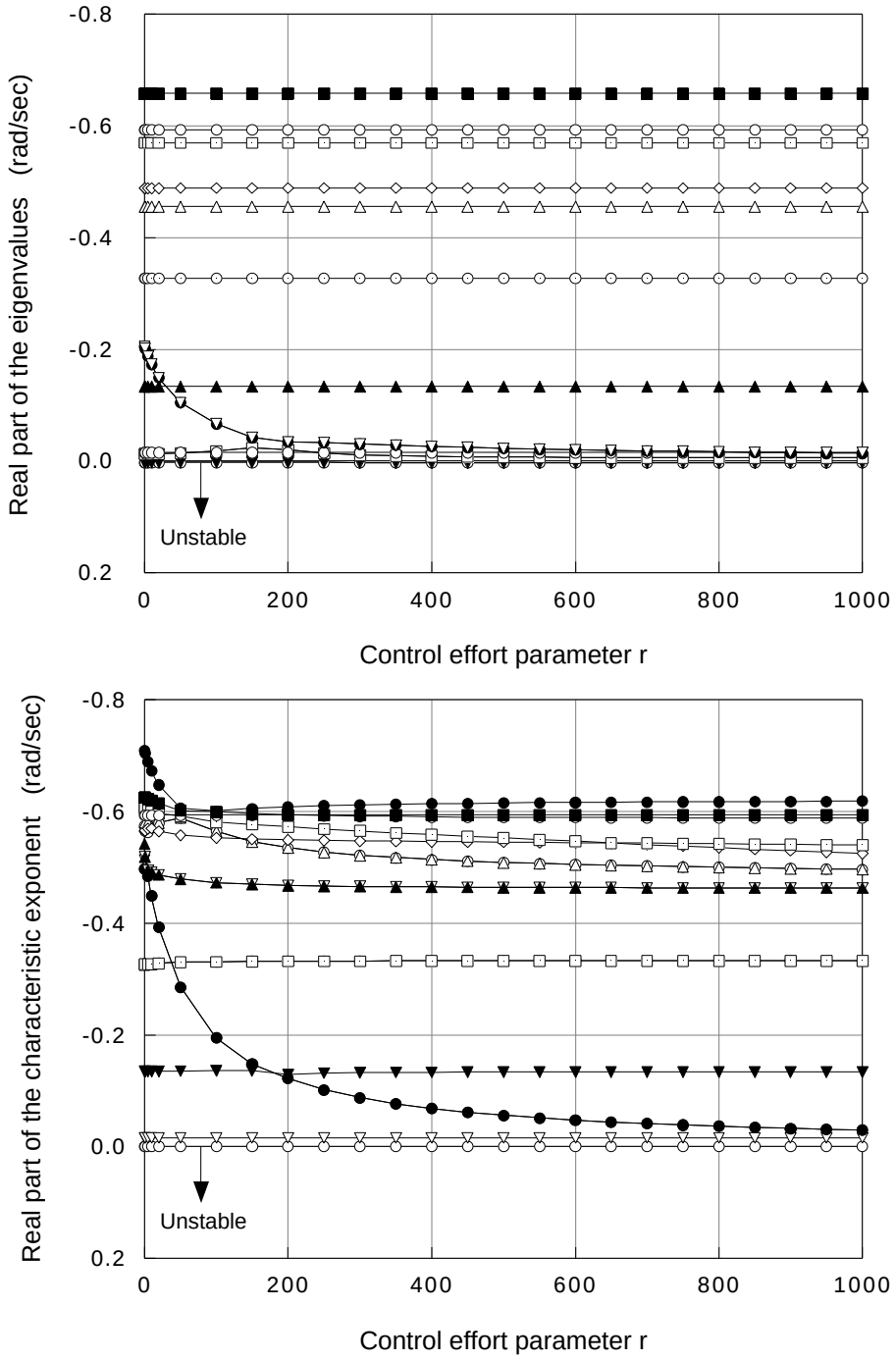

Figure 4.12: Real parts of eigenvalues (top) and characteristic exponents (bottom) of the least damped modes, V=140 kts.

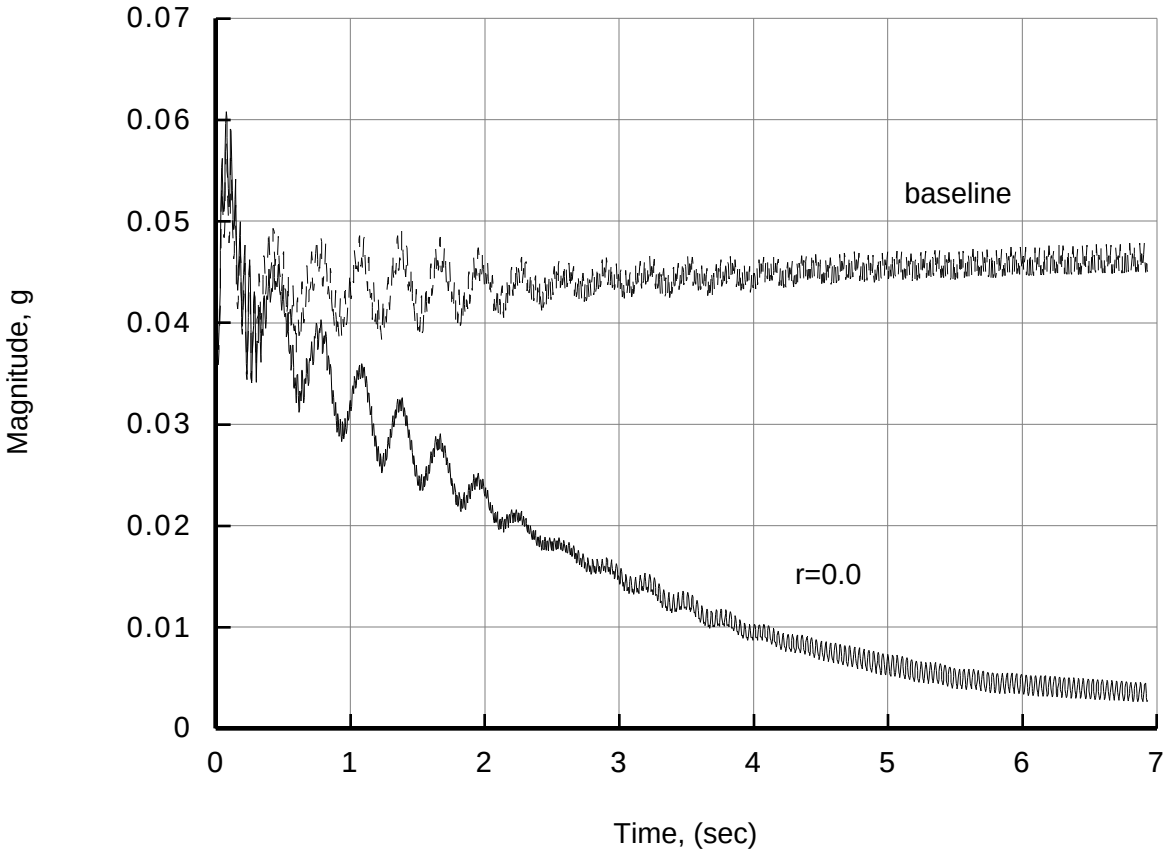

Figure 4.13: Peak-to-peak 4/rev vertical accelerations at the helicopter center of mass for V=170 kts ($\mu = 0.4$); reduced fuselage drag.

Chapter 5

Basic Concepts in the Treatment of Discrete Systems with Periodic Coefficients

5.1 State-space and input-output models for periodic systems

The state space description of a periodic system in discrete time is

$$x(t+1) = A(t)x(t) + B(t)u(t) \tag{5.1}$$

$$y(t) = C(t)x(t) + D(t)u(t) \tag{5.2}$$

where $x(t)$ is the state vector, of size n, $y(t)$ is the output vector, of size p, and $u(t)$ is the input vector, of size m. The matrices $A(\cdot), B(\cdot), C(\cdot)$, and $D(\cdot)$ are periodic of period T.

The stability of the system can be assessed by analyzing the so-called *monodromy matrix*. Precisely, let $\Phi_A(t,\tau)$ $(t \geq \tau)$ be the system transition matrix, i.e.

$$\Phi_A(t,\tau) = \begin{cases} A(t-1)A(t-2)\dots A(\tau) & t > \tau \\ I & t = \tau \end{cases} \tag{5.3}$$

The monodromy matrix is defined as the transition matrix over one period, e.g., $[\tau, \tau+T-1]$, and is denoted by $\Psi_A(\tau) = \Phi_A(\tau+T,\tau)$. Its eigenvalues do not depend upon τ and are named *characteristic multipliers*. The system is stable if and only if the characteristic multipliers lie in the open unit disk.

In the same way as for time-invariant systems, the external properties of a periodic system can also be studied in a fully input-output context. The basic causal relationship supplies

the output $y(t)$as a linear combination of past values of the input up to time τ:

$$\begin{aligned} y(t) &= M_0(t)u(t) + M_1(t)u(t-1) + M_2(t)u(t-2) + M_3(t)u(t-3) + \dots \\ &= \sum_{j=0}^{\infty} M_j(t)u(t-j) \end{aligned} \tag{5.4}$$

The matrix coefficients $M_i(t), i = 0, 1, 2, \dots$, are periodic functions of period T, known as *periodic Markov coefficients*. These Markov parameters are linked to the impulse response of the system in a way that can be easily assessed by making reference to the simple case where the input is a scalar variable ($m = 1$). Indeed, denoting by $\delta(t)$ the impulse function, i.e.,

$$\delta(t) = \begin{cases} 1 & t = 0 \\ 0 & \text{otherwise} \end{cases} \tag{5.5}$$

and by $y_{imp}^{(i)}(t)$ the response of the system at the impulsive input $u(t) = \delta(t - i)$ it follows from Eq. (5.4) that

$$y_{imp}^{(i)}(t) = M_{t-1}(t) \tag{5.6}$$

In the general multi-input case, the j-th column of the Markov coefficients $M_{t-1}(t)$ represents the output response of the system to an impulse applied at time i to the j-th component of the unit vector.

The periodicity of the Markov coefficients entails that the output response of the system at a generic time instant $t = kT + s$, where s is an integer such that $0 \leq s \leq T - 1$, can be written as a finite sum of the output responses of T time invariant systems indexed in the integer s. As a matter of fact, consider again Eq. (5.4), and evaluate $y(t)$ at the instant $t = kT + s$. We have

$$y(t) = \sum_{j=0}^{\infty} M_j(t)u(t-j) \quad \rightarrow \quad y(kT+s) = \sum_{j=0}^{\infty} M_j(kT+s)u(kT+s-j) \tag{5.7}$$

Focus now on the summation in Eq. (5.7). The summation index j counts the sample points as time progresses. The index j can be rewritten in terms of the period T as $j = \ell T + i$,

where ℓ counts the number of periods, and i is the sample point within the period. For example, assume that a period is composed of $T = 10$ time points. Then $j = 22$ can be seen as either the 22nd time point overall, or the second point of the third period, i.e., $22 = 2$ (number of periods) $\cdot$ 10 (length of one period) + 2 (2nd point in the period), and therefore $\ell = 2, T = 10$, and $i = 2$. With this in mind, one can replace j with $\ell T + i$ in Eq. (5.7), and replace the summation over j with a double summation over the number of points in one period and over the number of periods, i.e.,

$$\sum_{j=0}^{\infty} = \sum_{i=0}^{T-1} \sum_{\ell=0}^{\infty} \tag{5.8}$$

Making these substitutions in Eq. (5.7) one obtains

$$\begin{aligned}
y(kT+s) &= \sum_{j=0}^{\infty} M_j(kT+s)u(kT+s-j) \\
&= \sum_{i=0}^{T-1}\sum_{\ell=0}^{\infty} M_{i+\ell T}(kT+s)\; u[kT+s-(i+\ell T)] \\
&= \sum_{i=0}^{T-1}\sum_{\ell=0}^{\infty} M_{i+\ell T}(s)\; u[kT+s-(i+\ell T)] \\
&\quad \text{because } M \text{ is periodic, i.e.,} M_{i+\ell T}(kT+s) = M_{i+\ell T}(s) \\
&= \sum_{i=0}^{T-1} \underbrace{\sum_{\ell=0}^{\infty} M_{i+\ell T}(s)\; u[kT+s-i-\ell T)]}_{\stackrel{def}{=}\; \hat{y}_{i,s}(k)}
\end{aligned} \tag{5.9}$$

That is,

$$y(kT+s) = \sum_{i=0}^{T-1} \hat{y}_{i,s}(k) \tag{5.10}$$

and

$$\begin{aligned}
\hat{y}_{i,s}(k) &= \sum_{\ell=0}^{\infty} M_{i+\ell T}(s)\; u[kT+s-i-\ell T)] \\
&= \sum_{\ell=0}^{\infty} M_{i+\ell T}(s)\; u[(k-\ell)T+s-i)]
\end{aligned} \tag{5.11}$$

Now, if we define

$$\hat{u}_{i,s}(k) = u(kT + s - i) \tag{5.12}$$

then

$$\hat{u}_{i,s}(k - \ell) = u[(k - \ell)T + s - i)] \tag{5.13}$$

which appears in Eq. (5.11), which can therefore be rewritten as

$$\hat{y}_{i,s}(k) = \sum_{\ell=0}^{\infty} M_{i+\ell T}(s)\hat{u}_{i,s}(k - \ell) \tag{5.14}$$

From these expressions, it is apparent that $\hat{y}_{i,s}(k)$ is the output of a time-invariant system having $M_i(s), M_{i+T}(s), M_{i+2T}(s), \ldots$, as Markov parameters. Note the role of the different indexes appearing in these expressions: s is the chosen tag time index for the output variable, $s - i$ is the tag time index for the input variable, and k is the sampled time current variable.

Example: Use Eq. (5.9) with $k = 2, T = 4, s = 1$, and $kT + s = 9$.

$$
\begin{aligned}
y(9) &= \sum_{i=0}^{T-1} \sum_{\ell=0}^{\infty} M_{i+\ell T}(s)\, u[kT + s - i - \ell T)] \\
&= \sum_{i=0}^{T-1} \sum_{\ell=0}^{\infty} M_{i+4\ell}(1)\, u(9 - i - \ell T) \\
&= \sum_{i=0}^{3} \Bigg[\underbrace{M_i(1)\, u(9-i)}_{\ell=0} + \underbrace{M_{i+4}(1)\, u(9-i-4)}_{\ell=1} + \\
&\qquad \underbrace{M_{i+8}(1)\, u(9-i-8)}_{\ell=2} + \underbrace{M_{i+12}(1)\, u(9-i-12)}_{\ell=3} + \ldots \Bigg] \\
&= \sum_{i=0}^{3} M_i(1)\, u(9-i) + \sum_{i=0}^{3} M_{i+4}(1)\, u(5-i) + \\
&\qquad \sum_{i=0}^{3} M_{i+8}(1)\, u(1-i) + \sum_{i=0}^{3} M_{i+12}(1)\, u(-3-i) + \ldots \\
&= M_0(1)u(9) + M_1(1)u(8) + M_2(1)u(7) + M_3(1)u(6) + \\
&\quad M_4(1)u(5) + M_5(1)u(4) + M_6(1)u(3) + M_7(1)u(2) + \\
&\quad M_8(1)u(1) + M_9(1)u(0) + M_{10}(1)u(-1) + M_{11}(1)u(-2) + \\
&\quad M_{12}(1)u(-3) + M_{13}(1)u(-4) + M_{14}(1)u(-5) + M_{15}(1)u(-6) + \ldots \\
&= M_0(1)u(9) + M_1(1)u(8) + M_2(1)u(7) + M_3(1)u(6) + \\
&\quad M_4(1)u(5) + M_5(1)u(4) + M_6(1)u(3) + M_7(1)u(2) + \\
&\quad M_8(1)u(1) + M_9(1)u(0) \qquad (5.15)
\end{aligned}
$$

because we assume that the input starts at time $t = 0$, and therefore $u(t) = 0$ for $t < 0$. Compare Eq. (5.15) with the results of using directly Eq. (5.4):

$$
\begin{aligned}
y(t) &= \sum_{j=0}^{\infty} M_j(t) u(t-j) \\
&= M_0(1)u(9) + M_1(1)u(8) + M_2(1)u(7) + M_3(1)u(6) + M_4(1)u(5) + \\
&\quad M_5(1)u(4) + M_6(1)u(3) + M_7(1)u(2) + M_8(1)u(1) + M_9(1)u(0) \qquad (5.16)
\end{aligned}
$$

The two results are identical (this concludes the example).

For each $i = 0, 1, 2, \ldots, T-1$, (i.e., for each time point in the period T for the input), and each $s = 0, 1, 2, \ldots, T-1$, (i.e., for each time point in the period T for the output), one can define

$$\begin{aligned} H_i(z,s) &\stackrel{def}{=} \sum_{\ell=0}^{\infty} M_{\ell T+i}(s) z^{-\ell} && (5.17)\\ &= M_i(s) + M_{i+T}(s) z^{-1} + M_{i+2T}(s) z^{-2} + \ldots && (5.18)\\ &= M_i(s) + \frac{M_{i+T}(s)}{z} + \frac{M_{i+2T}(s)}{z^2} + \ldots && (5.19) \end{aligned}$$

This is the transfer function from the input $\hat{u}_{i,s}(k)$ to the output $\hat{y}_{i,s}(k)$ (both signals seen as functions of k). To see this, start by rewriting Eq. (5.14)

$$\begin{aligned} \hat{y}_{i,s}(k) &= \sum_{\ell=0}^{\infty} M_{i+\ell T}(s) \hat{u}_{i,s}(k-\ell) && \text{Eq. (5.14) repeated}\\ &= M_i(s)\hat{u}_{i,s}(k) + M_{i+T}(s)\hat{u}_{i,s}(k-1) + M_{i+2T}(s)\hat{u}_{i,s}(k-2) + \ldots && (5.20) \end{aligned}$$

From the basic properties of the z-transform we have

$$\begin{aligned} \hat{u}_{i,s}(k-1) &= z^{-1}\hat{u}_{i,s}(k) && (5.21)\\ \hat{u}_{i,s}(k-2) &= z^{-2}\hat{u}_{i,s}(k) && (5.22) \end{aligned}$$

$$\ldots$$

Substituting into Eq. (5.20) we have

$$\begin{aligned} \hat{y}_{i,s}(k) &= M_i(s)\hat{u}_{i,s}(k) + M_{i+T}(s)\hat{u}_{i,s}(k-1) + M_{i+2T}(s)\hat{u}_{i,s}(k-2) + \ldots\\ &= M_i(s)\hat{u}_{i,s}(k) + M_{i+T}(s)z^{-1}\hat{u}_{i,s}(k) + M_{i+2T}(s)z^{-2}\hat{u}_{i,s}(k) + \ldots\\ &= \underbrace{\left[M_i(s) + M_{i+T}(s)z^{-1} + M_{i+2T}(s)z^{-2} + \ldots\right]}_{\stackrel{def}{=} H_i(z,s) \text{ (see Eq. (5.18))}} \hat{u}_{i,s}(k)\\ &= H_i(z,s)\hat{u}_{i,s}(k) && (5.23) \end{aligned}$$

which confirms that $H_i(z,s)$ is the transfer function $\hat{u}_{i,s}(k)$ to $\hat{y}_{i,s}(k)$. By using z as the one-shift ahead operator in time k (namely, the T-shift operator in time t), and resorting to

a mixed z/k notation, one can connect the outputs $y(t)$ to the inputs $u(t)$ directly, without going through the intermediate quantities $\hat{y}(t)$ and $\hat{u}(t)$. To see this, begin by rewriting Eq. (5.10)

$$y(kT+s) = \sum_{i=0}^{T-1} \hat{y}_{i,s}(k) \qquad \text{Eq. (5.10) repeated}$$

expand the summation

$$= \hat{y}_{0,s}(k) + \hat{y}_{1,s}(k) + \hat{y}_{2,s}(k) + \ldots + \hat{y}_{T-1,s}(k)$$

use Eq. (5.23)

$$= H_0(z,s)\hat{u}_{0,s}(k) + H_1(z,s)\hat{u}_{1,s}(k) + \\ + H_2(z,s)\hat{u}_{2,s}(k) + \ldots + H_{T-1}(z,s)\hat{u}_{T-1,s}(k) \qquad (5.24)$$

Now recall that it was

$$\hat{u}_{i,s}(k) = u(kT+s-i) \qquad \text{Eq. (5.12) repeated}$$

from which

$$\begin{aligned} \hat{u}_{0,s}(k) &= u(kT+s) \\ \hat{u}_{1,s}(k) &= u(kT+s-1) \\ \hat{u}_{2,s}(k) &= u(kT+s-2) \\ &\vdots \\ \hat{u}_{T-1,s}(k) &= u(kT+s-(T-1)) \end{aligned}$$

Substitute into Eq. (5.24) to get

$$y(kT+s) = H_0(z,s)u(kT+s) + H_1(z,s)u(kT+s-1) + \\ + H_2(z,s)u(kT+s-2) + \ldots + H_{T-1}(z,s)u(kT+s-T+1) \quad (5.25)$$

but we would like to define $y(kT+s)$ in terms of

$$u(kT+s),\ u(kT+s+1),\ u(kT+s+2), \ldots,\ u(kT+s+T-1)$$

so we can then write input-output relations at the same time points, therefore we need to transform the terms $u(kT + s \underline{-} i)$ into $u(kT + s \underline{+} i)$. To do this, start by writing Eq. (5.25) in a different order

$$
\begin{array}{cc}
 & \text{Eq. (5.25)} \\
y(kT+s) & = H_0(z,s)u(kT+s)+ \\
 & +H_1(z,s)u(kT+s-1) \\
 & +H_2(z,s)u(kT+s-2) \\
 & \vdots \\
 & +H_{T-2}(z,s)u(kT+s-T+2) \\
 & +H_{T-2}(z,s)u(kT+s-T+1)
\end{array}
\qquad
\begin{array}{c}
\text{Eq. (5.25) rearranged} \\
 \\
+H_{T-1}(z,s)u(kT+s-T+1) \\
+H_{T-2}(z,s)u(kT+s-T+2) \\
\vdots \\
+H_2(z,s)u(kT+s-2) \\
+H_1(z,s)u(kT+s-1) \\
+H_0(z,s)u(kT+s)
\end{array}
$$

Then use the one-shift ahead operator in time z, $u(s-T) = z^{-1}u(s)$:

$$
\begin{array}{ccccc}
u(kT+s-(T-1)) & \rightarrow & u(kT+s+1-T) & = z^{-1}u(kT+s+1) \\
u(kT+s-(T-2)) & \rightarrow & u(kT+s+2-T) & = z^{-1}u(kT+s+2) \\
\vdots & & \vdots & \vdots \\
u(kT+s-(2)) & \rightarrow & u(kT+s-2) & = z^{-1}u(kT+s-2+T) \\
u(kT+s-(1)) & \rightarrow & u(kT+s-1) & = z^{-1}u(kT+s-1+T)
\end{array}
$$

and rewrite Eq. (5.25) rearranged

$$
\begin{aligned}
y(kT+s) \;=\; & H_0(z,s)u(kT+s)+ \\
& +H_{T-1}(z,s)z^{-1}u(kT+s+1) \\
& +H_{T-2}(z,s)z^{-1}u(kT+s+2) \\
& \cdots \\
& +H_2(z,s)z^{-1}u(kT+s+T-2) \\
& +H_1(z,s)z^{-1}u(kT+s+T-1)
\end{aligned}
\tag{5.26}
$$

The transfer function $H_i(z,s)$ will be referred to as the *sampled transfer function* at tag time s with input-output delay i.

The input-output periodic model is said to be *rational* if all transfer functions (5.17) are indeed rational, i.e., they are transfer functions of finite-dimensional (time-invariant)

systems. In this case, the periodic system can be given a state-space finite-dimensional realization, as shown in Ref. [13]. The problem of finding a minimal periodic realization in the form of difference equation is investigated in Refs. [3] and [26].

Introduce now the unit delay operator $\sigma(\cdot)$, which moves forward a signal by one step, i.e.,

$$\sigma u(t) = u(t+1) \qquad \sigma^{-1}u(t) = u(t-1) \qquad \sigma^{-k}u(t) = u(t-k) \tag{5.27}$$

Using $\sigma(\cdot)$, Eq. (5.4) can be given a compact form:

$$\begin{aligned}
y(t) &= M_0(t)u(t) + M_1(t)u(t-1) + M_2(t)u(t-2) + M_3(t)u(t-3) + \dots && \text{Eq. (5.4)} \\
&= M_0(t)u(t) + M_1(t)\sigma^{-1}u(t) + M_2(t)\sigma^{-2}u(t) + M_3(t)\sigma^{-3}u(t) + \dots \\
&= \underbrace{\left[M_0(t) + M_1(t)\sigma^{-1}(\cdot) + M_2(t)\sigma^{-2}(\cdot) + M_3(t)\sigma^{-3}(\cdot) + \dots\right]}_{\stackrel{def}{=}\ G(\sigma,\cdot)|_t} u(t) && (5.28) \\
&= G(\sigma,\cdot)|_t\, u(t) && (5.29)
\end{aligned}$$

where

$$G(\sigma,\cdot)|_t = M_0(t) + M_1(t)\sigma^{-1}(\cdot) + M_2(t)\sigma^{-2}(\cdot) + M_3(t)\sigma^{-3}(\cdot) + \dots \tag{5.30}$$

is the *input-output transfer operator*. The operator $G(\sigma,\cdot)|_t$ is periodic, i.e.,

$$G(\sigma,\cdot)|_{t+T} = G(\sigma,\cdot)|_t \qquad \text{for every } t \tag{5.31}$$

in fact,

$$\begin{aligned}
G(\sigma,\cdot)|_{t+T} &= \left[M_0(t+T) + M_1(t+T)\sigma^{-1}(\cdot) + M_2(t+T)\sigma^{-2}(\cdot) + \dots\right] \\
&= \left[M_0(t) + M_1(t)\sigma^{-1}(\cdot) + M_2(t)\sigma^{-2}(\cdot) + \dots\right] \\
&= G(\sigma,\cdot)|_t
\end{aligned}$$

because the Markov coefficients $M_i(t)$ are periodic. Moreover, $G(\sigma,\cdot)|_t$ enjoys a pseudo-commutative property with respect to the delays. Precisely

$$\sigma^{-k}\, G(\sigma,\cdot)|_t = G(\sigma,\cdot)|_{t-k}\, \sigma^{-k} \qquad \text{for every } t \tag{5.32}$$

To see this, write

$$\begin{aligned}\sigma^{-k}\left[M_0(t)u(t)\right] &= M_0(t-k)u(t-k)\\ &= M_0(t-k)\sigma^{-k}u(t) \qquad (5.33)\end{aligned}$$

$$\begin{aligned}\sigma^{-k}\left[M_1(t)\sigma^{-1}u(t)\right] &= \sigma^{-k}\left[M_1(t)u(t-1)\right]\\ &= M_1(t-k)u(t-1-k)\\ &= M_1(t-k)\sigma^{-k-1}u(t)\\ &= M_1(t-k)\sigma^{-1}\sigma^{-k}u(t) \qquad (5.34)\end{aligned}$$

$$\begin{aligned}\sigma^{-k}\left[M_2(t)\sigma^{-2}u(t)\right] &= \sigma^{-k}\left[M_2(t)u(t-2)\right]\\ &= M_2(t-k)u(t-2-k)\\ &= M_2(t-k)\sigma^{-k-2}u(t)\\ &= M_2(t-k)\sigma^{-2}\sigma^{-k}u(t) \qquad (5.35)\\ &\ldots\end{aligned}$$

Then

$$\begin{aligned}\sigma^{-k}\,G(\sigma,\cdot)\big|_t\,u(t) &= \sigma^{-k}\left[M_0(t)+M_1(t)\sigma^{-1}(\cdot)+M_2(t)\sigma^{-2}(\cdot)+\ldots\right]u(t)\\ &= \left[M_0(t-k)+M_1(t-k)\sigma^{-1}+M_2(t-k)\sigma^{-2}+\ldots\right]\sigma^{-k}u(t)\\ &= G(\sigma,\cdot)\big|_{t-k}\,\sigma^{-k}u(t)\end{aligned}$$

which implies

$$\sigma^{-k}\,G(\sigma,\cdot)\big|_t = G(\sigma,\cdot)\big|_{t-k}\,\sigma^{-k}$$

Because of this property, one can rewrite Eq. (5.30) as

$$\begin{aligned} G(\sigma,\cdot)|_t &= M_0(t) + M_1(t)\sigma^{-1}(\cdot) + M_2(t)\sigma^{-2}(\cdot) + M_3(t)\sigma^{-3}(\cdot) + \ldots \qquad \text{Eq. (5.30) repeated} \\ &= M_0(t) + \sigma^{-1}M_1(t+1)(\cdot) + \sigma^{-2}M_2(t+2)(\cdot) + \sigma^{-3}M_3(t+3)(\cdot) + \ldots \qquad (5.36) \end{aligned}$$

Hence, the operators σ^{-k} and $G(\sigma,\cdot)$ do commute if and only if the integer K is multiple of the period T.

If the transfer operator is evaluated in a specific time-point, say t, it results in a transfer function, henceforth denoted by $G(\sigma,t)$. In view of Eq. (5.17), such transfer function can be written as

$$G(\sigma,t) = \sum_{k=0}^{\infty} M_k(t)\sigma^{-k} = \sum_{i=0}^{T-1} H_i\left(\sigma^T,t\right)\sigma^{-i} \qquad (5.37)$$

In fact,

$$\begin{aligned} G(\sigma,t) &= \sum_{k=0}^{\infty} M_k(t)\sigma^{-k} \\ &\quad \text{rewrite } k \text{ as } jT+i \\ &= \sum_{i=0}^{T-1}\sum_{j=0}^{\infty} M_{jT+i}(t)\sigma^{jT+i} = \sum_{i=0}^{T-1}\sum_{j=0}^{\infty} M_{jT+i}(t)\left(\sigma^T\right)^{-j}\sigma^{-i} \\ &\quad \text{rewrite } t \text{ as } kT+s \\ &= \sum_{i=0}^{T-1}\sum_{j=0}^{\infty} M_{jT+i}(kT+s)\left(\sigma^T\right)^{-j}\sigma^{-i} \\ &\quad \text{but because } M \text{ is periodic, } M_{jT+i}(kT+s) = M_{jT+i}(s), \text{ and therefore} \\ &= \sum_{i=0}^{T-1}\sum_{j=0}^{\infty} M_{jT+i}(s)\left(\sigma^T\right)^{-j}\sigma^{-i} \\ &\quad \text{finally, use the definition, Eq. (5.17), } H_i(z,s) = \textstyle\sum_{j=0}^{\infty} M_{jT+i}(s)z^{-j}, \text{ with } z=\sigma^T \\ &= \sum_{i=0}^{T-1} H_i(\sigma^T,t)\sigma^{-i} \qquad (5.38) \end{aligned}$$

which is the right-hand-side of Eq. (5.37). Also note that σ generates a shift of one time step, whereas z generates a shift of one period. Therefore, if the period is composed of T time steps, to make one shift of Z it takes T shifts of σ, i.e., $z=\sigma^T$.

We now introduce the symbol ϕ which will be often used in the chapter:

$$\phi = \exp\left(\frac{2\pi i}{T}\right) = \cos\left(\frac{2\pi}{T}\right) + i\sin\left(\frac{2\pi}{T}\right) \tag{5.39}$$

Hence $1, \phi, \phi^2, \ldots, \phi^{T-1}$ are the T-roots of the unit. Note that

$$\frac{1}{T}\sum_{k=0}^{T-1}\phi^{sk} = \begin{cases} 1 & s = 0, \pm T, \pm 2T, \ldots \\ 0 & \text{otherwise} \end{cases} \tag{5.40}$$

Then, it is easy to see that one can recover the sampled transfer functions $H_i\left(\sigma^T, t\right)$ from a single transfer function $G(\sigma, t)$ as follows:

$$H_i\left(\sigma^T, t\right) = \frac{1}{T}\left[\sum_{k=0}^{T-1} G(\sigma\phi^k, t)\phi^{ki}\right]\sigma^i \tag{5.41}$$

5.2 Time-lifted reformulation

In this section we introduce the most classical time-invariant reformulation, namely the lifted reformulation. The simplest way to explain the idea of lifting is to make reference to a (discrete-time) signal, say $v(\cdot)$. Associated with $v(\cdot)$ one can introduce the augmented signal

$$v_\tau(k) = \begin{bmatrix} v(kT+\tau) \\ v(kT+\tau+1) \\ v(kT+\tau+2) \\ \vdots \\ v(kT+\tau+T-2) \\ v(kT+\tau+T-1) \end{bmatrix} \tag{5.42}$$

where τ is a tag point, arbitrarily chosen. We will also use the symbol $v^{(i)}(k)$ for the components of vector $v_\tau(k)$, i.e.,

$$v^{(i)}(k) = v(kT+\tau+i-1) \qquad i = 1, 2, \ldots, T \tag{5.43}$$

Note that $v^{(i)}(k)$ can itself be a vector. As apparent, $v_\tau(k)$ is constituted by the samples of the original signal over the interval $[\tau, \tau+T-1]$, T being any positive integer. For a proper

comprehension of the way in which signal lifting reflects into the input/output representation of a system, we start with by considering the effect of sampling in the z-domain. Then, we will pass to analyzing the action of lifting on time-invariant and T-periodic systems, both in state-space and input/output forms.

5.2.1 Sampling in the z-domain

Again, consider a discrete-time signal $v(\cdot)$, whose z-transform is given by the celebrated formula (written in terms of σ instead of z, and t instead of k, as more typically done)

$$V(\sigma) = \sum_{t=0}^{\infty} v(t)\sigma^{-t} \tag{5.44}$$

Hence, the z-transform of the periodically sampled signal

$$v^{(i)}(k) = v(kT + i - 1) \qquad i = 1, 2, \dots, T \tag{5.45}$$

is given by

$$V^{(i)}(z) = \sum_{k=0}^{\infty} v(kT + i - 1)z^{-k} \tag{5.46}$$

As can be seen in the expressions above, we use different symbols for the complex variables entering the z-transforms: σ for time t and z for the sampled time k. In fact, we are using two different time scales, shown in Fig. 5.1. In the discrete time scale t there are T samples for each sample of the time scale k. In other words, k indicates the number of periods, and t the number of samples, with T samples per period, i.e., $t = Tk$. The operator σ advances t by one, while the operator z advances k by one. Because it takes T shifts σ of time t to make one shift z of period k, we have $z = \sigma^T$.

Now denote by $\delta(t)$ the Kronecker symbol, i.e., $\delta(0) = 1$, and $\delta(t) = 0$ for $t \neq 0$. With this symbol we can write

$$v(q) = \sum_{t=0}^{\infty} v(t)\delta(t - q) \tag{5.47}$$

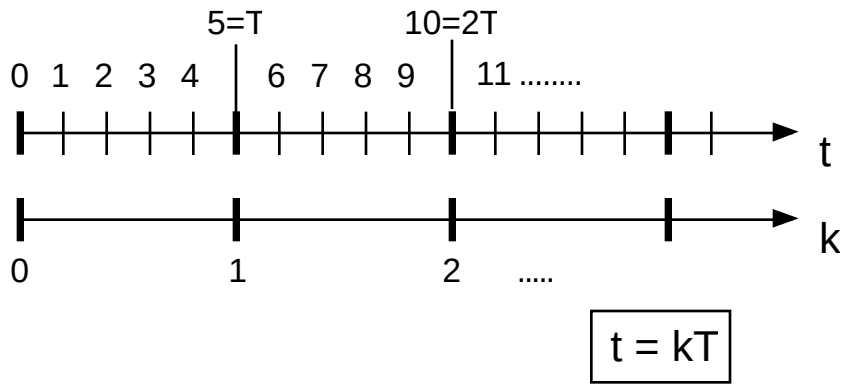

Figure 5.1: Time scales used in lifted-time reformulation; period T is equal to 5.

because the only nonzero term in the summation will be that for $t = q$, because only for that value of t will $\delta(t-q)$ be equal to 1. Similarly

$$v(q)\sigma^{-q} = \sum_{t=0}^{\infty} v(t)\sigma^{-t}\delta(t-q) \tag{5.48}$$

and if we let $q = kT + i - 1$

$$v(kT+i-1)\sigma^{-(kT+i-1)} = \sum_{t=0}^{\infty} v(t)\sigma^{-t}\delta[t-(kT+i-1)] \tag{5.49}$$

or, multiplying both sides by σ^{i-1}

$$v(kT+i-1)\sigma^{-kT} = \sum_{t=0}^{\infty} v(t)\sigma^{-t}\delta(t-kT-i+1)\sigma^{i-1} \tag{5.50}$$

Evaluating Eq. (5.46) in $z = \sigma^T$ it can be seen that

$$\begin{aligned} V^{(i)}(\sigma^T) &= \sum_{k=0}^{\infty} v(kT+i-1)\sigma^{-kT} \\ &\text{using Eq. (5.50)} \\ &= \sum_{k=0}^{\infty}\sum_{t=0}^{\infty} v(t)\sigma^{-t}\delta(t-kT-i+1)\sigma^{i-1} \\ &= \left[\sum_{k=0}^{\infty}\sum_{t=0}^{\infty} v(t)\sigma^{-t}\delta(t-kT-i+1)\right]\sigma^{i-1} \\ &\text{rearrange some terms inside the square brackets} \\ &= \left[\sum_{t=0}^{\infty} v(t) \underbrace{\sum_{k=0}^{\infty}\delta(t-kT-i+1)}_{\stackrel{def}{=} f_i(t)}\sigma^{-t}\right]\sigma^{i-1} \\ &= \left[\sum_{t=0}^{\infty} v(t) f_i(t)\sigma^{-t}\right]\sigma^{i-1} \end{aligned} \tag{5.51}$$

where

$$f_i(t) = \sum_{k=0}^{\infty}\delta(t-kT-i+1) \tag{5.52}$$

is a T periodic sequence of discrete pulses. Inside the parenthesis,

t	is the independent variable (will change with outer summation index)
kT	changes with the summation index
i	changes with the specific choice of $f_i(t)$

Now, recall definition (5.39) of the T-roots of the unit

$$\phi = \exp\left(\frac{2\pi i}{T}\right) = \cos\left(\frac{2\pi}{T}\right) + i\sin\left(\frac{2\pi}{T}\right) \qquad \text{(5.39) repeated}$$

and the associated property (5.40)

$$\frac{1}{T}\sum_{k=0}^{T-1}\phi^{sk} = \begin{cases} 1 & s = 0, \pm T, \pm 2T, \ldots \\ 0 & \text{otherwise} \end{cases} \qquad \text{(5.40) repeated}$$

which we can rewrite, with $s = i - 1 - t$

$$\frac{1}{T}\sum_{k=0}^{T-1}\phi^{k(i-1-t)} = \begin{cases} 1 & i-1-t = 0, \pm T, \pm 2T, \ldots \\ 0 & \text{otherwise} \end{cases} \tag{5.53}$$

Consider the conditions under which the summation is equal to zero:

$$\begin{cases} i-1-t &= 0 \\ i-1-t &= \pm T \\ i-1-t &= \pm 2T \\ & \vdots \end{cases} \quad \text{which imply} \quad \begin{cases} i-1-t &= 0 \\ i-1-t \pm T &= 0 \\ i-1-t \pm 2T &= 0 \\ & \vdots \end{cases} \tag{5.54}$$

and, multiplying by -1

$$\begin{cases} t-i+1 &= 0 \\ t \mp T - i + 1 &= 0 \\ t \mp 2T - i + 1 &= 0 \\ & \vdots \end{cases} \tag{5.55}$$

Comparing these conditions with those under which the summation inside Eq. (5.52) is equal to zero, it can be observed that they are the same, and therefore we can write

$$f_i(t) = \frac{1}{T}\sum_{k=0}^{T-1}\phi^{k(i-1-t)} \tag{5.56}$$

Note in passing that this expression is just the Fourier sum of the periodic function $f_i(t)$. Now rewrite Eqs. (5.51) and (5.52):

$$V^{(i)}(\sigma^T) = \left[\sum_{t=0}^{\infty} v(t) f_i(t) \sigma^{-t}\right] \sigma^{i-1} \qquad \text{(5.51) repeated}$$

$$f_i(t) = \sum_{k=0}^{\infty} \delta(t - kT - i + 1) \qquad \text{(5.52) repeated}$$

Use Eq. (5.56) for the underlined portion

$$\begin{aligned} V^{(i)}(\sigma^T) &= \left[\sum_{t=0}^{\infty} v(t)\underline{f_i(t)}\sigma^{-t}\right]\sigma^{i-1} \\ &= \left[\sum_{t=0}^{\infty} v(t)\cdot\frac{1}{T}\sum_{k=0}^{T-1}\phi^{k(i-1-t)}\cdot\sigma^{-t}\right]\sigma^{i-1} \end{aligned}$$

rearrange:

$$= \frac{1}{T}\left[\sum_{t=0}^{\infty} v(t)\sigma^{-t}\cdot\sum_{k=0}^{T-1}\phi^{k(i-1)}\phi^{-kt}\right]\sigma^{i-1}$$

rearrange again:

$$\begin{aligned} &= \frac{1}{T}\left[\sum_{k=0}^{T-1}\phi^{k(i-1)}\sum_{t=0}^{\infty} v(t)\left(\sigma\phi^k\right)^{-t}\right]\sigma^{i-1} \\ &= \frac{1}{T}\left[\sum_{k=0}^{T-1} V(\sigma\phi^k)\phi^{k(i-1)}\right]\sigma^{i-1} \end{aligned} \tag{5.57}$$

To understand the final step leading to Eq. (5.57), rewrite Eq. (5.44):

$$V(\sigma) = \sum_{t=0}^{\infty} v(t)\sigma^{-t} \qquad \text{(5.44) repeated}$$

and make the substitution $\sigma \leftrightarrow \sigma\phi^k$:

$$V(\sigma\phi^k) = \sum_{t=0}^{\infty} v(t)(\sigma\phi^k)^{-t}$$

Conversely, the z-transform $V(\sigma)$ of the original signal $v(t)$ can be recovered from the z-transform $V^(i)(z)$ of the sampled signals $v(kT+i)$. To see this, start from Eq. (5.44):

$$V(\sigma) = \sum_{t=0}^{\infty} v(t)\sigma^{-t} \qquad \text{(5.44) repeated}$$

rewrite t as $t = iT + k$ (where i counts the number of periods and k counts the sample points

within one period)

$$= \sum_{i=0}^{\infty} \sum_{k=0}^{T-1} v(iT+k)\sigma^{-(iT+k)}$$

rearrange:

$$= \sum_{k=0}^{T-1} \sigma^{-k} \sum_{i=0}^{\infty} v(iT+k)\sigma^{-(iT)}$$

add one to k:

$$= \sum_{k=1}^{T} \sigma^{-k+1} \sum_{i=0}^{\infty} v(iT+k+1)\sigma^{-(iT)} \tag{5.58}$$

For the next step in the derivation of $V(\sigma)$, first rewrite Eq. (5.46):

$$V^{(i)}(z) = \sum_{k=0}^{\infty} v(kT+i-1)z^{-k} \qquad \text{(5.46) repeated}$$

change notation $k \leftrightarrow i$:

$$V^{(i)}(z) = \sum_{i=0}^{\infty} v(iT+k-1)z^{-i}$$

change notation again $z \leftrightarrow \sigma^T$:

$$V^{(k)}(\sigma^T) = \sum_{i=0}^{\infty} v(iT+k-1)\sigma^{-iT}$$

which can be substituted into Eq. (5.58) to get the converse relation

$$V(\sigma) = \sum_{k=1}^{T} V^{(k)}(\sigma^T)\sigma^{-k+1} \tag{5.59}$$

Chapter 6

Constant-Coefficient Representations of Periodic-Coefficient Discrete Linear Systems

6.1 Introduction

Various types of active control of a helicopter rotor have been proposed as a means to reduce vibration and noise, and to improve performance. Very popular schemes are known as Higher Harmonic Control (HHC) and Individual Blade Control (IBC), typically defined as active controls implemented in the fixed system and in the rotating system, respectively. Extensive theoretical and experimental research has been performed on HHC and IBC for nearly three decades, and the first implementations on production aircraft are currently being considered.

Typical HHC/IBC implementations are based on frequency domain update formulas of the general type

$$Z_{n+1} = Z_n + T_n \Delta\theta_n \tag{6.1}$$

where Z and $\Delta\theta$ contain harmonics of outputs (usually a vector of hub load components) and inputs (a vector of HHC/IBC inputs), T is a transfer (or gain) matrix of suitable dimensions, which depends on the frequency response of the helicopter, and n is an index denoting the rotor revolution. Both the stability of the update formula of Eq. (6.1), and the effects on rotor vibrations, required power, and noise, have been studied extensively.

Although in steady state conditions they only apply harmonic input signals to the rotor, HHC and IBC are closed-loop dynamic control systems that act by modifying the rotor dynamics, so it is very important that they do not affect negatively the aeromechanical stability

of the helicopter. As for every active rotor control system, the potential for aeroservoelastic instabilities exists, especially for hingeless and bearingless rotor configurations, which typically have lowly damped rotor inplane modes or coupled rotor-fuselage modes.

However, until very recently, essentially no methodology existed in the published literature to study the coupled rotor-fuselage stability of a helicopter with an HHC or IBC system turned on, and no quantitative results were available. One probable contributing factor is that Eq. (6.1) does not readily lend itself to a state-space continuous representation that, when coupled to linearized models of rotor-fuselage dynamics, could provide closed-loop stability information in the form of stability eigenvalues or Floquet characteristic exponents. In fact, a state-space representation requires that it be possible to describe the entire dynamics of the system from a snapshot at any instant in time, and there are at least two aspects of Eq. (6.1) that appear to violate this requirement. Firstly, the extraction of the harmonics in Z requires a harmonic analysis, which cannot be carried out at a single instant in time, but requires a time *interval*, of at least one cycle. Secondly, Eq. (6.1) describes an update at discrete intervals in time.

The situation has been partially remedied by Refs. [9] and [28]. In both studies, the basic approach was to convert the discrete components of the model to continuous, or to neglect their discrete nature altogether. While this approach represents a very useful first step, the system described by Eq. (6.1) is discrete and should rigorously be treated as such.

A key ingredient of a *discrete* stability and response analysis is the reformulation of a discrete linear system with periodic coefficients into an equivalent one with constant coefficients. Therefore, the main objective of this chapter is to present four techniques to achieve this goal, namely: (i) time-lifted, (ii) cyclic, (iii) frequency-lifted, and (iv) Fourier reformulations. The theoretical development of these techniques is discussed in detail in Ref. [4]. This chapter summarizes the results of Ref. [4] of potential interest for the helicopter dynamics community, and presents the application of technique (i) to a simple example, i.e.,

the one-DOF flapping equation for an isolated, rigid, articulated rotor blade in a rotating coordinate system.

6.2 Discrete formulation of the blade flapping equation

The example that will be used in this chapter is the rigid flapping equation of motion of an isolated rotor blade hinged at the axis of rotation (see, for example, Ref.[24]):

$$\begin{aligned} \ddot{\beta} \;+\; & \frac{\gamma}{8}\left(1+\frac{4}{3}\mu\sin\psi\right)\dot{\beta}+\left[1+\frac{\gamma}{8}\left(\frac{4}{3}\mu\cos\psi+\mu^2\sin 2\psi\right)\right]\beta = \\ & = \frac{\gamma}{8}\left[\left(1+\frac{8}{3}\mu\sin\psi+2\mu^2\sin^2\psi\right)\theta(\psi)\right]-\frac{\gamma}{8}\left(\frac{4}{3}+2\mu\sin\psi\right)\lambda \end{aligned} \tag{6.2}$$

which can be rewritten in first-order form as:

$$\begin{cases} \dot{\mathbf{x}} &= A_c(\psi)\mathbf{x}+B_c(\psi)\mathbf{u} \\ \\ \mathbf{y} &= C_c(\psi)\mathbf{x}+D_c(\psi)\mathbf{u} \end{cases} \tag{6.3}$$

where $\mathbf{x}$ and $\mathbf{u}$ are, respectively, the state and control vector, defined as

$$\mathbf{x}=\begin{Bmatrix} \beta \\ \dot{\beta} \end{Bmatrix} \qquad \mathbf{u}=\begin{Bmatrix} \theta_0 \\ \theta 1c \\ \theta_{1s} \end{Bmatrix} \tag{6.4}$$

and the output vector $\mathbf{y}$ is chosen to be equal to $\mathbf{x}$. The system matrices are:

$$A_c(\psi) = \begin{bmatrix} 0 & 1 \\ A_{21}(\psi) & A_{22}(\psi) \end{bmatrix} \tag{6.5}$$

$$B_c(\psi) = \begin{bmatrix} 0 & 0 & 0 \\ f(\psi) & f(\psi)\cos\psi\, f & (\psi)\sin\psi \end{bmatrix} \tag{6.6}$$

$$C_c(\psi) = \begin{bmatrix} 1 & 0 \\ 0 & 1 \end{bmatrix} \tag{6.7}$$

$$D_c(\psi) = \begin{bmatrix} 0 & 0 & 0 \\ 0 & 0 & 0 \end{bmatrix} \tag{6.8}$$

with

$$f(\psi)=\frac{\gamma}{8}\left(1+\frac{8}{3}\mu\sin\psi+2\mu^2\sin^2\psi\right)$$

and

$$\begin{aligned} A_{21}(\psi) &= -\left[1+\frac{\gamma}{8}\left(\frac{4}{3}\mu\cos\psi+\mu^2\sin 2\psi\right)\right] \\ A_{22}(\psi) &= -\frac{\gamma}{8}\left(1+\frac{4}{3}\mu\sin\psi\right) \end{aligned}$$

Because of the simplicity of the flapping equation, all the system matrices above could be easily obtained by inspection. For more sophisticated mathematical models the matrices would typically be obtained numerically, by perturbing the governing equations about a steady-state equilibrium position.

In a discrete representation, the system is defined at discrete time intervals $\psi_k = k\Delta\psi k = 1, 2, \ldots$. The corresponding state-space description is given by

$$\begin{cases} \mathbf{x}(k+1) &= A(k)\mathbf{x}(k)+B(t)\mathbf{u}(k) \\ \mathbf{y}(k) &= C(k)\mathbf{x}(k)+D(k)\mathbf{u}(k) \end{cases} \tag{6.9}$$

where, for example, $\mathbf{x}(k)$ is a short-hand notation for $\mathbf{x}(k\Delta\psi)$. In a periodic system, such as a helicopter rotor blade, all the matrices have a common period equal to T samples, that is, $A(k) = A(k+\ell T)$ with $\ell = 1, 2, 3, \ldots$ Equation (6.9) yields the solution $\mathbf{x}(k+1)$ at time $\psi = (k+1)\Delta\psi$ in terms of the state $\mathbf{x}(k)$ and controls $\mathbf{u}(k)$ at time $\psi = k\Delta\psi$.

The starting point to link the continuous system matrices of Eq. (6.3) to the discrete system matrices of Eq. (6.9) is the continuous time solution formula [34]

$$\mathbf{x}(t) = \Phi_A(t,\tau)\mathbf{x}(\tau) + \int_\tau^t \Phi_A(t,\sigma)B_c(\sigma)\mathbf{u}(\sigma)\,d\sigma \tag{6.10}$$

which gives the solution vector $\mathbf{x}(t)$ starting from the initial time $t = \tau$, with an input vector $\mathbf{u}(t)$ and initial conditions $\mathbf{x}(\tau)$. The matrix $\Phi_A(t,\tau)$ is the state transition matrix of the system. Therefore, the solution $\mathbf{x}(k+1)$ at time $\psi = (k+1)\Delta\psi$, starting from time $\psi = k\Delta\psi$, and assuming that the input vector $\mathbf{u}$ is held constant over that time interval at

a value $\mathbf{u} = \mathbf{u}(k)$, is given by:

$$\begin{aligned}\mathbf{x}[(k+1)\Delta\psi] &= \Phi_A\,[(k+1)\Delta\psi k\ \ \Delta\psi]\,\mathbf{x}(k\Delta\psi) \\ &\quad + \int_{k\Delta\psi}^{(k+1)\Delta\psi} \Phi_A[(k+1)\Delta\psi\sigma\ \ ]B_c(\sigma)\,d\sigma\cdot\mathbf{u}(\sigma) \qquad (6.11)\end{aligned}$$

Comparing Eq. (6.11) and the first row of Eq. (6.9) it can be seen that:

$$A(k) = \Phi_A\,[(k+1)\Delta\psi k\ \ \Delta\psi] \qquad (6.12)$$

$$B(k) = \int_{k\Delta\psi}^{(k+1)\Delta\psi} \Phi_A[(k+1)\Delta\psi\sigma\ \ ]B_c(\sigma)\,d\sigma \qquad (6.13)$$

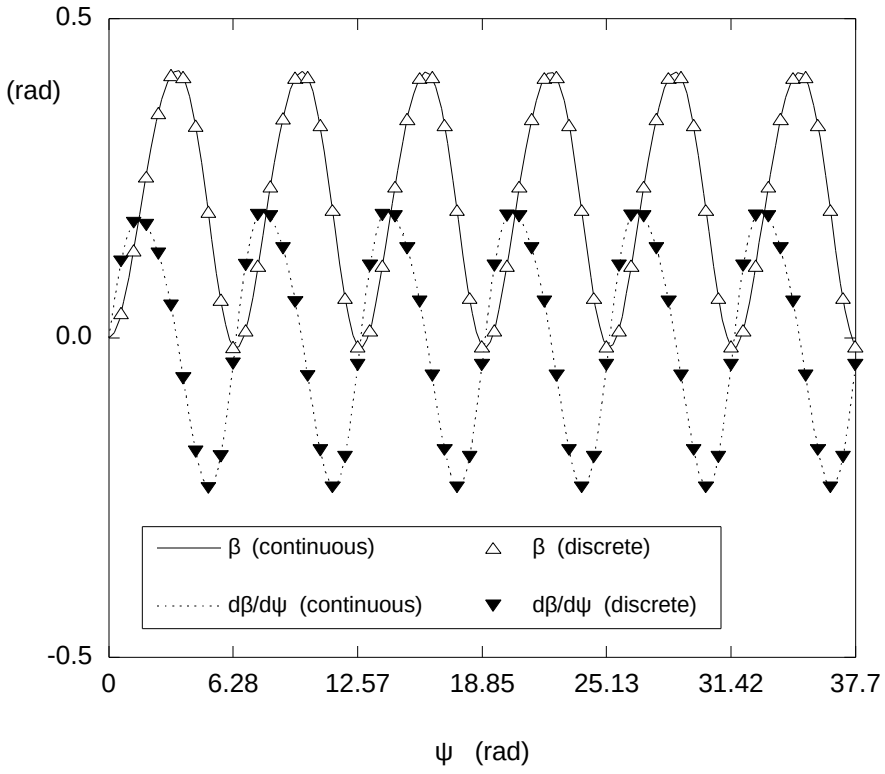

Figure 6.1: Continuous and discrete solutions of flapping equation.

To compute $A(k)$, recall that for the special case $\tau = 0$, the i-th column of $\Phi_A(t,0)$ can be obtained by integrating from τ to t the homogeneous system $\dot{\mathbf{x}} = A_c(\psi)\mathbf{x}$ with an initial condition vector $\mathbf{x}(0)$ equal to zero except for its i-th component which is set to 1.

Therefore, first compute the two transition matrices $\Phi_A[k\Delta\psi\ \ 0]$ and $\Phi_A[(k+1)\Delta\psi\ \ 0]$. Then, the property of transition matrices [34]

$$\Phi(t_2, 0) = \Phi(t_2, t_1)\Phi(t_1, 0) \tag{6.14}$$

can be used to obtain

$$\begin{aligned} \Phi_A\left[(k+1)\Delta\psi k\ \ \Delta\psi\right] &= \Phi_A\left[(k+1)\Delta\psi\ \ 0\right]\Phi_A^{-1}\left[k\Delta\psi\ \ 0\right] \\ &= A(k) \end{aligned} \tag{6.15}$$

The discrete control matrix $B(k)$ can be obtained from Eq. (6.13) numerically using a trapezoidal rule, which gives

$$B(k) \approx \Delta\sigma_i \sum_{i=0}^{m} \alpha_i \Phi_A[(k+1)\Delta\psi\sigma\ \ _i] B_c(\sigma_i) \tag{6.16}$$

where m is the number of intervals in which the sample $\Delta\psi$ has been divided for the purpose of computing the integral, $\Delta\sigma = \Delta\psi m\ \ $, $\sigma_i = k\Delta\psi + i\Delta\sigma$, and $\alpha = 1/2$ if $i = 1$ or $i = m$ and $\alpha = 1$ otherwise. The transition matrix $\Phi_A[(k+1)\Delta\psi\sigma\ \ _i]$ is computed as described in the calculation of $A(k)$, and is therefore given by:

$$\Phi_A[(k+1)\Delta\psi\sigma\ \ _i] = \Phi_A[(k+1)\Delta\psi\ \ 0]\Phi_A^{-1}[\sigma_i, 0] \tag{6.17}$$

The continuous and discrete solutions of the flapping equation for a typical case are shown in Fig. 6.1. The numerical details are provided in the Appendix.

6.3 Transfer Functions

The output $\mathbf{x}(k)$ at a certain time $k\Delta\psi$ of a linear time-periodic system can be written as a linear combination of the past values of the input up to time $k\Delta\psi$:

$$\begin{aligned} \mathbf{x}(k) &= M_0(k)\mathbf{u}(k) + M_1(k)\mathbf{u}(k-1) + M_2(k)\mathbf{u}(k-2) + \ldots \\ &= \sum_{j=0}^{\infty} M_j(k)\mathbf{u}(t-k) \end{aligned} \tag{6.18}$$

The coefficients $M_i(k)$ are periodic matrices with a period equal to T samples, known as *periodic Markov coefficients*. Physically, the j-th column of the Markov coefficient $M_{k-i}(k)$ represents the output response $\mathbf{x}(k)$ of the system to an impulse applied at time $k\Delta\psi$ to the j-th component of the input vector.

Express now the generic time point k in terms of the total number ℓ of elapsed periods (or rotor revolutions), i.e.

$$k = \ell T + s \tag{6.19}$$

For example, if $k = 24$ and a rotor revolution is discretized into $T = 10$ samples, then $\ell = 2$ (two complete revolutions have taken place) and $s = 4$ (this is the fourth sample in the third revolution). With this in mind, it can be shown [4] that the response of a time-periodic system at a generic time instant k can be written as the finite sum of the response of T time-*invariant* systems, indexed in the integer s. Therefore, it is:

$$\mathbf{x}(\ell T + s) = \sum_{i=0}^{T-1} \hat{\mathbf{x}}_{i,s}(\ell) \tag{6.20}$$

where $\hat{\mathbf{x}}_{i,s}(\ell)$ is the output of a time-invariant system having $M_i(s), M_{i+T}(s), M_{i+2T}(s), \ldots$ as Markov parameters. Each of these time-invariant systems is forced only once per period. An important reason why this can be done is the periodicity of the Markov parameters, so that $M_{i+T}(s+T) = M_{i+T}(s), M_{i+2T}(s+2T) = M_{i+2T}(s), \ldots$.

Equation (6.20) expresses the fundamental concept that the response of a system with periodic coefficients can be expressed in terms of the responses of multiple systems with *constant* coefficients. This is the basis for invariant, or constant-coefficient, representations of linear periodic systems.

Introduce now, as usual in the representation of discrete systems, the "one-shift ahead in time" operator z. The shift is of T samples in time, not just one sample, because we are interested in describing the behavior of each of the constant-coefficient systems in which we

have decomposed the original periodic-coefficient system. In other words, z shifts from a generic sample $\ell T + s$ to $(\ell + 1)T + s$, rather than $\ell T + s + 1$.

We can then define a *sampled transfer function* as:

$$H_i(z, s) \stackrel{def}{=} \sum_{\ell=0}^{\infty} M_{\ell T+i}(s) z^{-\ell} \tag{6.21}$$

and rewrite the system response as:

$$\begin{aligned}
\mathbf{x}(\ell T + s) &= H_0(z, s)\mathbf{u}(\ell T + s) + H_1(z, s)\mathbf{u}(\ell T + s - 1) + \ldots \\
&\quad + H_{T-2}(z, s)\mathbf{u}(\ell T + s - T + 2) + H_{T-1}(z, s)\mathbf{u}(\ell T + s - T + 1) \quad (6.22) \\
&= H_0(z, s)\mathbf{u}(\ell T + s) + H_{T-1}(z, s)z^{-1}\mathbf{u}(\ell T + s + 1) + \ldots \\
&\quad + H_2(z, s)z^{-1}\mathbf{u}(\ell T + s + T - 2) + H_1(z, s)z^{-1}\mathbf{u}(\ell T + s + T - 1) \quad (6.23)
\end{aligned}$$

Note that now the output at a generic time sample $\ell T + s$ is expressed entirely in terms of inputs $\mathbf{u}$ over one period T, written backward, Eq. (6.22), or forward, Eq. (6.23), in time.

The Markov coefficients in Eqs. (6.18) and (6.21) can be expressed in terms of the system matrices:

$$\begin{aligned}
M_0(k) &= D(k) && (6.24) \\
M_1(k) &= C(k)B(k-1) && (6.25) \\
M_2(k) &= C(k)A(k-1)B(k-2) && (6.26) \\
M_3(k) &= C(k)A(k-2)B(k-3) && (6.27) \\
&\ldots
\end{aligned}$$

or, equivalently:

$$\begin{aligned}
M_0(k) &= D(k) && (6.28) \\
M_{\ell T+i} &= C(k)\Psi_A^{\ell}(k)\Phi_A(k, k-i+1)B(k-i) && (6.29)
\end{aligned}$$

Substituting into Eq. (6.21) yields for the transfer functions $H(z,k)$, after some manipulations:

$$H_0(z,k) = D(k) + C(k)\left[zI - \Psi_A(k)\right]^{-1}\Phi_A(k,k-T+1)B(k) \tag{6.30}$$

$$H_i(z,k) = zC(k)\left[zI - \Psi_A(k)\right]^{-1}\Phi_A(k,k-i+1)B(k-i) \qquad i = 1,2,\ldots,T-1 \tag{6.31}$$

Additional details and numerical values for the flapping blade example can be found in the Appendix.

A second type of transfer function is very useful for the construction of time-invariant representations of periodic systems. Using the unit delay operator σ^{-1} (e.g., $\mathbf{u}(k-1) = \sigma^{-1}\mathbf{u}(k)$), Eq. (6.18) can be rewritten as

$$\begin{aligned}\mathbf{x}(k) &= \left[M_0(k) + M_1(k)\sigma^{-1} + M_2(k)\sigma^{-2} + \ldots\right]\mathbf{u}(k) \\ &= G(\sigma,\cdot)|_k\,\mathbf{u}(k)\end{aligned} \tag{6.32}$$

where the *input-output transfer operator* $G(\sigma,\cdot)|_k$ is defined as

$$G(\sigma,\cdot)|_k \stackrel{def}{=} \left[M_0(k) + M_1(k)\sigma^{-1} + M_2(k)\sigma^{-2} + \ldots\right] \tag{6.33}$$

Note that $G(\sigma,\cdot)|_k$ in Eq. (6.32) is an operator on $\mathbf{u}(k)$, not a multiplicative factor for $\mathbf{u}(k)$, i.e., it is a more elaborate way of writing $f(\mathbf{u}(k))$.

If the input-output transfer operator is evaluated in a specific time point, say k, it results in a transfer function, denoted by $G(\sigma,k)$. Because they both describe the same dynamic system, this transfer function is obviously related to the sampled transfer function $H_i(z,s)$, defined in Eq. (6.21). It can be shown [4] that the two transfer functions are related by:

$$G(\sigma,k) = \sum_{i=0}^{T-1} H_i(\sigma^T,k)\sigma^{-i} \tag{6.34}$$

and the inverse relationship

$$H_i(\sigma^T, k) = \frac{1}{T}\left[\sum_{\ell=0}^{T-1} G(\sigma\phi^\ell, k)\phi^{\ell i}\right]\sigma^i \tag{6.35}$$

where $\phi = \exp(2\pi j/T) = \cos(2\pi/T) + j\sin(2\pi/T)$. Note that if the original periodic system is time-invariant, i.e., $T = 1$ and hence $\sigma = z$, then the transfer function $G(\sigma, k)$ is not a function of k and reduces to the transfer function $G(\sigma)$ of the time-invariant system. Additional details and numerical values for the flapping blade example can be found in the Appendix.

6.4 Time-invariant reformulations

6.4.1 Time-lifted reformulation

The operation of "lifting" consists in "packing" the values of a signal over one period into a new enlarged signal. Time-lifting results in a constant coefficient state-space system of the type

$$\mathbf{x}^{(k)}(\ell+1) = F_k\mathbf{x}^{(k)}(\ell) + G_k\mathbf{u}_k(\ell) \tag{6.36}$$

$$\mathbf{y}(\ell) = H_k\mathbf{x}^{(k)}(\ell) + E_k\mathbf{u}_k(\ell) \tag{6.37}$$

where $\mathbf{x}^{(k)}(\ell)$ is a shorthand notation for $\mathbf{x}(\ell T + k)$, with ℓ the number of periods elapsed from time zero, and k the time within the period at which the sample is taken. The vector $\mathbf{u}_k(\ell)$ is the "packed" input vector, defined as:

$$\mathbf{u}_k(\ell) = \begin{bmatrix} \mathbf{u}(\ell T + k) \\ \mathbf{u}(\ell T + k + 1) \\ \mathbf{u}(\ell T + k + 2) \\ \vdots \\ \mathbf{u}(\ell T + k + T - 2) \\ \mathbf{u}(\ell T + k + T - 1) \end{bmatrix} \tag{6.38}$$

The packed output vector $\mathbf{y}_k(\ell)$ is defined in a similar way. Therefore, if the system has n states, m controls, and p outputs, and is sampled T times over one period, the dimensions

of the state matrix F_k, the control matrix G_k, the output matrix H_k, and the feed-through matrix E_k, will be n by n, n by mT, pT by n, and pT by mT, respectively.

The matrices in Eqs. (6.36) and (6.37) are given by [4]:

$$F_k = \Psi_A(k) \tag{6.39}$$

$$G_k = \left[G_{k1} \middle| G_{k2} \middle| \dots \middle| G_{kT} \right] \tag{6.40}$$

with:

$$G_{k1} = \Phi_A(k+T, k+1)B(k)$$

$$G_{k2} = \Phi_A(k+T, k+2)B(k+1)$$

$$G_{kT} = \Phi_A(k+T, k+T)B(k+T-1)$$

$$H_k = \begin{bmatrix} C(k) \\ C(k+1)\Phi_A(k+1,k) \\ \vdots \\ C(k+T-1)\Phi_A(k+T-1,k) \end{bmatrix} \tag{6.41}$$

$$E_k \rightarrow (E_k)_{ij} = \begin{cases} 0 & i < j \\ D(k+i-1) & i = j \\ C(k+i-1)\Phi_A(k+i-1, k+j)\times & \\ \quad \times B(k+j-1) & i > j \end{cases} \tag{6.42}$$

For the derivations of the present chapter it will be $\ell = 0$, i.e., the starting point is the first point of the period. Also, the subscript k will be dropped from all the system matrices.

The time-lifted matrix F is given by Eq. (6.39) as $F = \Psi_A(0)$, where $\Psi_A(0) \stackrel{def}{=} \Phi_A(T, 0)$ is the transition matrix at the end of one period. Therefore, the periodic system will be stable if and only if the time-lifted, constant coefficient system is stable. The time-lifted state matrix F is given by $\Phi_A[10\Delta\psi\ \ 0] = \Phi_A[6.2832, 0]$, in the Appendix.

Note that the open loop stability characteristics of the discrete systems, in both the periodic and the time-lifted formulations, are identical to those of the corresponding continuous system. In fact, the discrete state matrices $A(k)$, and therefore also $\Psi_A(0)$, have been built from the continuous time solution formula, Eq. (6.10). Therefore the transition matrices at the end of one period for the continuous and the discrete systems are identical and identical

are their eigenvalues, which determine the stability levels.

From Eq. (6.40), the time-lifted control matrix G for the flapping blade example is given by:

$$G = \left[G_1 \middle| G_2 \middle| \dots \middle| G_{T-1} \middle| G_T \right] \tag{6.43}$$

with:

$$G_1 = \Phi_A(T,1)B(0)$$

$$G_2 = \Phi_A(T,2)B(1)$$

$$G_{T-1} = \Phi_A(T,T-1)B(T-2)$$

$$G_T = \underbrace{\Phi_A(T,T)}_{=[I]} B(T-1)$$

The control matrices $B(\dots)$ are given in Table in the Appendix. The transition matrices $\Phi_A(T,1)$, $\Phi_A(T,2), \dots$ can be obtained from the transition matrix property, Eq. (6.14) as

follows

$$\begin{aligned}
\Phi_A(T,T) &= [I] \\
\Phi_A(T,T-1) &= A(T-1) \\
\Phi_A(T,T-2) &= \Phi_A(T,T-1)\Phi_A(T-1,T-2) \\
&= \Phi_A(T,T-1)A(T-2) \\
&= A(T-1)A(T-2) \\
\Phi_A(T,T-3) &= \Phi_A(T,T-2)\Phi_A(T-2,T-3) \\
&= \Phi_A(T,T-2)A(T-3) \\
&= A(T-1)A(T-2)A(T-3) \\
&\dots \\
\Phi_A(T,1) &= \Phi_A(T,2)\Phi_A(2,1) \\
&= \Phi_A(T,2)A(1) \\
&= A(T-1)A(T-2)A(T-3) \times \\
&\qquad \dots \times A(2)A(1)
\end{aligned}$$

where the state matrices $A(\dots)$ are given in the Appendix. For the blade flapping equation, which has 2 states and 3 controls, and for a period discretized in $T = 10$ intervals, the time-lifted control matrix G has 2 rows and 30 columns (see the Appendix, Eq. (6.70) for the numeric values of the matrix).

From Eq. (6.41), the time-lifted output matrix H for the flapping blade example is given by:

$$H = \begin{bmatrix} C(0) \\ C(1)\Phi_A(1,0) \\ C(2)\Phi_A(2,0) \\ \vdots \\ C(9)\Phi_A(9,0) \end{bmatrix} = \begin{bmatrix} I \\ \Phi_A(1,0) \\ \Phi_A(2,0) \\ \vdots \\ \Phi_A(9,0) \end{bmatrix} \tag{6.44}$$

because for the blade example all the discrete output matrices $C(k)$ are taken to be equal to the identity matrix. With 2 states and 2 outputs, and for a period discretized in $T = 10$ intervals, the time-lifted output matrix G has 20 rows and 2 columns. The transition matrices $\Phi_A(k, 0)$ and the output matrix H are given in the Appendix.

Finally, from Eq. (6.41), the time-lifted feedthrough matrix E for the flapping blade example is given by:

$$E \to E_{ij} = \begin{cases} 0_{2\times 3} & i < j \\ D(i-1)_{2\times 3} = 0 & i = j \\ C(i-1)\Phi_A(i-1,j)B(j-1) = & \\ \qquad = \Phi_A(i-1,j)B(j-1) & i > j \end{cases} \tag{6.45}$$

because for the blade example all the discrete output matrices $C(k)$ are taken to be equal to the identity matrix and all the $D(k)$ are zero matrices. The transition matrices $\Phi_A(i-1, j)$ are obtained using $\Phi_A(i-1, j) = \Phi_A(i-1, 0)\Phi_A^{-1}(j, 0)$. The notation E_{ij} indicates the i-th 2×3 block rowwise and j-th columnwise of E. With 2 outputs and 3 controls, and for a period discretized in $T = 10$ intervals, the time-lifted feedthrough matrix E has 20 rows and 30 columns. The matrix is given by Eq. (6.72) in the Appendix.

6.4.2 Cycled reformulation

In the time-lifted reformulation shown in the previous section, the state vector remains of its original dimension, i.e., it is not lifted or augmented in any form. In the cycled reformulation, all the state, input, and output vectors are augmented. For a generic signal vector $\mathbf{v}(k)$, which can represent any of those vectors, the operation of "cycling" results in a vector $\hat{\mathbf{v}}_\tau^{(i)}(k)$ defined as [4]:

$$\hat{\mathbf{v}}_\tau^{(i)}(k) = \begin{cases} \mathbf{v}(k) & k = \tau + i - 1 + \ell T \\ 0 & \text{otherwise} \end{cases} \tag{6.46}$$

where the superscript (i) in $\hat{\mathbf{v}}_\tau^{(i)}(k)$ denotes the partition of the cycled vector $\hat{\mathbf{v}}_\tau(k)$. In other words, at each time point, the vector $\hat{\mathbf{v}}_\tau(k)$ has a unique nonzero sub-vector, which cyclically

shifts, e.g.

$$\hat{\mathbf{v}}_\tau(\tau) = \begin{bmatrix} \mathbf{v}(\tau) \\ 0 \\ \vdots \\ 0 \end{bmatrix}, \quad \hat{\mathbf{v}}_\tau(\tau+1) = \begin{bmatrix} 0 \\ \mathbf{v}(\tau+1) \\ \vdots \\ 0 \end{bmatrix},$$

$$, \cdots, \quad \hat{\mathbf{v}}_\tau(\tau+1) = \begin{bmatrix} 0 \\ 0 \\ \vdots \\ \mathbf{v}(\tau+T-1) \end{bmatrix} \tag{6.47}$$

Cycling results in a constant coefficient state-space system of the type

$$\hat{\mathbf{x}}_\tau(k+1) = \hat{F}_\tau \hat{\mathbf{x}}_\tau(k) + \hat{G}_\tau \hat{\mathbf{u}}_\tau(k) \tag{6.48}$$

$$\hat{\mathbf{y}}(k) = \hat{H}_\tau \hat{\mathbf{x}}_\tau(k) + \hat{E}_\tau \hat{\mathbf{u}}_\tau(k) \tag{6.49}$$

where the "state" matrix $\hat{F}_\tau$ is given by:

$$\hat{F}_\tau = \begin{bmatrix} 0 & 0 & \dots & 0 & A(\tau+T-1) \\ A(\tau) & 0 & \dots & 0 & 0 \\ 0 & A(\tau+1) & \dots & 0 & 0 \\ \dots & \dots & \ddots & \dots & \dots \\ 0 & 0 & \dots & A(\tau+T-2) & 0 \end{bmatrix} \tag{6.50}$$

the control matrix $\hat{G}_\tau$ has exactly the same structure as $\hat{F}_\tau$, but with $B(\cdot)$ instead of $A(\cdot)$, the output matrix $\hat{H}_\tau$ is given by:

$$\hat{H}_\tau = \begin{bmatrix} C(\tau) & 0 & \dots & 0 \\ 0 & C(\tau+1) & \dots & 0 \\ \dots & \dots & \ddots & \dots \\ 0 & 0 & \dots & C(\tau+T-1) \end{bmatrix} \tag{6.51}$$

and the feedthrough matrix $\hat{E}_\tau$ has exactly the same structure as $\hat{H}_\tau$, but with $D(\cdot)$ instead of $C(\cdot)$.

Considering the matrix $\hat{F}_\tau$, it can be shown [4] that its eigenvalues coincide with all the T-th roots of the characteristic multipliers of the discrete state matrix $A(\cdot)$. Therefore, the periodic system is stable if and only if its cycled reformulation is stable. Additional properties, important from a control system standpoint, can be found in Ref. [4].

6.4.3 Frequency-lifted reformulation

The frequency lifting is conceptually similar to the time lifting, except that in this case the enlarged vectors contain all the harmonics of the input and of the output signals. Therefore, this is a frequency domain representation. This reformulation is naturally set in the z-domain directly.

Consider a generic discrete signal $\mathbf{v}(k)$, the z-transform of which is $\mathbf{V}(\sigma)$ (recall that while z shifts signals by one sample, σ shifts signals by T samples, and therefore it is the z-transform equivalent when we wish to consider the behavior of the system every T samples). Then, we can define a *frequency-lifted vector* $\tilde{\mathbf{V}}(\sigma)$ as:

$$\tilde{\mathbf{V}}(\sigma) = \left\{ \begin{array}{c} \mathbf{V}(\sigma) \\ \mathbf{V}(\sigma\phi) \\ \mathbf{V}(\sigma\phi^2) \\ \vdots \\ \mathbf{V}(\sigma\phi^{T-1}) \end{array} \right\} \tag{6.52}$$

where again $\phi = \exp(j2\pi/T)$. Notice that the i-th component of this vector is nothing but the z-transform of the complex signal obtained by multiplying the signal $\mathbf{v}(t)$ by the complex number $\phi^{(-i+1)k}$.

When the general definition of Eq. (6.52) is specialized to the state vector $\mathbf{x}(k)$, the control vector $\mathbf{u}(k)$, and the output vector $\mathbf{y}(k)$, we obtain frequency-lifted vectors $\tilde{\mathbf{X}}(\sigma)$, $\tilde{\mathbf{U}}(\sigma)$, and $\tilde{\mathbf{Y}}(\sigma)$, each with T subvectors, and total size of nT, mT, and pT, respectively.

The frequency-lifted input vector $\tilde{\mathbf{U}}(\sigma)$ and output vector $\tilde{\mathbf{Y}}(\sigma)$ are related by:

$$\tilde{\mathbf{Y}}(\sigma) = \tilde{W}(\sigma)\tilde{\mathbf{U}}(\sigma) \tag{6.53}$$

where $\tilde{W}(\sigma)$ is the *frequency-lifted transfer function* of the periodic system. The matrix has dimensions pT by mT, and it is composed of T by T blocks of p rows and m columns. The submatrix $\left[\tilde{W}(\sigma)\right]_{q+1,r+1}$ in row $q+1$ and column $r+1$, with $r, q = 0, 1, 2, ..., T-1$ is given

by [4]

$$\left[\tilde{W}(\sigma)\right]_{q+1,r+1} = \frac{1}{T}\sum_{\ell=0}^{T-1} G(\sigma\phi^r, \ell)\phi^{\ell(r-q)} \tag{6.54}$$

Therefore, for example

$$\begin{aligned} q=0, r=0 \quad \left[\tilde{W}(\sigma)\right]_{1,1} &= \frac{1}{T}\sum_{\ell=0}^{T-1} G(\sigma, \ell) \\ q=1, r=0 \quad \left[\tilde{W}(\sigma)\right]_{2,1} &= \frac{1}{T}\sum_{\ell=0}^{T-1} G(\sigma, \ell)\phi^{-\ell} \\ q=0, r=1 \quad \left[\tilde{W}(\sigma)\right]_{1,2} &= \frac{1}{T}\sum_{\ell=0}^{T-1} G(\sigma, \ell)\phi^{\ell} \end{aligned}$$

All these matrices will generally have complex coefficients. Note that the various elements of the frequency-lifted transfer function are expressed in terms of the input-output transfer function $G(\sigma, k)$.

6.4.4 Fourier reformulation

The Fourier reformulation is closely related to the frequency-lifted reformulation, and is also a frequency-domain representation. This formulation is obtained by considering the periodic system in an Exponentially Modulated Periodic (EMP) regime.

A signal $\mathbf{v}(k)$ is said to be EMP if there exists a (complex) number $\lambda \neq 0$ such that

$$\mathbf{v}(\ell T + s) = \mathbf{v}(s)\lambda^{\ell T} \tag{6.55}$$

where s is any of the T samples that make up one period. For $\lambda = 1$ or any T-root of 1 an EMP signal is also periodic. Any EMP signal $\mathbf{v}(k)$ can also be written as the following *EMP Fourier expansion* [4]

$$\mathbf{v}(k) = \sum_{\ell=0}^{T-1} \bar{\mathbf{v}}_\ell \phi^{\ell k}\lambda^k \tag{6.56}$$

where $\bar{\mathbf{v}}_\ell$ are the coefficients of the Fourier expansion of the periodic signal $\bar{\mathbf{v}(k)} = \mathbf{v}(k)\lambda^{-k}$.

To obtain the Fourier reformulation, the state vector $\mathbf{x}(k)$, the control vector $\mathbf{u}(k)$, and the output vector $\mathbf{y}(k)$, are all expressed as EMP Fourier expansions. For example

$$\mathbf{u}(k) = \sum_{\ell=0}^{T-1} \bar{\mathbf{u}}_\ell \sigma^{\ell k} \sigma^k \tag{6.57}$$

(see Ref. [4] for details of the substitution of λ^k in Eq. (6.56) with σ^k in Eq. (6.57)). The system matrices are similarly expanded. For example, for the state matrix $A(k)$ we have

$$A(k) = \sum_{\ell=0}^{T-1} A_\ell \phi^{\ell k} \tag{6.58}$$

Substituting the EMP expansions of the system matrices into the system equations, Eq. (6.9), and equating all terms at the same frequency, we obtain the following matrix equation

$$\sigma \mathcal{N} \tilde{\mathbf{x}} = \mathcal{A}\tilde{\mathbf{x}} + \mathcal{B}\tilde{\mathbf{u}} \tag{6.59}$$

$$\tilde{\mathbf{y}} = \mathcal{C}\tilde{\mathbf{x}} + \mathcal{D}\tilde{\mathbf{u}} \tag{6.60}$$

where $\tilde{\mathbf{x}}$, $\tilde{\mathbf{u}}$, and $\tilde{\mathbf{y}}$ are vectors formed with the harmonics of $\mathbf{x}(k)$, $\mathbf{u}(k)$, and $\mathbf{y}(k)$, respectively, organized in the following fashion

$$\tilde{\mathbf{x}} = \left\{ \begin{array}{c} \bar{\mathbf{x}}_0 \\ \bar{\mathbf{x}}_1 \\ \vdots \\ \bar{\mathbf{x}}_{T-1} \end{array} \right\} \tag{6.61}$$

and similarly for $\tilde{\mathbf{u}}$ and $\tilde{\mathbf{y}}$. $\mathcal{A}, \mathcal{B}, \mathcal{C}$, and $\mathcal{D}$ are formed with the harmonics of $A(k), B(k), C(k)$, and $D(k)$, respectively. For example

$$\mathcal{A} = \left[\begin{array}{ccccc} A_0 & A_{T-1} & A_{T-2} & \dots & A_1 \\ A_1 & A_0 & A_{T-1} & \dots & A_2 \\ \vdots & \vdots & \vdots & & \vdots \\ A_{T-2} & A_{T-3} & A_{T-4} & \dots & A_{T-1} \\ A_{T-1} & A_{T-2} & A_{T-3} & \dots & A_0 \end{array} \right] \tag{6.62}$$

and similarly for $\mathcal{B}, \mathcal{C}$, and $\mathcal{D}$. The matrix $\mathcal{N}$ is the block diagonal matrix

$$\mathcal{N} = \text{blkdiag}\left[\phi^k I\right] \qquad k = 0, 1, 2, ..., T-1 \tag{6.63}$$

Then, one can define the *harmonic transfer function* as

$$\mathcal{G}(\sigma) = \mathcal{C}\left[\sigma\mathcal{N}I - \mathcal{A}\right]^{-1}\mathcal{B} + \mathcal{D} \tag{6.64}$$

This transfer function provides a connection between the input harmonics $\tilde{\mathbf{U}}$ and the output harmonics $\tilde{\mathbf{Y}}$. Note that for the steady-state periodic case $\sigma = 1$. Finally, it can be shown [4] that the harmonic transfer function, Eq. (6.64), coincides with the frequency-lifted transfer function, Eq. (6.53).

6.5 Other considerations

Taken together, the four constant coefficient reformulations described in the previous sections provide the foundation required to study a coupled rotor-fuselage system with a closed loop IBC or HHC system entirely as a discrete system. This is important because the effects on stability and performance characteristics of discrete elements (e.g., control updates, harmonic analyses, etc.) and sensor and computation delays can then be studied rigorously. The approximations intrinsic in converting discrete elements to continuous, especially if the sampling or update rates are low, are eliminated.

Because the reformulated systems have constant coefficients, all the control system design tools for discrete time-invariant systems can be used to design both time-invariant and periodic rotor controllers. Possible interactions with flight control systems can also be studied, and gain and phase margins can be established. However, it is important to point out that while a periodic coefficient system has always an equivalent constant coefficient representation, the reverse is not true. For example, a constant coefficient system will have a periodic coefficient analogue only if the direct feed-through matrix E_τ of the time-lifted

system, Eq. (6.45), is block lower triangular [12]. This has practical implications on the design of active rotor controls in the rotating system.

6.6 Summary

The fully discrete modeling of a coupled rotor-fuselage system allows a rigorous treatment of closed-loop HHC or IBC systems, including the discrete elements with multiple sampling and update rates.

The extraction of a linearized discrete model from the continuous one is very simple. The Floquet characteristic multipliers and characteristic exponents are the same for the discrete and continuous systems, and therefore the open loop stability characteristics of the two systems are exactly the same.

Time-lifting converts a system with periodic coefficients into a larger system, but with constant coefficients. Time-lifting is based on two properties of discrete periodic systems, namely: (i) the response of the periodic system can be modeled as the combination of the responses of multiple constant-coefficient systems, one per sample, and (ii) using shifting operators, it is possible to "move" all the system inputs at the same sample in multiple periods to that sample in a single period.

Other discrete, constant coefficient reformulations are available, and can be useful for theoretical studies and practical applications.

6.7 Appendix

This appendix contains numerical details for the blade flapping examples presented in this chapter. The parameters used in the flapping equations were: Lock number $\gamma = 8$, inflow ratio $\lambda = 0$, advance ratio $\mu = 0.3$, collective pitch $\theta_0 = 10$ deg, lateral cyclic $\theta_{1c} = 2$ deg, longitudinal cyclic $\theta_{1s} = 3$. The choice of setting $\lambda = 0$, not very realistic from a practical point of view, was simply made to simplify the calculations: in fact, for the mathematical

model of this study λ is neither a state nor a control. In a more accurate mathematical model, λ would probably be a state, have its governing equations, and be part of the state vector $\mathbf{x}$. To take it into account in the present study, it could be added to the $\mathbf{u}$ vector as if it were a pseudo-control.

The transition matrices $\Phi_A[k\Delta\psi\ 0]$, $k = 1, 2, \ldots, 10$, which are 2 by 2 matrices, are listed below. Note that $\Phi_A[10\Delta\psi\ 0]$ is the transition matrix at the end of one period, the eigenvalues of which determine the stability of the periodic system.

$$\Phi_A[\Delta\psi\ 0] = \Phi_A[0.6283, 0] = \begin{bmatrix} 0.7849 & 0.4154 \\ -0.5769 & 0.3244 \end{bmatrix}$$

$$\Phi_A[2\Delta\psi\ 0] = \Phi_A[1.2566, 0] = \begin{bmatrix} 0.4025 & 0.4616 \\ -0.5661 & -0.1129 \end{bmatrix}$$

$$\Phi_A[3\Delta\psi\ 0] = \Phi_A[1.8850, 0] = \begin{bmatrix} 0.1189 & 0.3466 \\ -0.3322 & -0.2118 \end{bmatrix}$$

$$\Phi_A[4\Delta\psi\ 0] = \Phi_A[2.5133, 0] = \begin{bmatrix} -0.0285 & 0.2234 \\ -0.1538 & -0.1730 \end{bmatrix}$$

$$\Phi_A[5\Delta\psi\ 0] = \Phi_A[3.1416, 0] = \begin{bmatrix} -0.0919 & 0.1293 \\ -0.0578 & -0.1299 \end{bmatrix}$$

$$\Phi_A[6\Delta\psi\ 0] = \Phi_A[3.7699, 0] = \begin{bmatrix} -0.1086 & 0.0564 \\ 0.0016 & -0.1037 \end{bmatrix}$$

$$\Phi_A[7\Delta\psi\ 0] = \Phi_A[4.3982, 0] = \begin{bmatrix} -0.0929 & -0.0011 \\ 0.0460 & -0.0779 \end{bmatrix}$$

$$\Phi_A[8\Delta\psi\ 0] = \Phi_A[5.0265, 0] = \begin{bmatrix} -0.0550 & -0.0390 \\ 0.0701 & -0.0408 \end{bmatrix}$$

$$\Phi_A[9\Delta\psi\ 0] = \Phi_A[5.6549, 0] = \begin{bmatrix} -0.0113 & -0.0512 \\ 0.0637 & 0.0015 \end{bmatrix}$$

$$\Phi_A[10\Delta\psi\ 0] = \Phi_A[6.2832, 0] = \begin{bmatrix} 0.0195 & -0.0399 \\ 0.0319 & 0.0304 \end{bmatrix}$$

The discrete state transition matrices $A(k)$, $k = 1, 2, \ldots, 10$, which are 2 by 2 matrices, are listed below:

$$
\begin{aligned}
A(1) &= A(0.6283) = \begin{bmatrix} 0.7849 & 0.4154 \\ -0.5769 & 0.3244 \end{bmatrix} \\
A(2) &= A(1.2566) = \begin{bmatrix} 0.8030 & 0.3947 \\ -0.5033 & 0.2965 \end{bmatrix} \\
A(3) &= A(1.8850) = \begin{bmatrix} 0.8467 & 0.3920 \\ -0.3818 & 0.3153 \end{bmatrix} \\
A(4) &= A(2.5133) = \begin{bmatrix} 0.8923 & 0.4053 \\ -0.2768 & 0.3638 \end{bmatrix} \\
A(5) &= A(3.1416) = \begin{bmatrix} 0.9108 & 0.4289 \\ -0.2536 & 0.4232 \end{bmatrix} \\
A(6) &= A(3.7699) = \begin{bmatrix} 0.8946 & 0.4561 \\ -0.3194 & 0.4809 \end{bmatrix} \\
A(7) &= A(4.3982) = \begin{bmatrix} 0.8622 & 0.4793 \\ -0.4163 & 0.5244 \end{bmatrix} \\
A(8) &= A(5.0265) = \begin{bmatrix} 0.8346 & 0.4888 \\ -0.4911 & 0.5309 \end{bmatrix} \\
A(9) &= A(5.6549) = \begin{bmatrix} 0.8134 & 0.4771 \\ -0.5435 & 0.4823 \end{bmatrix} \\
A(10) &= A(6.2832) = \begin{bmatrix} 0.7936 & 0.4477 \\ -0.5817 & 0.3974 \end{bmatrix}
\end{aligned}
$$

The discrete control matrices $B(k)$, $k = 1, 2, \ldots, 10$, are listed below:

$$
\begin{aligned}
B(1) &= \begin{bmatrix} 0.1792 & 0.1720 & 0.0419 \\ 0.5319 & 0.4847 & 0.1996 \end{bmatrix} \\
B(2) &= \begin{bmatrix} 0.2482 & 0.1597 & 0.1861 \\ 0.6993 & 0.3643 & 0.5848 \end{bmatrix} \\
B(3) &= \begin{bmatrix} 0.2860 & 0.0251 & 0.2816 \\ 0.7739 & -0.0442 & 0.7608 \end{bmatrix} \\
B(4) &= \begin{bmatrix} 0.2700 & -0.1350 & 0.2304 \\ 0.7108 & -0.4336 & 0.5490 \end{bmatrix} \\
B(5) &= \begin{bmatrix} 0.2085 & -0.1882 & 0.0844 \\ 0.5394 & -0.5082 & 0.1527 \end{bmatrix} \\
B(6) &= \begin{bmatrix} 0.1360 & -0.1318 & -0.0268 \\ 0.3517 & -0.3279 & -0.1103 \end{bmatrix} \\
B(7) &= \begin{bmatrix} 0.0850 & -0.0567 & -0.0621 \\ 0.2279 & -0.1294 & -0.1830 \end{bmatrix} \\
B(8) &= \begin{bmatrix} 0.0654 & -0.0064 & -0.0643 \\ 0.1889 & 0.0062 & -0.1857 \end{bmatrix} \\
B(9) &= \begin{bmatrix} 0.0745 & 0.0382 & -0.0630 \\ 0.2298 & 0.1433 & -0.1750 \end{bmatrix} \\
B(10) &= \begin{bmatrix} 0.1136 & 0.1039 & -0.0426 \\ 0.3522 & 0.3369 & -0.0829 \end{bmatrix}
\end{aligned}
$$

Transfer functions $H_i(z,k)$ and $G(\sigma,k)$

For the blade flapping example, there are 100 transfer function matrices $H_i(z,k)$ because both $i = 0, 1, 2, \ldots, T-1$ and $k = 1, 2, \ldots, T$. Each of the matrices has 2 rows and 3 columns. Denoting, for convenience, $B'(k) = \Phi_A(k, k-T+1)B(k)$, and recalling that $D(k) = 0$, the expression for $H_0(z,k)$, Eq. (6.30) becomes

$$
H_0(z,k) = C(k)\left[zI - \Psi_A(k)\right]^{-1} B'(k) \tag{6.65}
$$

which represents a conversion from state space to transfer function that can be carried out, for example, using the Matlab function `ss2tf`. For illustration, consider the case $k = 0$, i.e.,

compute $H_0(z,0)$. We have:

$$\Psi_A(0) = A(9)A(8) \times \ldots \times A(0) \tag{6.66}$$

$$\Phi_A(0,-9) = A(9)A(8) \times \ldots \times A(1) \tag{6.67}$$

$B(0) = B(10)$, $C(0)$ is the identity matrix, and $D(0)$ is zero. Using `ss2tf`, the first column of $H_0(z,0)$ can be computed using `ss2tf(A9*A8*A7*A6*A5*A4*A3*A2*A1*A0` and `A9*A8*A7*A6*A5*A4*A3*A2*A1*B0,C,D,1)`, where `A0, A1, ...` denote $A(0), A(1), \ldots$, respectively. To compute the second and third columns, the last argument `1` is replaced by `2` and `3`, respectively.

The result is

$$\begin{aligned} H_0(z,0) &= \frac{1}{z^2 - 0.0499z + 0.0019} \times \\ &\times \begin{bmatrix} -0.0193z + 0.0004 & -0.0186z + 0.0004 & -0.0047z + 0.0001 \\ 0.0077z - 0.011 & 0.0071z - 0.011 & 0.0028z - 0.003 \end{bmatrix} \end{aligned} \tag{6.68}$$

Note that, although the 100 $H_i(z,k)$ matrices will generally have different coefficients, the characteristic polynomial $z^2 - 0.0499z + 0.0019$ will be the same for all of them.

The transfer function $G(\sigma,k)$ is calculated using Eq. (6.34):

$$G(\sigma,k) = \sum_{i=0}^{T-1} H_i(\sigma^T,k)\sigma^{-i} \qquad \text{Eq. (6.34) repeated}$$

For the blade flapping example there are 10 different $G(\sigma,k)$, i.e., one for each value of $k = 0,1,2,\ldots,T-1$. For example, for $k=0$ and $T=10$

$$G(\sigma,0) = \sum_{i=0}^{9} H_i(\sigma^9,0)\sigma^{-i} \tag{6.69}$$

The first term in the summation, $i = 0$, is $H_0(\sigma^9,0)$. The matrix $H_0(z,0)$ is given by Eq. (6.68). Therefore $H_0(\sigma^9,0)$ is obtained from $H_0(z,0)$ by replacing z with σ^9 in all the elements. This can be done with either numerical or symbolic manipulation software.

Time-lifted reformulation

The time-lifted state matrix F is given by $\Phi_A[10\Delta\psi\ 0]$. The time-lifted control matrix G is given by:

$$G = \begin{bmatrix} G_1 & G_2 & G_3 & G_4 & G_5 & G_6 & G_7 & G_8 \end{bmatrix}$$

where: (6.70)

$$G_1 = \begin{bmatrix} -0.0200 & -0.0189 & 0.0056 & -0.0306 \\ -0.0064 & -0.0065 & 0.0004 & -0.0092 \end{bmatrix}$$

$$G_2 = \begin{bmatrix} -0.0284 & -0.0101 & -0.0312 & -0.0187 \\ -0.0077 & -0.0052 & -0.0869 & -0.0453 \end{bmatrix}$$

$$G_3 = \begin{bmatrix} -0.0243 & 0.0138 & -0.0038 & 0.0136 \\ -0.0726 & -0.2159 & 0.0064 & -0.2123 \end{bmatrix}$$

$$G_4 = \begin{bmatrix} 0.1103 & -0.0677 & 0.0849 & 0.2028 \\ -0.3155 & 0.1831 & -0.2506 & -0.2965 \end{bmatrix}$$

$$G_5 = \begin{bmatrix} -0.1904 & 0.0597 & 0.2280 & -0.2139 \\ 0.2755 & -0.0958 & -0.1763 & 0.1674 \end{bmatrix}$$

$$G_6 = \begin{bmatrix} -0.0675 & 0.1934 & -0.1142 & -0.1522 \\ 0.0459 & -0.0449 & 0.0310 & 0.0321 \end{bmatrix}$$

$$G_7 = \begin{bmatrix} 0.1469 & -0.0023 & -0.1444 & 0.0745 \\ 0.0682 & 0.0064 & -0.0670 & 0.2298 \end{bmatrix}$$

$$G_8 = \begin{bmatrix} 0.0382 & -0.0630 \\ 0.1433 & -0.1750 \end{bmatrix}$$

The time-lifted output matrix H is given by:

$$H^T = \begin{bmatrix} H_1 & H_2 & H_3 & H_4 & H_5 \end{bmatrix} \tag{6.71}$$

where:

$$H_1 = \begin{bmatrix} 1.0000 & 0 & 0.7849 & -0.5769 \\ 0 & 1.0000 & 0.4154 & 0.3244 \end{bmatrix}$$

$$H_2 = \begin{bmatrix} 0.4025 & -0.5661 & 0.1189 & -0.3322 \\ 0.4616 & -0.1129 & 0.3466 & -0.2118 \end{bmatrix}$$

$$H_3 = \begin{bmatrix} -0.0285 & -0.1538 & -0.0919 & -0.0578 \\ 0.2234 & -0.1730 & 0.1293 & -0.1299 \end{bmatrix}$$

$$H_4 = \begin{bmatrix} -0.1086 & 0.0016 & -0.0929 & 0.0460 \\ 0.0564 & -0.1037 & -0.0011 & -0.0779 \end{bmatrix}$$

$$H_5 = \begin{bmatrix} -0.0550 & 0.0701 & -0.0113 & 0.0637 \\ -0.0390 & -0.0408 & -0.0512 & 0.0015 \end{bmatrix}$$

Finally the time-lifted feedthrough matrix E is a matrix with 30 rows and 20 columns. For reasons of space, only the first 4 rows will be listed below, transposed:

$$E^T = \begin{bmatrix} 0.0000 & 0.0000 & 0.0000 & 0.0000 & \\ 0.0000 & 0.0000 & 0.0000 & 0.0000 & \\ 0.1136 & 0.1039 & -0.0426 & 0.0000 & \\ 0.3522 & 0.3369 & -0.0829 & 0.0000 & \\ 0.2303 & 0.2164 & -0.0669 & 0.1792 & \\ 0.0472 & 0.0476 & -0.0032 & 0.5319 & \\ 0.2135 & 0.2019 & -0.0579 & 0.3602 & \\ -0.0730 & -0.0676 & 0.0246 & 0.0993 & \\ 0.1609 & 0.1527 & -0.0417 & 0.3617 & \\ -0.0857 & -0.0805 & 0.0250 & -0.0636 & \cdots \\ 0.1098 & 0.1046 & -0.0273 & 0.3021 & \\ -0.0771 & -0.0728 & 0.0211 & -0.1186 & \\ 0.0631 & 0.0604 & -0.0148 & 0.2162 & \\ -0.0721 & -0.0684 & 0.0189 & -0.1535 & \\ 0.0198 & 0.0193 & -0.0037 & 0.1128 & \\ -0.0641 & -0.0610 & 0.0160 & -0.1705 & \\ -0.0148 & -0.0138 & 0.0048 & 0.0108 & \\ -0.0438 & -0.0418 & 0.0103 & -0.1459 & \\ -0.0329 & -0.0311 & 0.0088 & -0.0608 & \\ -0.0131 & -0.0127 & 0.0024 & -0.0762 & \end{bmatrix} \tag{6.72}$$

Chapter 7

Discrete-Time, Closed-Loop Aeromechanical Stability Analysis of Helicopters With Higher Harmonic Control

7.1 Introduction

Higher Harmonic Control (HHC) is an active vibration control technology that tries to reduce N/rev (N being the number of rotor blades) vibratory components in the fuselage by adding higher harmonic components to the rotor controls. Amplitude and phase of these harmonics are determined on line by a suitable control law. If the higher harmonic inputs are applied in the rotating system, via rotating high frequency actuators, the technique is usually called Individual Blade Control (IBC). IBC and HHC are generally considered as effective techniques for vibration reduction, but issues of power requirements and reliability have until now prevented widespread application on production helicopters [39].

HHC has been the subject of extensive research over the last three decades. The research until 1982 has been reviewed by Johnson [25] as part of an extensive study of several types of HHC algorithms and implementation techniques that remains relevant to this date. More recent survey papers have been written by Friedmann and Millott [20] and Teves *et al.* [37]. Although HHC is generally studied in the context of rotor control, the basic HHC algorithm has also been successfully used for fuselage-mounted active vibration reduction [22].

Figure 7.1 shows a typical architecture of an HHC system. While this is not the only possible architecture, nor is it necessarily the best, it is important for historical and practical reasons, and has been extensively studied theoretically and experimentally (e.g., [35]). Some

helicopter outputs, typically N/rev components of fuselage vibrations are extracted through a harmonic analysis, fed to a controller that computes appropriate values of the higher harmonic outputs, which are then injected into the rotor controls. Figure 7.2 depicts a hypothetical situation in which the HHC system is inoperative over the first quarter of the revolution of a reference blade, samples the desired output over the next quarter to build the desired harmonics to attenuate, computes the required inputs over the next half revolution, and updates the HHC inputs at the end of the revolution. These steps are not instantaneous, but are carried out over finite time intervals, and therefore cannot be rigorously described in state space form.

This modeling problem is the probable reason why, although the basic characteristics of HHC algorithms have been investigated extensively in the published literature, the influence of the aeromechanic behavior of the entire helicopter on the performance and, especially, the stability of the HHC system has been typically ignored. The helicopter dynamics have only been considered indirectly, through their contribution to the gain, or T-, matrix. Stability analyses have focused on the stability of the HHC update algorithm, with or without on-line identification, not on the closed loop stability of the complete helicopter with the HHC system turned on. Also, no study on the potential interactions between an HHC system and a flight control system was available in the literature. These analyses require mathematical representation in state-space form, preferably with constant coefficients.

Some recent studies have addressed this gap. Cheng *et al.* [9] have extracted a linearized, state-space, time-invariant model of the helicopter, and have used it for a study of the interaction between the HHC and the flight control system. The harmonic analyzer is essentially modeled as if it was an analog analyzer, continuously extracting the required N/rev vibration harmonics. The computation delays are modeled using Padè approximants and the HHC input is updated continuously. The gain matrix T is fixed. One important conclusion is that while the HHC has little influence on the flight control system and on the handling qualities,

the reverse is not true. There is a significant effect of maneuvers on vibration, which leads to higher required crossover frequencies for the HHC loop.

Lovera *et al.* [28] have studied the closed loop stability of a hingeless rotor helicopter equipped with an HHC system. The T-matrix is constant, and the HHC algorithm is written as a linear time-invariant dynamic compensator using the technique developed by Wereley and Hall [40], extended to cover inputs and outputs at different harmonics. This compensator is coupled to a high-order, coupled rotor-fuselage model, and the closed loop stability is studied using Floquet theory and constant coefficient approximations. The key results of the study are that: (i) the HHC system does not degrade the aeromechanic stability, (ii) the time constants of the HHC are such that interactions with a flight control system could occur, and (iii) that the effects of periodic coefficients need to be taken into account.

A gap in the analysis of HHC systems however remains open, because the issues related to the actual discrete-time implementation were not included in Ref. [28] and have never been studied in detail in the literature. Discrete-time issues are likely to play a major role in determining the closed loop behavior of the system. In fact, the typical update frequency for HHC control inputs is 1/rev, which is comparable with the bandwidth of the dynamics of the open loop, i.e., uncontrolled helicopter rotor. Previous work on this problem (see, e.g., [27, 28, 40]) tried to overcome this difficulty by developing continuous-time, time domain counterparts of the discrete elements. On the other hand, a more complete and rigorous picture of the operation of HHC can be obtained by looking at the entire control loop, including the coupled rotor-fuselage dynamics, in discrete time rather than in continuous time.

In the light of the preceding discussion, this chapter has the following objectives:

1. To describe a typical discrete-time HHC architecture and derive suitable linearized, state-space, discrete models for all the components present in the control loop;

2. To formulate a coupled helicopter-HHC discrete model, and convert it from a periodic, multiple sampling rate model to a constant coefficient, single sampling rate model using time-lifting techniques; and

3. To perform a closed loop, aeromechanic stability and response analysis of the discrete-time, coupled helicopter-HHC model, and compare it with the corresponding results obtained using a continuous-time model.

7.2 Helicopter Model

The baseline simulation model used in this study is a nonreal-time, blade element type, coupled rotor-fuselage simulation model. The model is discussed in detail in Ref. [38], and only a brief description will be provided here. The fuselage is assumed to be rigid and dynamically coupled with the rotor. A total of nine states describe fuselage motion through the nonlinear Euler equations. Fuselage and blades aerodynamics are described through tables of aerodynamic coefficients, and no small angle assumption is required. A coupled flap-lag-torsion elastic rotor model is used. Blades are modeled as Bernoulli-Euler beams. The rotor is discretized using finite elements, with a modal coordinate transformation to reduce the number of degrees of freedom. The elastic deflections are not required to be small. Blade element theory is used to obtain the aerodynamic characteristics on each blade section. Quasi-steady aerodynamics is used, with a 3-state dynamic inflow model. The trim procedure is the same as in Ref. [8]. The rotor equations of motion are transformed into a system of nonlinear algebraic equations using a Galerkin method. The algebraic equations enforcing force and moment equilibrium, the Euler kinematic equations, the inflow equations and the rotor equations are combined in a single coupled system. The solution yields the harmonics of a Fourier expansion of the rotor degrees of freedom, the pitch control settings, trim attitudes and rates of the entire helicopter, and main and tail rotor inflow.

Linearized models are extracted numerically, by perturbing rotor, fuselage, and inflow states about a trimmed equilibrium position. The resulting continuous-time, linearized, time periodic model of the helicopter is in the form

$$\begin{aligned} \dot{\mathbf{x}}_H(t) &= A_H(t)\mathbf{x}_H(t) + B_{FCS}(t)\mathbf{u}_{FCS}(t) + B_{HHC}(t)\mathbf{u}_{HHC}(t) \\ \mathbf{y}_H(t) &= C_H(t)\mathbf{x}_H(t) + D_{FCS}(t)\mathbf{u}_{FCS}(t) + D_{HHC}(t)\mathbf{u}_{HHC}(t). \end{aligned} \tag{7.1}$$

where all the matrices are periodic, with period corresponding to N/rev; the control vectors $\mathbf{u}_{FCS}(t)$ and $\mathbf{u}_{HHC}(t)$ are defined as in Eqs. (7.4) and (7.5), while the outputs are the body frame accelerations measured by the control system.

The matrices of the linearized model are generated as Fourier series. For example, the state matrix $A_H(\psi)$ is given as:

$$A_H(\psi) = A_{H0} + \sum_{k=1}^{K} \left(A_{Hkc}\cos kN\psi + A_{Hks}\sin kN\psi\right) \tag{7.2}$$

with $\psi = \Omega t$, and where the matrices A_{H0}, A_{Hkc}, and A_{Hks} are constant.

The control matrices $B_{FCS}(\psi)$ and $B_{HHC}(\psi)$ are obtained in the same Fourier series form as $A_H(\psi)$, Eq. (7.2), by assuming that the pitch control angle of the i-th blade is given by

$$\begin{aligned} \theta_i(\psi) &= \theta_0 + \theta_{1c}\cos\psi + \theta_{1s}\sin\psi + \theta_{3c}\cos 3\psi + \theta_{3s}\sin 3\psi + \\ &\quad + \theta_{4c}\cos 4\psi + \theta_{4s}\sin 4\psi + \theta_{5c}\cos 5\psi + \theta_{5s}\sin 5\psi \end{aligned} \tag{7.3}$$

where $\psi_i = \psi + 2\pi i/N, i = 0, \ldots, N-1$ is the azimuth angle, and the number of blades $N = 4$. Therefore, the input harmonics are defined in the rotating system, but they are identical for each blade. This arrangement will be defined as HHC, although it could also fall under some definitions of IBC. Note that the theoretical development that follows is entirely independent of the specific configuration for actuators and sensors.

The vector $\mathbf{u}_{FCS}(t)$ contains the controls that would be applied by the pilot or the flight control system. For the derivations of this chapter $\mathbf{u}_{FCS}(t)$ is defined as

$$\mathbf{u}_{FCS}(t) = \left[\theta_0(t) \;\; \theta_{1c}(t) \;\; \theta_{1s}(t)\right]^T \tag{7.4}$$

The input vector $\mathbf{u}_{FCS}(t)$ actually used in the simulations also includes the tail rotor collective pitch $\theta_t(t)$. The partition $\mathbf{u}_{HHC}(t)$ contains the harmonics of the HHC system, that is

$$\mathbf{u}_{HHC}(t) = [\theta_{3c}(t) \;\; \theta_{3s}(t) \;\; \theta_{4c}(t) \;\; \theta_{4s}(t) \;\; \theta_{5c}(t) \;\; \theta_{5s}(t)]^T \tag{7.5}$$

The development that follows only addresses the HHC control loop. The HHC analysis holds, under linearity assumptions, regardless of whether the FCS loops are open or closed.

The output vector $\mathbf{y}_H(t)$ can be formed with any of the three linear and three angular components of the accelerations, measured at one or more points of the airframe (the dimensions of $\mathbf{u}(t)$ and $\mathbf{y}(t)$ need not be the same). The output matrices $C_H(t)$, $D_{FCS}(t)$ and $D_{HHC}(t)$ in Eq. (7.1) therefore depend on the specific form of the output vector $\mathbf{y}_H(t)$ (i.e., on the specific arrangement of sensors), and will be provided later in the chapter.

7.3 Higher Harmonic Control

The HHC controller used in the present study is based on a linear, steady state, frequency domain representation of the dynamics of the helicopter. The vector $\tilde{\mathbf{u}}_{HHC}(k)$ of the harmonics of the rotor controls computed by the HHC system is defined as

$$\tilde{\mathbf{u}}_{HHC}(k) = \left[\theta_{3c}(k) \;\; \theta_{3s}(k) \;\; \theta_{4c}(k) \;\; \theta_{4s}(k) \;\; \cdots \;\; \theta_{5c}(k) \;\; \theta_{5s}(k)\right]^T \tag{7.6}$$

where k is the discrete-time index associated with the sample time at which the control loop operates (1/rev). The vector $\tilde{\mathbf{y}}_{HHC}(k)$ contains the N/rev cosine and sine harmonics of the fuselage accelerations, and is defined as

$$\tilde{\mathbf{y}}_{HHC}(k) = \left[\tilde{y}^1_{Nc}(k) \;\; \tilde{y}^2_{Nc}(k) \;\; \ldots \;\; \tilde{y}^n_{Nc}(k) \;\; \tilde{y}^1_{Ns}(k) \;\; \tilde{y}^2_{Ns}(k) \;\; \ldots \;\; \tilde{y}^n_{Ns}(k)\right]^T \tag{7.7}$$

where $\tilde{y}^i_{Nc}(k)$ and $\tilde{y}^i_{Ns}(k),\ i = 1, \ldots, n$ are, respectively, the cosine and sine components of the i-th N/rev output $\tilde{y}^i(k)$, each defined as

$$\tilde{y}^i_{Nc}(k) = \frac{1}{\pi}\int_{k\pi}^{(k+1)\pi} y^i_H(\psi)\ \cos N\psi d\psi \tag{7.8}$$

$$\tilde{y}^i_{Ns}(k) = \frac{1}{\pi}\int_{k\pi}^{(k+1)\pi} y^i_H(\psi)\ \sin N\psi d\psi \tag{7.9}$$

The generic output $\tilde{y}^i(k)$ can be one of the linear or angular components of the accelerations, which in turn can be measured at one or more locations. In general, there will be n such measurements, and therefore the measurement vector will have $p = 2n$ elements. Finally, $\tilde{\mathbf{y}}^o$ is the vector of N/rev disturbance components corresponding to $\tilde{\mathbf{y}}_{HHC}(k)$.

Then, assuming that the accelerations are linearly related to the HHC harmonics, the variables defined above can be related by

$$\tilde{\mathbf{y}}_{HHC}(k) = T_C\tilde{\mathbf{u}}_{HHC}(k) + \tilde{\mathbf{y}}^o(k) \tag{7.10}$$

where T_C is a real, constant coefficient matrix that links the harmonics of the HHC inputs to those of the acceleration response (see Ref. [28] for details). The matrix T_C can be either estimated from measured data using on line or off line identification algorithms, or computed on the basis of a mathematical model of the helicopter as done in the present study. In general, T_C is a function of the flight condition. At each discrete time step the HHC controller selects the value of the input harmonics $\tilde{\mathbf{u}}_{HHC}$ to reduce the effect of $\tilde{\mathbf{y}}^o$ on $\tilde{\mathbf{y}}_{HHC}$. Assuming that the baseline acceleration vector $\tilde{\mathbf{y}}^o$ is constant over the time step, the optimal open loop solution is given by

$$\tilde{\mathbf{u}}_{HHC}(k) = -T_C^\dagger\tilde{\mathbf{y}}^o(k) \tag{7.11}$$

where $T_C^\dagger$ is the pseudoinverse of the T_C matrix (which is not necessarily square). Since in general $\tilde{\mathbf{y}}^o$ cannot be measured directly, the same result can be obtained by using a discrete-time integral control law in closed loop, i.e., based on the measurements of $\tilde{\mathbf{y}}_{HHC}$:

$$\tilde{\mathbf{u}}_{HHC}(k+1) = \tilde{\mathbf{u}}_{HHC}(k) - T_C^\dagger\tilde{\mathbf{y}}_{HHC}(k) \tag{7.12}$$

The HHC control algorithm used in the present study is defined in terms of the minimization of a quadratic cost function J of the form [33]

$$J = \tilde{\mathbf{y}}_{HHC}^T W \tilde{\mathbf{y}}_{HHC} + \Delta\tilde{\mathbf{u}}_{HHC}^T R \Delta\tilde{\mathbf{u}}_{HHC} \tag{7.13}$$

where $W = W^T \geq 0$ and $R = R^T > 0$ are matrices that allow different weighting of acceleration outputs and $\Delta\tilde{\mathbf{u}}_{HHC}$ is the increment of $\tilde{\mathbf{u}}_{HHC}$ from one iteration to the next:

$$\Delta\tilde{\mathbf{u}}_{HHC}(k+1) = \tilde{\mathbf{u}}_{HHC}(k+1) - \tilde{\mathbf{u}}_{HHC}(k) \tag{7.14}$$

The minimization of J, Eq. (7.13) leads to the control law

$$\Delta\tilde{\mathbf{u}}_{HHC}(k+1) = -(T_C^T W T_C + R)^{-1} T_C^T W \tilde{\mathbf{y}}_{HHC}(k) \tag{7.15}$$

The T_C matrix links the N/rev harmonics of the output to the harmonics of the HHC input vector $\tilde{\mathbf{u}}_{HHC}$. The matrix is fixed, and is obtained from the linearized model of the complete helicopter using a methodology based on the harmonic transfer function. The derivation is presented in detail in Ref. [28].

7.4 Architecture of the HHC System

The present study focuses on the simulation of the HHC architecture shown in Fig. 7.1. The operation of the system consists of the following three steps, which are performed at every rotor revolution: (i) the determination of the N/rev acceleration output vector $\tilde{\mathbf{y}}_{HHC}(k)$; (ii) the update $\tilde{\mathbf{u}}_{HHC}(k+1)$ of the control input using Eq. (7.15); and (iii) the actual application of $\tilde{\mathbf{u}}_{HHC}(k+1)$ via a simple zero-order-hold.

Two different sampling rates are used. The first, and faster, corresponds to the sampling of the acceleration signals required to reconstruct the N/rev harmonics. The second, and slower, is that corresponding to the 1/rev update of the HHC inputs. The portions of the block diagram where each sampling rate is used are shown in Fig. 7.1.

The closed-loop analysis of the helicopter with the HHC system is carried out as follows:

1. Discrete-time models are obtained for each of the components of the control loop, including the block representing the dynamics of the helicopter;

2. A complete model is obtained for the series connection of hold circuit, helicopter, and harmonic analyzer: this model will prove to be time-periodic;

3. A time-invariant reformulation of the complete model is obtained using the theory of time-lifting of periodic systems, using the slower sampling rate (i.e., that of the controller);

4. The overall closed-loop stability analysis is carried out in discrete-time.

7.5 Discrete Models of the Loop Components

In this section, discrete-time models of all the elements in the closed loop scheme of Fig. 7.1 are derived. They include: (i) the helicopter model, (ii) the harmonic analyzer, (iii) the controller, and (iv) the zero-order-hold.

According to the architecture defined in the previous section, the HHC inputs are updated at 1/rev, while the outputs are sampled at a higher frequency in order to allow the reconstruction of the N/rev component of the accelerations of interest.

7.5.1 Discrete helicopter model

The discrete-time helicopter dynamic model is obtained from the linearized continuous-time model of Eq. (7.1). The sampling frequency is the faster of the two in the system, i.e., that required to allow the reconstruction of the N/rev component of the accelerations of interest.

Writing the state and output equations, Eq. (7.1), for the helicopter model over a sampling interval P, under the usual assumption of constant input in the interval, one can write

the analytical solution for the continuous state vector $\mathbf{x}_H(t)$ at time $t = \eta P + P$ as

$$\mathbf{x}_H(\eta P + P) = \Phi_H(\eta P + P, \eta P)\mathbf{x}_H(\eta P) + \int_{\eta P}^{\eta P + P} \Phi_H(\eta P + P, \tau) B_{HHC}(\tau)\mathbf{u}_{HHC}(\tau) d\tau \tag{7.16}$$

$$\mathbf{y}_H(\eta P) = C_H(\eta P)\mathbf{x}_H(\eta P) + D_{HHC}(\eta P)\mathbf{u}_{HHC}(\eta P) \tag{7.17}$$

where Φ_H is the state transition matrix associated with the state matrix A_H. Defining the discrete-time state vector $\tilde{\mathbf{x}}_H$ as $\tilde{\mathbf{x}}_H(\eta) = \mathbf{x}_H(\eta P)$ (similarly for the control vector $\mathbf{u}_{HHC}$ and the output vector $\mathbf{y}_H$) results in the following discrete-time, state-space linearized model of the helicopter

$$\begin{aligned} \tilde{\mathbf{x}}_H(\eta + 1) &= \tilde{A}_H(\eta)\tilde{\mathbf{x}}_H(\eta) + \tilde{B}_{HHC}(\eta)\tilde{\mathbf{u}}_{HHC}(\eta) \\ \tilde{\mathbf{y}}_H(\eta) &= \tilde{C}_H(\eta)\tilde{\mathbf{x}}_H(\eta) + \tilde{D}_{HHC}(\eta)\tilde{\mathbf{u}}_{HHC}(\eta) \end{aligned} \tag{7.18}$$

where the system matrices are defined as

$$\tilde{A}_H(\eta) = \Phi_H(\eta P + P, \eta P) \tag{7.19}$$

$$\tilde{B}_H(\eta) = \int_0^P \Phi_H(\eta P + P, \tau' + \eta P) B_{HHC}(\tau' + \eta P) d\tau' \tag{7.20}$$

$$\tilde{C}_H(\eta) = C_H(\eta P) \tag{7.21}$$

$$\tilde{D}_{HHC}(\eta) = D_{HHC}(\eta P) \tag{7.22}$$

The system matrices are periodic, with a common period equal to n_s samples.

7.5.2 Harmonic Analysis

To implement the HHC control algorithm, the N/rev components $\tilde{\mathbf{y}}_{HHC}$ of the output accelerations must be extracted from their time domain measurements $\tilde{\mathbf{y}}_H$. In each period, the information about $\mathbf{y}_H$ is available starting from $\eta = n_s/2 - 1 + Kn_s$, $K = 1, 2, \ldots$ but is provided as output only at $\eta = (K + 1)n_s$. The operation of the harmonic analyzer can be described mathematically by a linear time-periodic model with discrete time η and period

n_s:

$$\begin{aligned} \tilde{\mathbf{x}}_F(\eta+1) &= \tilde{A}_F(\eta)\tilde{\mathbf{x}}_F(\eta) + \tilde{B}_F(\eta)\tilde{\mathbf{y}}_H(\eta) \\ \tilde{\mathbf{y}}_{HHC}(\eta) &= \tilde{C}_F(\eta)\tilde{\mathbf{x}}_F(\eta) \end{aligned} \tag{7.23}$$

The matrices $\tilde{A}_F(\eta)$, $\tilde{B}_F(\eta)$ and $\tilde{C}_F(\eta)$ are defined in a way that reflects the various phases of the harmonic analysis that occur over one rotor revolution. For the four-bladed rotor of this study there are three distinct phases, defined as follows (see also Figure 7.2):

1. *During the first quarter of the period*, $\eta = 1, 2, \ldots, n_s/4$, the output signal $\mathbf{y}_H$ is allowed to reach steady state following the update of the control input $\mathbf{u}_{HHC}$ at the end of the previous rotor revolution. During this time, the output of the harmonic analyzer is set to zero and the $\mathbf{y}_H$s measured are not accumulated in the integrals, Eqs. (7.8) and (7.9). Therefore the state space matrices of the harmonic analyzer are given by

$$\tilde{A}_F(\eta) = I \quad \tilde{B}_F(\eta) = 0 \quad \tilde{C}_F(\eta) = 0 \tag{7.24}$$

2. *During the second quarter of the period*, $\eta = n_s/4{+}1, n_s/4{+}2, \ldots, n_s/2$, the outputs $\mathbf{y}_H$ are actually sampled and the integrals, Eqs. (7.8) and (7.9), computed, but the output of the analyzer is still kept to zero. Note that the state of the harmonic analyzer must be reset to zero at the beginning of the second quarter of the period, so the state space matrices will be defined as:

$$\tilde{A}_F(\eta) = \begin{cases} 0 & \eta = \dfrac{n_s}{4} \\ I & \text{elsewhere} \end{cases} \tag{7.25}$$

$$\tilde{B}_F(\eta) = \text{blkdiag}\left\{ \begin{bmatrix} \sin\left(\dfrac{2N\pi}{n_s}\eta\right) \\ \cos\left(\dfrac{2N\pi}{n_s}\eta\right) \end{bmatrix} \right\} \tag{7.26}$$

$$\tilde{C}_F(\eta) = 0 \tag{7.27}$$

3. *During the remaining half period*, $\eta = n_s/2+1, n_s/2+2, \ldots, n_s$ the new value of the control input $\tilde{\mathbf{u}}_{HHC}$ is computed and applied to the rotor; therefore the operation of the analyzer is stopped and the computed value for the N/rev harmonic of $\mathbf{y}_H$ is made available at the end of the period:

$$\tilde{A}_F(\eta) = I \tag{7.28}$$

$$\tilde{B}_F(\eta) = 0 \tag{7.29}$$

$$\tilde{C}_F(\eta) = \begin{cases} \dfrac{8}{n_s} I & \eta = n_s \\ 0 & \text{elsewhere} \end{cases} \tag{7.30}$$

The entire sequence of operations described above can be summarized in the following expressions for the state space matrices of the harmonic analyzer, which hold for a generic value of the 1/rev discrete time index k (i.e., for the generic, k-th rotor revolution):

$$\tilde{A}_F(\eta) = \begin{cases} 0 & \eta = kn_s + \dfrac{n_s}{4} \\ I & \text{elsewhere} \end{cases} \tag{7.31}$$

$$\beta_F(\eta) = \begin{cases} 1 & kn_s + \dfrac{n_s}{4} \le \eta < kn_s + \dfrac{n_s}{2} \\ 0 & \text{elsewhere} \end{cases} \tag{7.32}$$

$$\tilde{B}_F(\eta) = \beta_F(\eta)\text{blkdiag}\left\{ \begin{bmatrix} \sin\left(\dfrac{2N\pi}{n_s}\eta\right) \\ \cos\left(\dfrac{2N\pi}{n_s}\eta\right) \end{bmatrix} \right\} \tag{7.33}$$

$$\tilde{C}_F(\eta) = \begin{cases} \dfrac{8}{n_s} I & \eta = kn_s + n_s \\ 0 & \text{elsewhere} \end{cases} \tag{7.34}$$

Therefore, the output of the above model is nonzero only for $\eta = 0, n_s, 2n_s, \ldots$.

7.5.3 Controller

The control law given by Eq. (7.15) can be written in state-space form as a linear time-invariant system

$$\tilde{\mathbf{x}}_C(k+1) = \tilde{A}_C\tilde{\mathbf{x}}_C(k) + \tilde{B}_C\tilde{\mathbf{y}}_{HHC}(k) \tag{7.35}$$

$$\tilde{\mathbf{u}}_{HHC}(k) = \tilde{C}_C\tilde{\mathbf{x}}_C(k) \tag{7.36}$$

where

$$\tilde{A}_C = I \tag{7.37}$$

$$\tilde{B}_C = -\{T_C^T W T_C + R\}^{-1} T_C^T W \tag{7.38}$$

$$\tilde{C}_C = I \tag{7.39}$$

7.5.4 Zero-Order-Hold circuit

The hold circuit is the interface between the controller and the helicopter. Since the controller operates at the discrete-time k (i.e., once per revolution) while the helicopter model has been obtained at the discrete-time η (i.e., once per sample needed to extract the N/rev harmonics), the controller provides a new value of the control variables only at $\eta = kn_s$, $k = 1, 2, \ldots$, and this output must be kept constant for the intervening samples $kn_s \leq \eta < (k+1)n_s$. Therefore, the model of the hold circuit is linear, discrete-time periodic, with discrete time η and period n_s, and is given by

$$\tilde{\mathbf{x}}_Z(\eta+1) = \tilde{A}_Z(\eta)\tilde{\mathbf{x}}_Z(\eta) + \tilde{B}_Z(\eta)\tilde{\mathbf{u}}_{HHC}(\eta) \tag{7.40}$$

$$\mathbf{u}_{HHC}(\eta) = \tilde{C}_Z(\eta)\tilde{\mathbf{x}}_Z(\eta) + \tilde{D}_Z(\eta)\tilde{\mathbf{u}}_{HHC}(\eta) \tag{7.41}$$

where

$$\tilde{A}_Z(\eta) = \delta(\eta) \tag{7.42}$$

$$\tilde{B}_Z(\eta) = I - \delta(\eta) \tag{7.43}$$

$$\tilde{C}_Z(\eta) = \delta(\eta) \tag{7.44}$$

$$\tilde{D}_Z(\eta) = I - \delta(\eta) \tag{7.45}$$

and

$$\delta(\eta) = \begin{cases} 0 & \eta = kn_s, \quad k = 1, 2, \ldots \\ I & \text{elsewhere} \end{cases} \tag{7.46}$$

7.5.5 Series connection of zero order hold, helicopter model and harmonic analyzer

The overall discrete HHC model, which relates the harmonics of the HHC input $\tilde{\mathbf{u}}_{HHC}$ to the harmonics of the acceleration output $\tilde{\mathbf{y}}_{HHC}$ can be obtained by connecting in series the harmonic analyzer, Eq. (7.23), the discrete model for the response of the helicopter to HHC inputs, Eq. (7.16), and that of the zero order hold, Eq. (7.40). The model, with discrete-time η, is given by

$$\tilde{\mathbf{x}}_Z(\eta+1) = \tilde{A}_Z\tilde{\mathbf{x}}_Z(\eta) + \tilde{B}_Z\tilde{\mathbf{u}}_{HHC}(\eta) \tag{7.47}$$

$$\tilde{\mathbf{x}}_H(\eta+1) = \tilde{A}_H\tilde{\mathbf{x}}_H(\eta) + \tilde{B}_{HHC}\tilde{C}_Z\tilde{\mathbf{x}}_Z(\eta) + \tilde{B}_{HHC}\tilde{D}_Z\tilde{\mathbf{u}}_{HHC}(\eta) \tag{7.48}$$

$$\begin{aligned} \tilde{\mathbf{x}}_F(\eta+1) = {} & \tilde{A}_F\tilde{\mathbf{x}}_F(\eta) + \tilde{B}_F\tilde{C}_H\tilde{\mathbf{x}}_H(\eta) + \tilde{B}_F\tilde{D}_{HHC}\tilde{C}_Z\tilde{\mathbf{x}}_Z(\eta) + \\ & + \tilde{B}_F\tilde{D}_{HHC}\tilde{D}_Z\tilde{\mathbf{u}}_{HHC}(\eta) \end{aligned} \tag{7.49}$$

$$\tilde{\mathbf{y}}_{HHC}(\eta) = \tilde{C}_F\tilde{\mathbf{x}}_F(\eta) \tag{7.50}$$

(the argument η in the matrices has been omitted for simplicity). This model cannot be connected directly to the HHC controller because its sampling rate is still different from that of the discrete HHC control law (n_s/rev vs. 1/rev). A combined model at the same sampling

rate as the HHC controller can be obtained using the theory of time-invariant reformulations of linear time-periodic systems and, more precisely, through a time-lifted reformulation.

7.6 Time-lifted Formulation of the Closed Loop System

A closed-loop stability analysis requires a single sampling period for the entire system. Therefore, the model will be reformulated using the shorter sampling period $P = T/n_S$ as the common period. The implicit assumption that the longer sampling period T, corresponding to one rotor revolution, is an integer multiple of the acceleration sampling period P is clearly quite reasonable. This reformulation is carried out using time lifting, and results in a discrete model with overall sampling period T and time index k. Time lifting is described in detail in Ref. [4] and is summarized in Ref. [11], which also contains numerical examples of the application to a flapping rigid rotor blade. A useful byproduct of the use of a lifted reformulation is that the resulting model has constant coefficients, which simplifies the closed loop stability analysis.

7.6.1 Time lifting of periodic systems

Time lifting is based on the idea that the knowledge of the state vector at time k and of the inputs between time k and $k+1$ is sufficient to determine the value of the state at time $k+1$ and the value of the outputs between k and $k+1$. The key steps of time lifting will be briefly outlined here.

Consider the linear, discrete-time periodic system with a period equal to n_s samples, and with m inputs and p outputs

$$\begin{aligned} \tilde{\mathbf{x}}(t+1) &= A(t)\tilde{\mathbf{x}}(t) + B(t)\tilde{\mathbf{u}}(t) \\ \tilde{\mathbf{y}}(t) &= C(t)\tilde{\mathbf{x}}(t) + D(t)\tilde{\mathbf{u}}(t) \end{aligned} \tag{7.51}$$

where $t = 0, 1, 2, \ldots, n_s - 1$. Then, the state vector at time $t > \tau$ is given by the discrete-time

Lagrange formula [34]

$$\tilde{\mathbf{x}}(t) = \Psi(t,\tau)\tilde{\mathbf{x}}(\tau) + \sum_{j=\tau+1}^{t} \Psi(t,j)B(j-1)\tilde{\mathbf{u}}(j-1). \tag{7.52}$$

where $\Psi(t,\tau) = A(t-1)A(t-2)\cdots A(\tau)$ is the transition matrix from time τ (also an integer between 0 and $n_s - 1$) to time t for the state equation, Eq. (7.51). Equation (7.52) can be used to build an equivalent (i.e., with the same output given the same input) time-invariant system by sampling the state vector at a frequency of n_s, and packing the input and output vectors for each sample into larger input and output vectors. This results in the "lifted" reformulation [4, 11]

$$\begin{aligned} \tilde{\mathbf{x}}(k+1) &= F\tilde{\mathbf{x}}(k) + G\mathbf{u}_{lift}(k) \\ \mathbf{y}_{lift}(k) &= H\tilde{\mathbf{x}}(k) + E\mathbf{u}_{lift}(k) \end{aligned} \tag{7.53}$$

where the extended input vector $u_{lift}(k)$ has size mn_s and is defined as

$$\mathbf{u}_{lift}(k) = \left[\tilde{\mathbf{u}}(kn_s)^T \quad \cdots \quad \tilde{\mathbf{u}}(kn_s + n_s - 1)^T\right]^T$$

and the extended output vector $\mathbf{y}_{lift}(k)$ has size pn_s and is defined as

$$\mathbf{y}_{lift}(k) = \left[\ \tilde{\mathbf{y}}(kn_s)^T \quad \cdots \quad \tilde{\mathbf{y}}(kn_s + n_s - 1)^T\ \right]^T$$

The time invariant system matrices F, G, H, and E have dimensions, respectively, of n by n, n by mn_s, pn_s by n, and pn_s by mn_s and are given by [4, 11]

$$F = A(n_s-1)A(n_s-2)\cdots A(0) \tag{7.54}$$

$$G = \left[\Psi(n_s,1)B(0) \ \ \Psi(n_s,2)B(1) \ \ \Psi(n_s,n_s)B(n_s-1)\right] \tag{7.55}$$

$$H = \left[C(0)^T \ \ \Psi(1,0)^T C(1)^T \ \ \Psi(n_s-1,0)^T C(n_s-1)^T\right]^T \tag{7.56}$$

$$E = \{(E_{ij})\}, \quad i,j = 1,2,\ldots n_s \tag{7.57}$$

$$\text{with } E_{ij} = \begin{cases} 0 & i < j \\ D(i-1) & i = j \\ C(i-1)\Psi(i-1,j)B(j-1) & i > j \end{cases} \tag{7.58}$$

It should be noted that the matrix F is the Floquet Transition matrix of the discrete-time periodic system, Eq. (7.51), therefore the constant-coefficient lifted system of Eq. (7.53) has exactly the same stability characteristics as the time-periodic system. This Floquet Transition Matrix is also the same as that of the original continuous system, and therefore continuous and discrete systems also have the same stability characteristics [4, 11].

7.6.2 Lifted form of the HHC loop

Time lifting can be directly applied to the coupled helicopter/HHC system, Eqs. (7.47)-(7.50). The corresponding lifted form is given by:

$$\tilde{\mathbf{x}}(k+1) = F\tilde{\mathbf{x}}(k) + G\mathbf{u}_{lift}(k) \tag{7.59}$$

$$\mathbf{y}_{lift}(k) = H\tilde{\mathbf{x}}(k) + E\mathbf{u}_{lift}(k) \tag{7.60}$$

The input vector $\mathbf{u}_{lift}(k)$ is given by

$$\mathbf{u}_{lift}(k) = \begin{bmatrix} I \\ I \\ \vdots \\ I \end{bmatrix} \tilde{\mathbf{u}}_{HHC}(k) \tag{7.61}$$

where the mn_s by m matrix that relates $\mathbf{u}_{lift}(k)$ and $\tilde{\mathbf{u}}_{HHC}(k)$ is obtained by assembling n_s identity matrices because the HHC input vector $\tilde{\mathbf{u}}_{HHC}(k)$ is held constant over all the n_s samples that make up one rotor revolution.

Similarly, once the lifted output vector $\mathbf{y}_{lift}$ has been obtained as the output of the lifted system, Eqs. (7.59)-(7.60), the actual discrete output vector $\tilde{\mathbf{y}}_{HHC}(k)$ can be recovered by observing that it is the output of the Fourier coefficients extractor, which is only evaluated once per revolution, i.e., at times $\eta = 0, n_s, 2n_s, \ldots$. Therefore

$$\tilde{\mathbf{y}}_{HHC}(k) = [I \quad 0]\, \mathbf{y}_{lift}(k) \tag{7.62}$$

where $\mathbf{y}_{HHC}(k)$ has size p and $\mathbf{y}_{lift}(k)$ has size pn_s. On the basis of Eqs. (7.61) and (7.62), and recalling the state space form for the discrete HHC controller, Eqs. (7.35)-(7.36) the

overall closed loop system can be constructed as follows:

$$\tilde{\mathbf{x}}(k+1) = F\tilde{\mathbf{x}}(k) + G \begin{bmatrix} I \\ I \\ \vdots \\ I \end{bmatrix} \tilde{C}_C \mathbf{x}_C(k) \tag{7.63}$$

$$\tilde{\mathbf{x}}_C(k+1) = B_C \begin{bmatrix} I & 0 \end{bmatrix} H\tilde{\mathbf{x}}(k) + \left(\tilde{A}_C + \begin{bmatrix} I & 0 \end{bmatrix} E \begin{bmatrix} I \\ I \\ \vdots \\ I \end{bmatrix} \right) \tilde{\mathbf{x}}_C(k) \tag{7.64}$$

This closed loop helicopter/HHC system is now linear time-invariant, with discrete-time k and state variables $\tilde{x}_Z$, $\tilde{x}_H$, $\tilde{x}_F$, and $\tilde{x}_C$. Therefore, the closed loop stability analysis can be carried out by checking the eigenvalues of the closed loop system.

7.7 Results

This section presents closed-loop stability and response results for a coupled helicopter-HHC system. The stability results and the linearized time histories are obtained from the linearized, time-lifted model of Eqs. (7.63) and (7.64). The closed-loop response results are obtained from the full nonlinear simulation of the coupled helicopter-HHC system.

The helicopter configuration used for the present study is similar to the Eurocopter B0-105, with a thrust coefficient $C_T/\sigma = 0.071$. Three blade modes are used in the modal coordinate transformation, namely, the fundamental flap, lag, and torsion modes, with natural frequencies of 1.12/rev, 0.7/rev, and 3.4/rev, respectively. Because the aerodynamic model consists of a simple linear inflow with quasi-steady aerodynamics, vibratory loads and CG accelerations, and consequently also HHC inputs, tend to be underestimated. Therefore, their absolute values can be considered representative only in a qualitative sense. However, the overall simulation model is likely reasonable for stability studies, and for a general assessment of the design and closed-loop analysis methodology.

For all the vibratory response results, the helicopter is first trimmed in steady, straight

flight at the desired velocity with the HHC system turned off. Then, the nonlinear simulation begins, with the pilot controls held fixed at their trim values and the HHC system turned on at time $t = 0$.

The controller has been implemented in discrete time using a "fast" sampling rate of 16 samples per rotor revolution. The weighting matrices W and R which define the HHC quadratic performance index, Eq. (7.13), have been chosen to be proportional to the identity matrix, i.e., $W = wI$ and $R = rI$.

7.7.1 Results for V=80 kts

Figure 7.3 shows the closed-loop, vertical acceleration response $\dot{w}$ for three different values of the tuning parameter r, namely $r = 2 \cdot 10^4$ (top plot), $r = 5 \cdot 10^4$ (center plot), and $r = 10^5$ (bottom plot), corresponding to increasing restrictions on the control effort or, equivalently, to decreasing gain. Note that the scales on the vertical axis are different for each plot. For the value $r = 2 \cdot 10^4$ the response loosely resembles a limit cycle, but the values of the accelerations are of up to $\pm 1g$, and therefore unacceptably high. For this value of r the linearized analysis predicts an instability. For the value $r = 5 \cdot 10^4$ the response is unstable, but the values of $\dot{w}$ are now considerably smaller, and remain within $\pm 0.04g$ within the first seven seconds. The linearized analysis indicates a mild instability. Finally, for $r = 10^5$, the response becomes stable and the HHC is very effective in suppressing $\dot{w}$. This is also predicted by the linearized analysis. The behavior of roll and pitch accelerations is qualitatively very similar to that of $\dot{w}$, and it will not be shown here.

Similar plots had been presented in Ref. [28] for the same flight condition and helicopter configuration, but with the HHC closed loop modeled as entirely continuous, and the harmonic analysis, the computation delay, and the zero-order-hold not modeled at all. For values of the tuning parameter r ranging from 0 to 10^4 the response was stable, and the HHC would effectively suppress vibrations in 10 seconds or less. Comparing these results

with those shown in Fig. 7.3, it is clear that the allowable gains of the HHC system must be lower because of the reduction in phase margin brought about by the delays in the HHC loop.

Selected closed loop stability eigenvalues are shown in Fig. 7.4 as a function of r. In the top portion of the figure the eigenvalues are presented in root locus plot form, in the bottom portion the real parts of the eigenvalues are plotted as a function of r. These are the eigenvalues of the discrete system, converted to continuous form. The closed loop system becomes unstable for $r < 1.5 \cdot 10^5$. This instability was not captured by the approximate continuous HHC model of Ref. [28], which instead predicted closed loop stability for every value of r. This clearly demonstrates that neglecting the discrete nature of the HHC loop is unconservative, and should be avoided.

Figure 7.5 shows the time history of the response of just the 4/rev harmonic of $\dot{w}$. The three curves show, respectively, the baseline response with the HHC system turned off, the response predicted by the nonlinear simulation model, and that predicted by the linearized, time periodic model used to design the HHC system. Apart from a small initial transient, caused by a small initial mismatch between the trimmed and the time-marching solution, the baseline 4/rev response rapidly converges to a constant, nonzero steady value. The nonlinear closed-loop response exhibits a brief but strong transient, during which the acceleration increases by almost three times the baseline value. The transient lasts for less than 2 seconds, after which the 4/rev response is rapidly reduced to almost zero. This strong transient is not present in the $\dot{p}$ and $\dot{q}$ 4/rev responses, not shown in the figure, which start being attenuated as soon as the HHC is turned on. The figure also shows that the 4/rev responses predicted by the LTP and by the nonlinear model are nearly identical. This indicates that, for the type of mathematical model used in this study, and for the flight condition considered, (i) the effect of nonlinearities on the 4/rev $\dot{w}$ response is small, and the response is adequately captured by a linearized model as long as the periodicity is retained

(the same conclusions hold for $\dot{p}$ and $\dot{q}$), and (ii) the LTP model is sufficiently accurate for the HHC design.

The magnitude of the 3/, 4/, and 5/rev control harmonics are plotted in Fig. 7.6 as a function of time. The controls for both the rigorous discrete model and the approximate continuous model are shown in the figure. Discrete and continuous controls tend to the same magnitude value, but the initial transients are quite different. The magnitudes of the discrete controls grow much faster than those of the continuous controls. The magnitudes of the 3/ and 4/rev harmonics of the discrete controller reach essentially the respective steady state values in about 2 seconds, that of the 5/rev harmonic in about 6 seconds. The respective values for the continuous case are well over 6 seconds for the 3/ and 5/rev, and about 6 seconds for the 4/rev. This behavior, which is to some extent counterintuitive given that the discrete HHC is operating at a lower gain than the continuous HHC, is responsible for the faster vibration reduction of the discrete HHC.

Better agreement between the phases of the discrete and continuous model can be seen in Fig. 7.7. Except for the first 1-2 rotor revolutions (slightly more for the 4/rev control), discrete and continuous phases are almost identical.

7.7.2 Results for V=140 kts

Figure 7.8 shows the closed-loop, vertical acceleration response $\dot{w}$ for three different values of the tuning parameter r, namely $r = 10^4$ (top plot), $r = 5 \cdot 10^4$ (center plot), and $r = 10^5$ (bottom plot). The scale on the vertical axis of the top plot is different from those of the other two. As in the 80 kts case, for the value $r = 10^4$ the acceleration response is very high and erratic, with peaks well over $1g$ in absolute value, and loosely resembling a limit cycle. For this value of r the linearized analysis predicts an instability. For the value $r = 5 \cdot 10^4$ the response is stable, and slowly decreases in magnitude. Finally, for $r = 10^5$, the response is stable and the vibrations are reduced very quickly, in less than 2 seconds

from the application of HHC. The linearized analysis also indicates that these last two cases are stable. The behavior of roll and pitch accelerations is qualitatively very similar to that of $\dot{w}$, and it will not be shown here.

Compared with the corresponding plots of Ref. [28], for the same flight condition but with a continuous HHC model, the allowable gains are lower. In Ref. [28] the closed-loop system was studied for values of r ranging from 0 to 1000, and in all cases it was stable.

Figure 7.9 is similar to Fig. 7.5, but refers to $V = 140$ kts. As in Fig. 7.5, after a small initial transient, the baseline 4/rev response rapidly converges to a constant, nonzero steady value. The nonlinear closed-loop response no longer exhibits the strong transient observed at $V = 80$ kts, and the 4/rev response is substantially reduced after just one second. The same happens for the $\dot{p}$ and $\dot{q}$ 4/rev responses, not shown in the figure. As in the $V = 80$ kts case, the 4/rev responses predicted by the LTP and by the nonlinear model are nearly identical, and the same conclusions on the effect of nonlinearities and the adequacy of the LTP model for design purposes apply.

The magnitude of the 3/, 4/, and 5/rev harmonics are plotted in Fig. 7.10 as a function of time. The controls for both the discrete and the continuous model are shown in the figure. As in the $V = 80$ kts case, discrete and continuous controls tend to the same magnitude value, although the initial transients are quite different and the magnitudes of the discrete controls grow much faster than those of the continuous controls. The magnitudes of all the harmonics of the discrete controller reach their respective steady state values in about 2 seconds. The respective values for the continuous case are of 6 seconds and more. An almost perfect agreement between the phases of the discrete and continuous model can be seen in Fig. 7.11. Except for the first few rotor revolutions, discrete and continuous phases are almost identical.

7.7.3 Other considerations

The results presented in this section underscore the importance of a correct modeling of "real life" effects such as discrete sampling, computations, and control updates, even for the simplified, fixed T-matrix scheme used in this study. Several additional effects were neglected, and should be included or more carefully analyzed in future research. First, in the scheme of Fig. 7.2, it was assumed that the transient following each HHC update would take one quarter of a rotor revolution to die out. Simulation results not presented here indicate that a more realistic figure is 1-2 rotor revolutions for well-damped rotors with mechanical lag dampers, and up to 4-6 revolutions for lowly damped hingeless rotors. Second, the HHC update at each rotor revolution was simulated as a pure step. While rotating system HHC actuators are very fast, they cannot generate such steps, and therefore they add their own delay. Third, perfect measurements were assumed, whereas real sensors introduce their own dynamics in the loop. Finally, practical digital harmonic analyses will require the use of windows, which may introduce further delays and spurious dynamics. All these effects must be taken into account to obtain realistic predictions of the maximum performance achievable by an HHC system.

7.8 Conclusions

This chapter presented an aeromechanical closed loop stability and response analysis of a hingeless rotor helicopter with an HHC system for vibration reduction. The analysis fully included the rigid body dynamics of the helicopter and the flexibility of the rotor blades. It was assumed that the gain matrix T was fixed and computed off-line. The discrete elements of the HHC control loop were rigorously modeled, including the presence of two different time scales in the loop. By also formulating the coupled rotor-fuselage dynamics in discrete form, the entire coupled helicopter-HHC system could be rigorously modeled as a discrete

system. Finally, the effect of the periodicity of the equations of motion was rigorously taken into account by converting the system with periodic coefficients into an equivalent system with constant coefficients and identical stability properties using a time lifting technique.

The most important conclusion of the present study is that the discrete elements in the HHC loop must be modeled in any HHC analysis. Not doing so is unconservative. For the helicopter configuration and HHC structure used in this study, an approximate continuous modeling of the HHC system indicated that the closed loop, coupled helicopter-HHC system was always stable, whereas the more rigorous discrete analysis shows that closed loop instabilities can occur. The HHC gains must be reduced to account for the loss of gain margin brought about by the discrete elements.

Other conclusions of the study are: (i) the HHC is effective in quickly reducing vibrations, at least at its design condition; (ii) a linearized model of helicopter dynamics is adequate for HHC design, as long as the periodicity of the system is correctly taken into account, i.e., periodicity is more important than nonlinearity, at least for the mathematical model used in this study; and (iii) when discrete and continuous systems are both stable, the predicted HHC control harmonics are in good agreement, although the initial transient behavior can be considerably different.

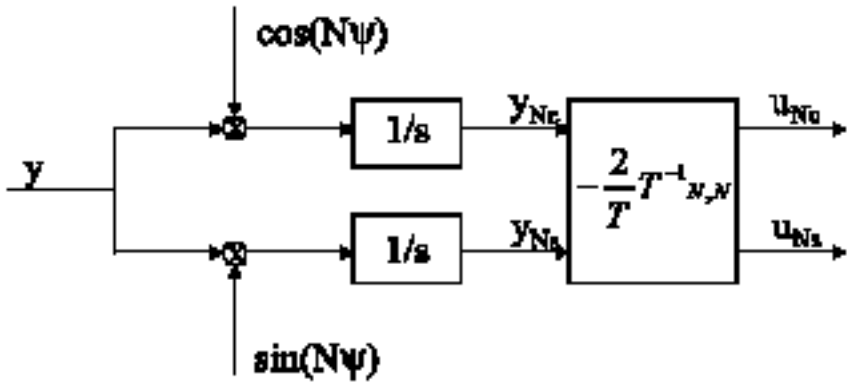

Figure 7.1: Block diagram of a HHC loop (Thin lines: continuous signals; thick lines: "fast sampling" discrete signals; double lines: 1/rev sampling signals.)

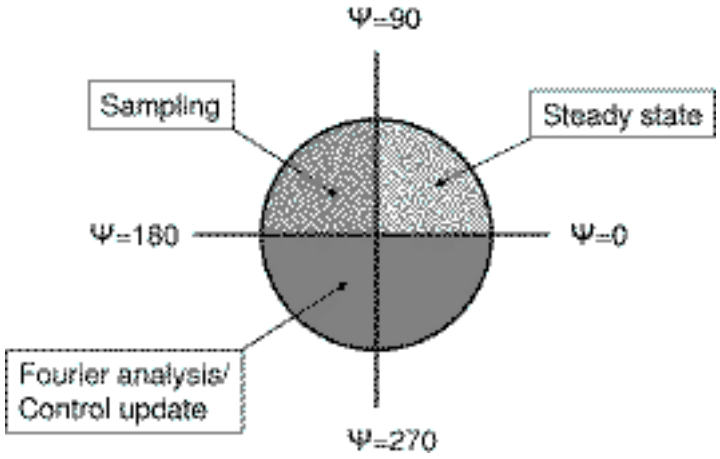

Figure 7.2: Operation of the control system over one rotor revolution period T, as a function of the azimuth angle ψ.

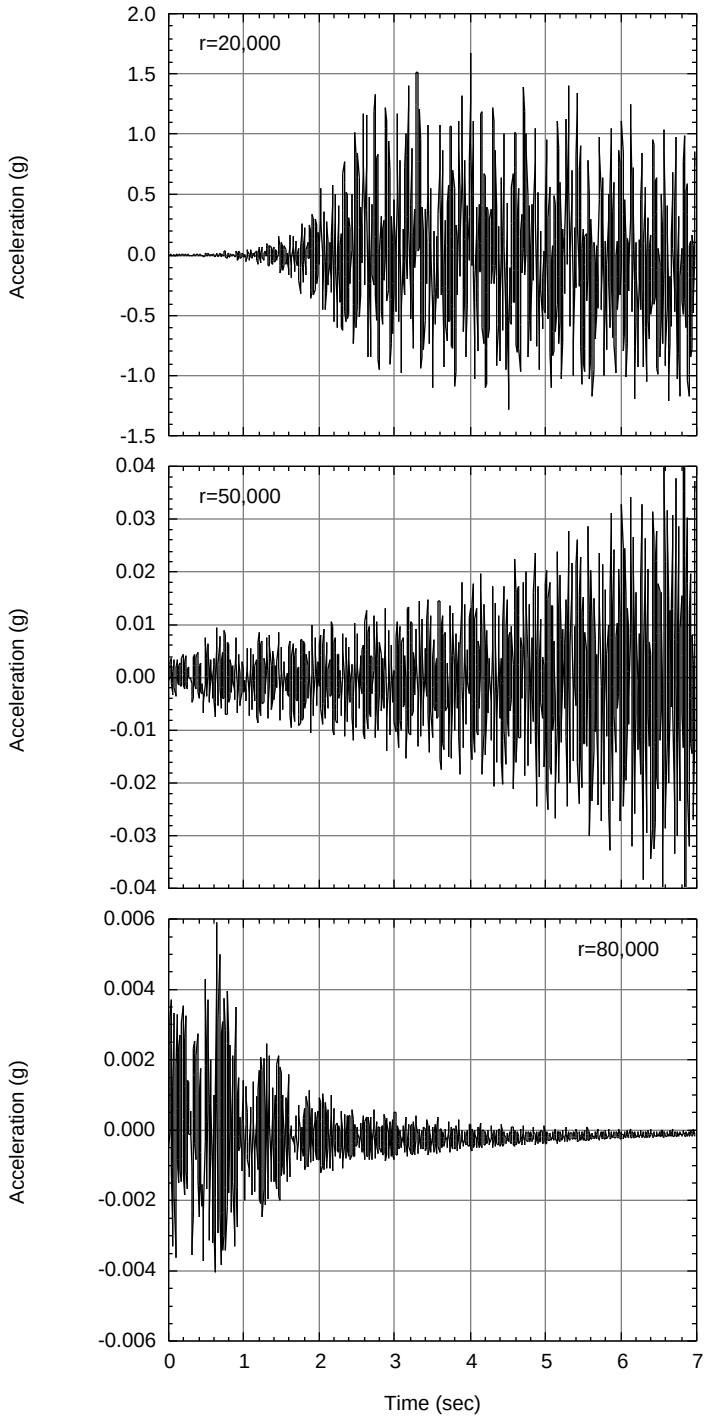

Figure 7.3: Vertical accelerations $\dot{w}$ at the helicopter center of mass for V=80 kts ($\mu = 0.188$) and tuning parameter $r = 2 \cdot 10^4$ (top), $r = 5 \cdot 10^4$ (center), and $r = 10^5$ (bottom).

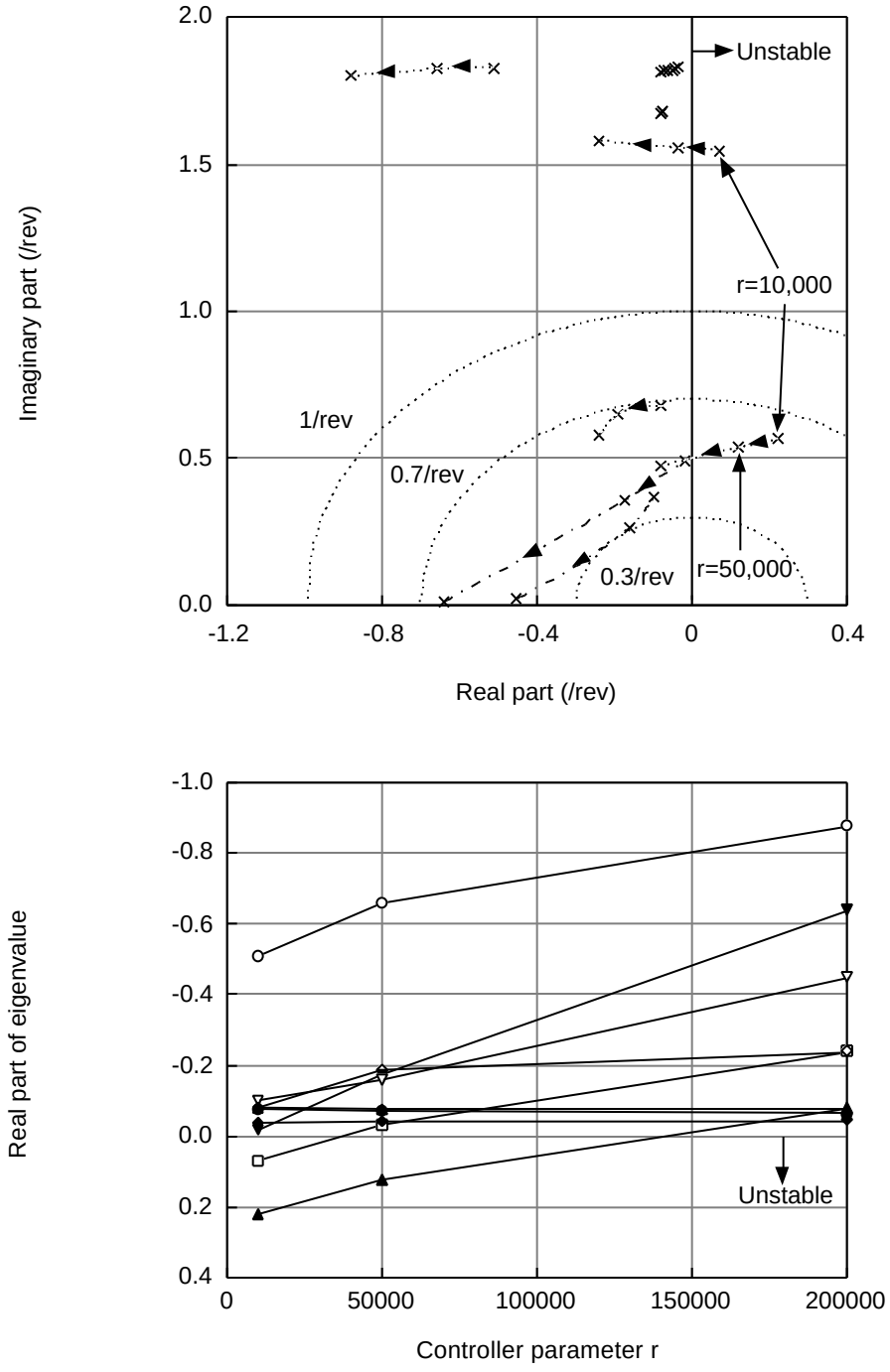

Figure 7.4: Selected closed loop stability eigenvalues for V=80 kts ($\mu = 0.188$) as a function of the controller tuning parameter r; root locus plot (top) and real parts only (bottom).

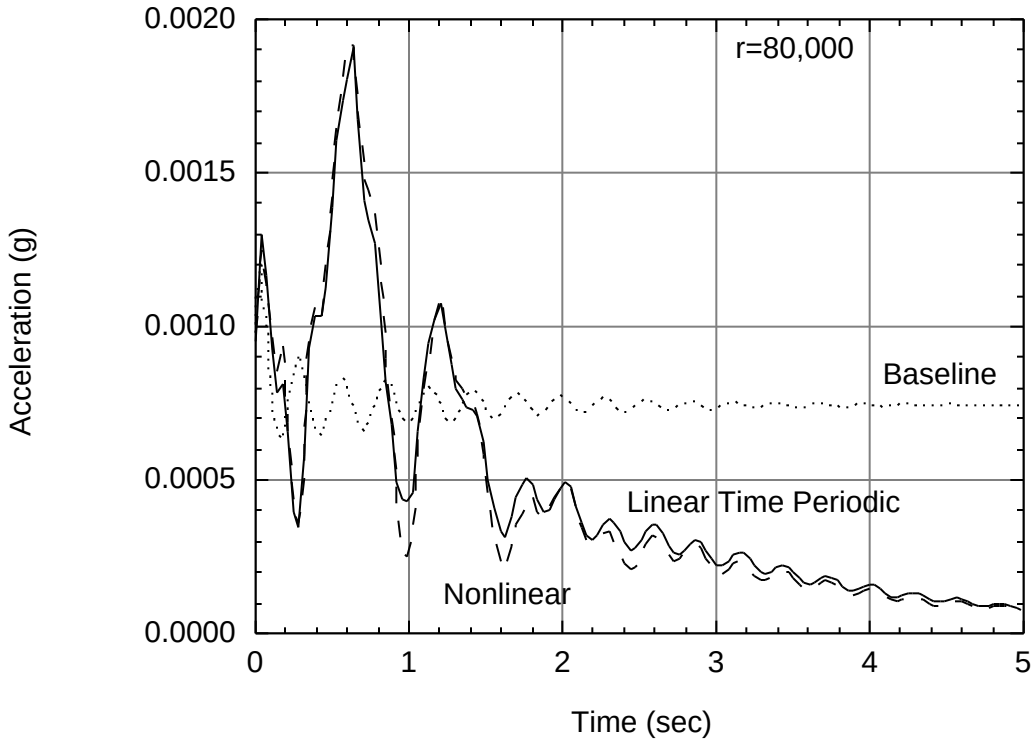

Figure 7.5: Closed loop 4/rev vertical acceleration response $\dot{w}$ at the helicopter center of mass for V=80 kts ($\mu = 0.188$); baseline open-loop response, and prediction with linear and nonlinear simulation model.

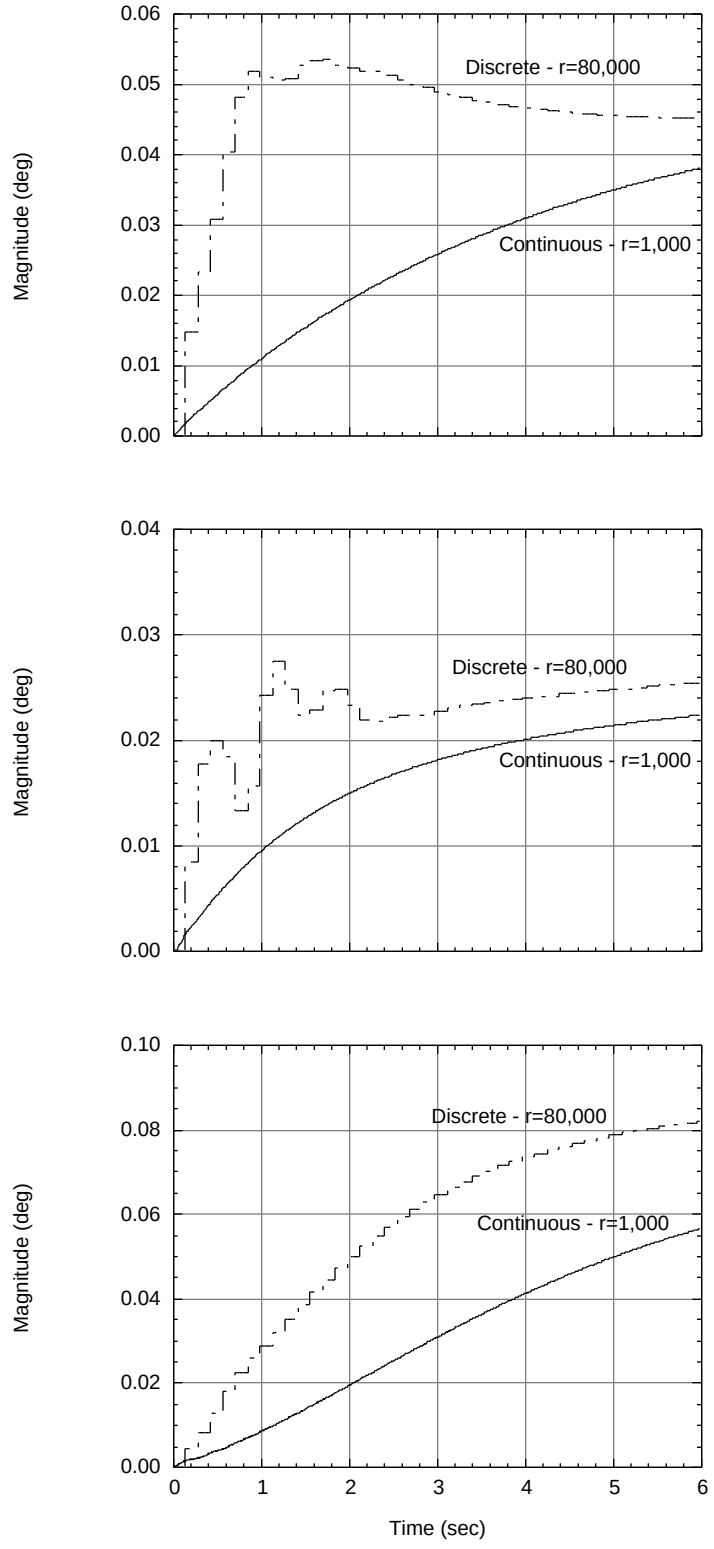

Figure 7.6: HHC control input magnitude in degrees for continuous and discrete models, V=80 kts ($\mu \approx 0.189$); 3/rev (top), 4/rev (center), 5/rev (bottom).

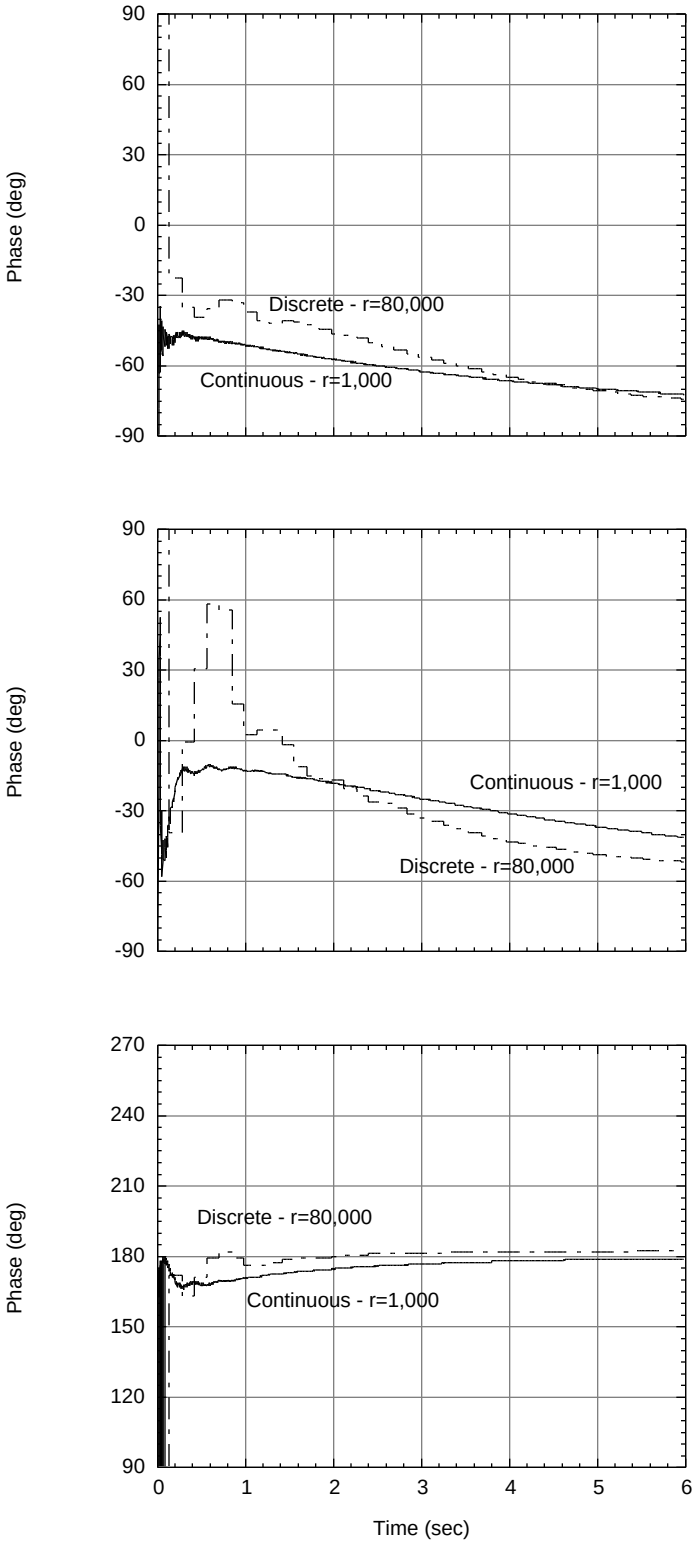

Figure 7.7: HHC control input phase in degrees for continuous and discrete models, V=80 kts ($\mu \approx 0.189$); 3/rev (top), 4/rev (center), 5/rev (bottom).

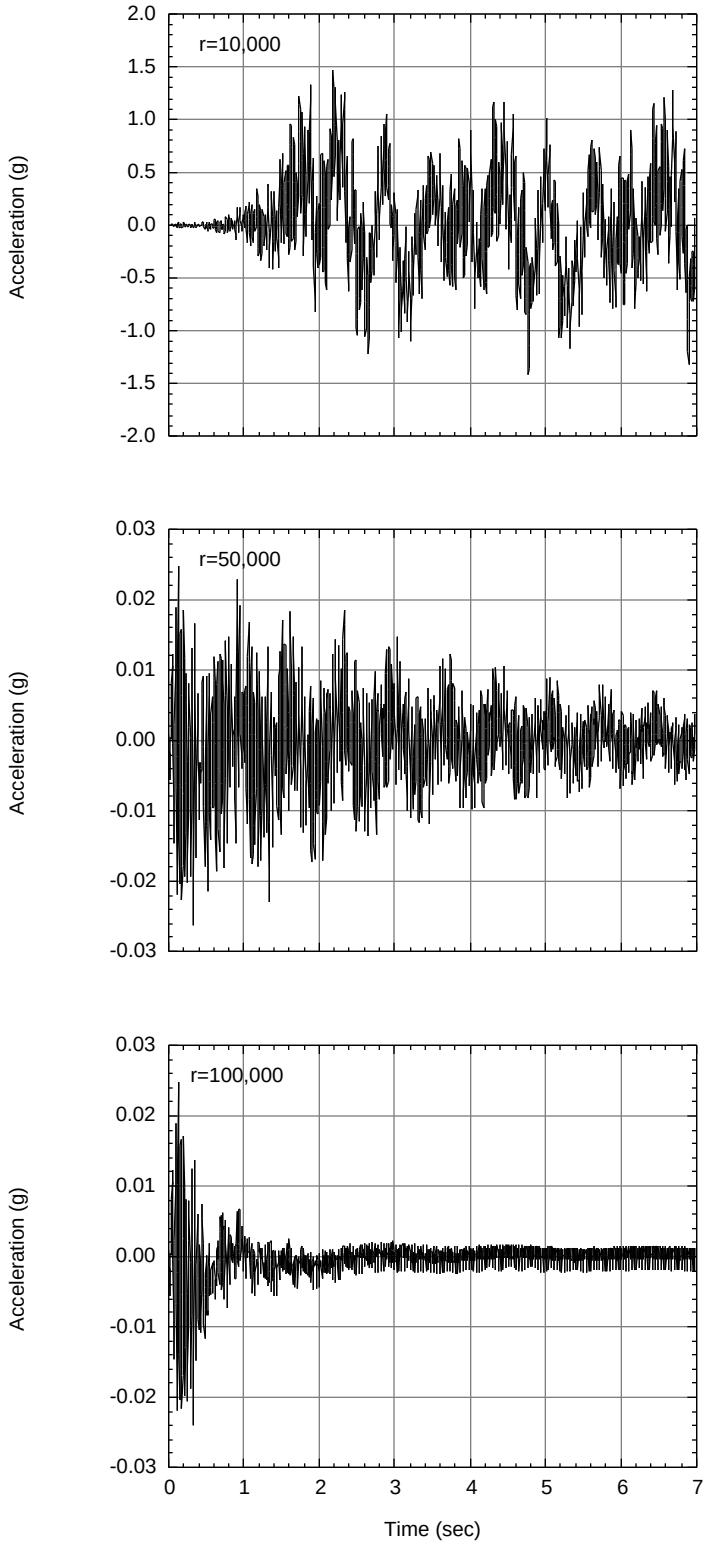

Figure 7.8: Vertical accelerations $\dot{w}$ at the helicopter center of mass for V=140 kts ($\mu = 0.330$) and tuning parameter $r = 10^4$ (top), $r = 5 \cdot 10^4$ (center), and $r = 10^5$ (bottom).

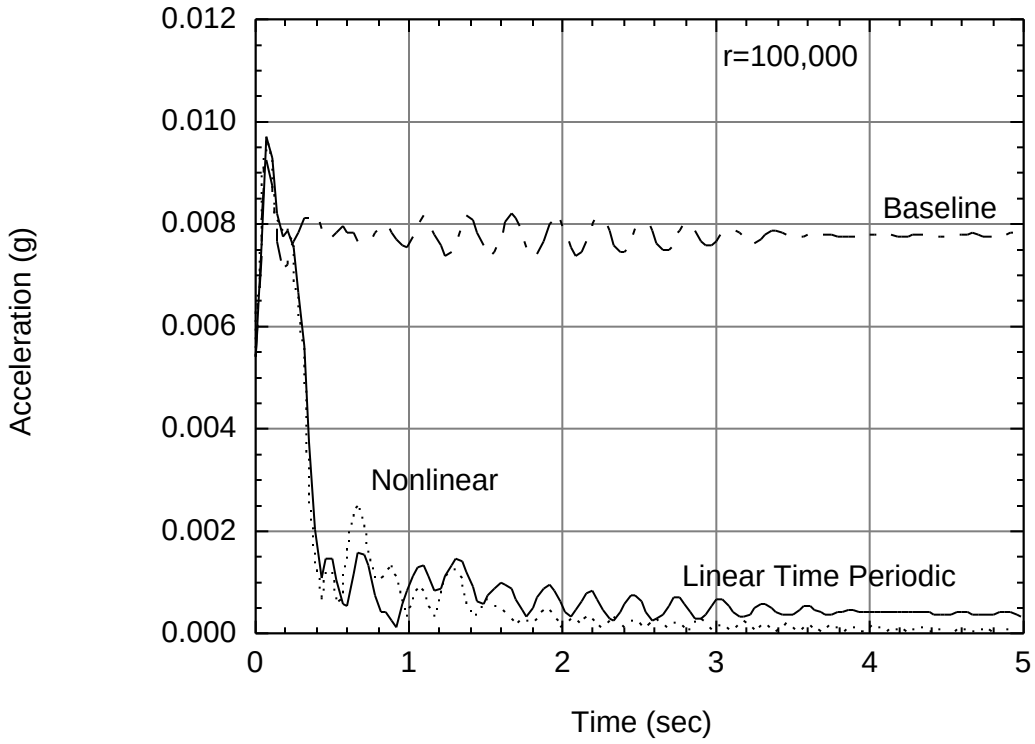

Figure 7.9: Closed loop 4/rev acceleration response $\dot{w}$ at the helicopter center of mass for V=140 kts ($\mu = 0.330$); baseline open-loop response, and prediction with linear and nonlinear simulation model.

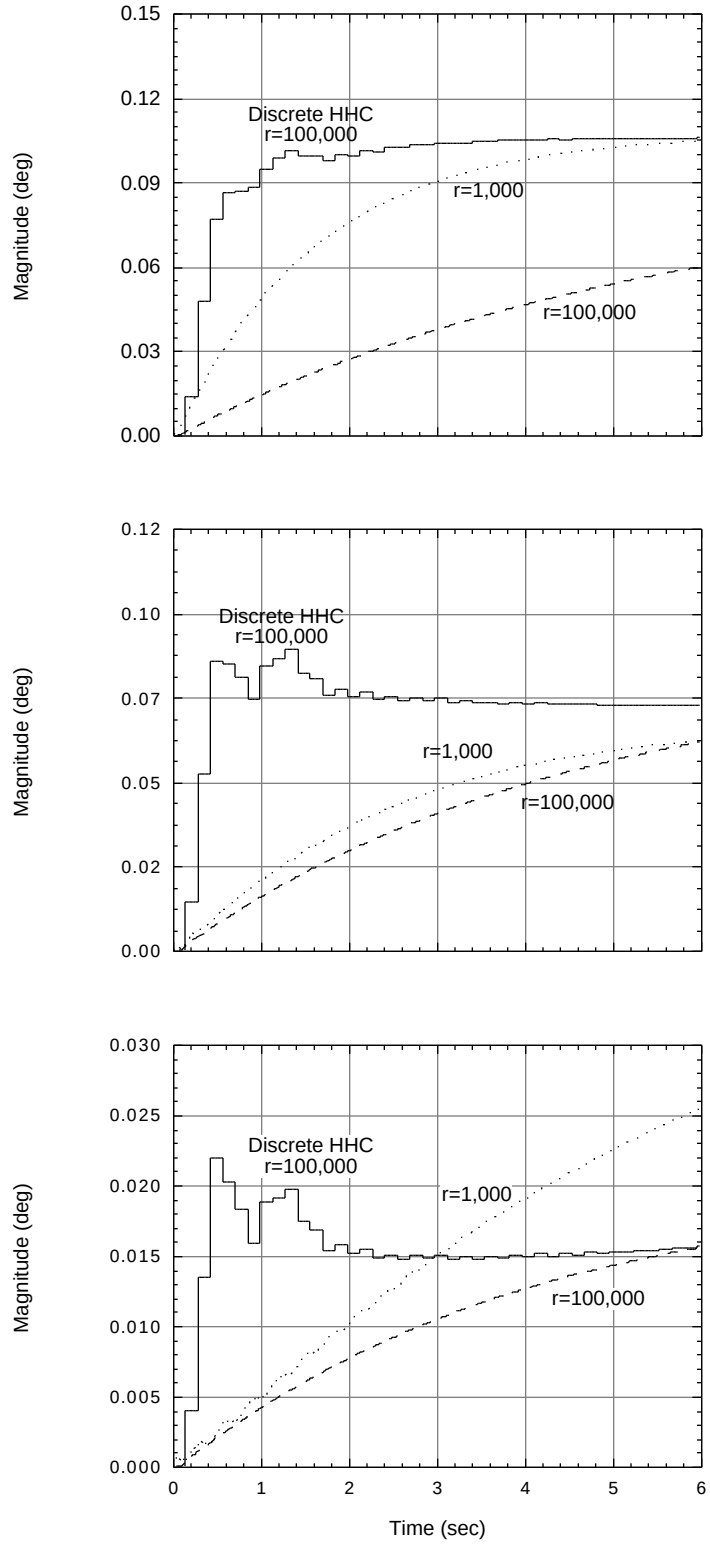

Figure 7.10: HHC control input magnitude in degrees for continuous and discrete models, V=140 kts ($\mu = 0.330$); 3/rev (top), 4/rev (center), 5/rev (bottom).

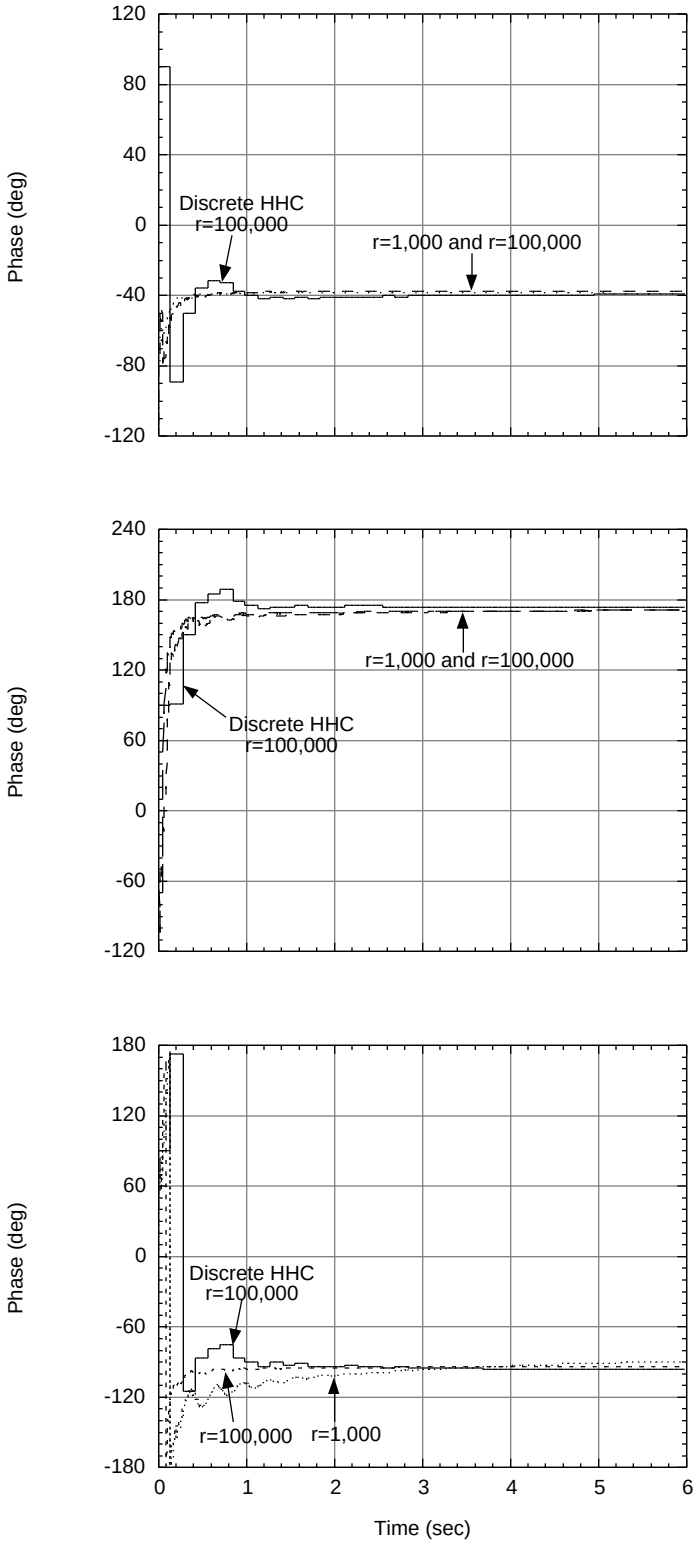

Figure 7.11: HHC control input phase in degrees for continuous and discrete models, V=140 kts ($\mu = 0.330$); 3/rev (top), 4/rev (center), 5/rev (bottom).

Bibliography

[1] Bittanti, S., and Colaneri, P., "Periodic control," in J.G. Webster, editor, *Wiley Encyclopedia of Electrical and Electronic Engineering*, John Wiley and Sons, New York, 1999, pp. 59-73.

[2] Bittanti, S., and Bolzern, P., "Discrete Linear Periodic Systems: Gramian and Modal Criteria for Reachability and Controllability," *International Journal of Control*, Vol. 41, (4), 1985, pp. 909-928.

[3] Bittanti, S., Bolzern, P., and Guardabassi, G., "Some Critical Issues Concerning the State-Representation of Time-Varying ARMA Models," *Proceedings of the 7th IFAC Symposium on Identification and System Parameter Estimation*, York, England, 1985, pp. 1479-1484.

[4] Bittanti, S., and Colaneri, P., "Invariant Representations of Discrete-Time Periodic Systems," *Automatica*, Vol. 36, pp. 1777-1793, 2000.

[5] Bittanti, S., and Lovera, M., "On the Zero Dynamics of Helicopter Rotor Loads," *European Journal of Control*, Vol. 1, Jan 1996, pp. 57-68.

[6] Bojanczyk, A., Golub, G., and Van Dooren, P., "The Periodic Schur Form. Algorithms and Applications," *Proceedings SPIE Conference, San Diego, USA*, 1992, pp. 31–42.

[7] Bolzern, P., Colaneri, P., and Scattolini, R., "Zeros of Discrete Time Linear Periodic Systems," *IEEE Transactions on Automatic Control*, Vol. 31, 1986, pp. 1057-1058.

[8] Celi, R., "Hingeless Rotor Dynamics in Coordinated Turns," *Journal of the American Helicopter Society*, Vol. 36, No. 4, 1991, pp. 39-47.

[9] Cheng, R. P., Tischler, M. B., and Celi, R., "A High-Order, Time Invariant Linearized Model for Application to HHC/AFCS Interaction Studies," *Proceedings of the 59th Annual Forum of the American Helicopter Society*, Phoenix, AZ, 2003.

[10] Chopra, I., "Perspectives in Aeromechanical Stability of Helicopter Rotors," *Vertica*, Vol. 14, (1), 1990.

[11] Colaneri, P., Celi, R., and Bittanti, S., "Constant-Coefficient Representations of Periodic-Coefficient Discrete Linear Systems," *Proceedings of the AHS 4th Decennium Specialist's Conference on Aeromechanics*, San Francisco, CA, Jan 2004.

[12] Colaneri, P., and Longhi, S., "The realization problem for linear periodic systems," *Automatica*, Vol. 31, pp. 775-779, 1995.

[13] Colaneri, P., and Longhi, S., "The Minimal Realization Problem for Discrete-Time Periodic Systems," *Automatica*, Vol. 31, 1995, pp. 779-783.

[14] D'Angelo, H., *Linear Time-Varying Systems: Analysis and Synthesis*, Allyn and Bacon, 1970, pp. 193-220.

[15] De Nicolao, G., and Ferrari-Trecate, G., "On the Zeros of Discrete Time Linear Periodic Systems," *Circuits, Systems, Signal Processing*, Vol. 16, 1997, pp. 703-718.

[16] De Nicolao, G., Ferrari-Trecate, G., and Pinzoni, S., "Zeros of Continuous-Time Linear Periodic Systems," *Automatica*, Vol. 34, (12), 1998, pp. 1651-1655.

[17] Du Val, R., Gregory, C., and Gupta, N., "Design and Evaluation of a State Feedback Vibration Controller," *Journal of the American Helicopter Society*, Vol. 29, No. 3, 1984, pp. 30-37.

[18] Friedmann, P. P., "Recent Trends in Rotary-Wing Aeroelasticity," *Vertica*, Vol. 11, (1/2), 1987.

[19] Friedmann, P. P., "Helicopter Rotor Dynamics and Aeroelasticity—Some Key Ideas and Insights," *Vertica*, Vol. 14, (1), 1990.

[20] Friedmann, P.P., and Millott, T., "Vibration Reduction in Rotorcraft Using Active Control-A Comparison of Various Approaches," *Journal of Guidance, Control and Dynamics*, Vol. 18, No. 4, 1995, pp. 664-673.

[21] Golub, G., and Van Loan, C., *Matrix Computations*, Johns Hopkins University Press, 1989.

[22] Goodman, R. K., and Millott, T. A., "Design, Development, and Flight Testing of the Active Vibration Control System for the Sikorsky S-92," *Proceedings of the 56th Forum of the American Helicopter Society*, Virginia Beach, VA, May 2000.

[23] Grasselli, O., and Longhi, S., "Zeros and Poles of Linear Periodic Multivariable Discrete Time Systems," *Circuits, Systems, Signal Processing*, Vol. 7, 1988, pp. 361-380.

[24] Johnson, W., *Helicopter Theory*, Princeton University Press, 1980.

[25] Johnson, W., "Self-Tuning Regulators for Multicyclic Control of Helicopter Vibration," NASA TP 1996, March 1992.

[26] Kuijper, M., and Willems, J. C., "A Behavioral Framework for Periodically Time-Varying Systems," *Proceedings of the IEEE Conference on Decision and Control*, San Diego, CA, 1997, pp. 2013-2016.

[27] Lovera, M., Colaneri, P., and Celi, R., "Periodic Analysis of Higher Harmonic Control Techniques for Helicopter Vibration Attenuation," *Proceedings of the 2003 American Control Conference*, Denver, CO, 2003.

[28] Lovera, M., Colaneri, P., Malpica, C., and Celi, R., "Closed-Loop Aeromechanical Stability Analysis of HHC and IBC, with Application to a Hingeless Rotor Helicopter," *Proceedings of the 2003 European Rotorcraft Forum*, Friedrichshafen, Germany, September 2003.

[29] Lovera, M., Colaneri, P., Malpica, C., and Celi, R., "Discrete-Time, Closed-Loop Aeromechanical Stability Analysis of Helicopters With Higher Harmonic Control," *Proceedings of the 60th Annual Forum of the American Helicopter Society*, Baltimore, MD, June 2004.

[30] Lust, K., "Numerical Bifurcation Analysis of Periodic Solutions of Partial Differential Equations," Ph.D Dissertation, Katholieke Universiteit Leuven, Belgium, 1997.

[31] Lust, K., "Improved Numerical Floquet Multipliers," *International Journal of Bifurcation and Chaos*, Vol. 11, (9), 2001, pp. 2389–2410.

[32] Muller, M., Arnold, U. T. P., and Morbitzer, D., "On the Importance and Effectiveness of 2/rev IBC for Noise, Vibration and Pitch Link Load Reduction," *Proceedings of the 55th Annual Forum of the American Helicopter Society*, Virginia Beach, VA, 2000.

[33] Pearson, J. T., and Goodall, R.M., "Adaptive schemes for the active control of helicopter structural response," *IEEE Transactions on Control Systems Technology*, Vol. 2, No. 2, Jun 1994, pp. 61-72.

[34] Rugh, W. J., *Linear System Theory*, 2nd edition, Prentice Hall, 1996.

[35] Shaw, J., and Albion, N, "Active Control of the Helicopter Rotor for Vibration Reduction," *Journal of the American Helicopter Society*, Vol. 26, No. 4, 1981, pp. 32-39.

[36] Sinha, S. C., and Butcher, E. A., "Symbolic Computation of Fundamental Solution Matrices for Linear Time-Periodic Dynamical Systems," *Journal of Sound and Vibration*, Vol. 206, (1), 1997, pp. 61-85.

[37] Teves, D., Niesl, G., Blaas, A., and Jacklin, S., "The Role of Active Control in Future Rotorcraft," Paper III.10.1–17, *Proceedings of the 21st European Rotorcraft Forum*, Saint Petersburg, Russia, 1995.

[38] Theodore, C., and Celi, R., "Helicopter Flight Dynamic Simulation with Refined Aerodynamic and Flexible Blade Modeling," *Journal of Aircraft*, Vol. 39, No. 4, 2002, pp. 577-586.

[39] Welsh, W. A., "Evolution of Active Vibration Control Technology," *Proceedings of the AHS 4th Decennium Specialist's Conference on Aeromechanics*, San Francisco, CA, Jan 2004.

[40] Wereley, N., and Hall, S., "Linear Control Issues in the Higher Harmonic Control of Helicopter Vibrations," *Proceedings of the 45th Forum of the American Helicopter Society*, Boston, MA, 1989, pp. 955-972.

[41] Wereley, N., and Hall, S. "Frequency Response of Linear Time Periodic Systems," *Proceedings of the 29th IEEE Conference on Decision and Control*, 1990, Honolulu, HI, pp. 3650-3655.

[42] Zhou, J., and Hagiwara, T., "H_2 and H_∞ Norm Computations of Linear Continuous-Time Periodic Systems Via the Skew Analysis of Frequency Response Operators," *Automatica*, Vol. 38, No. 8, 2002, pp. 1381-1387.

[43] Zhou, J., Hagiwara, T., and Araki, M., "Stability Analysis of Continuous-Time Periodic Systems Via the Harmonic Analysis," *IEEE Transactions on Automatic Control*, Vol. 47, (2), 2002, pp. 292-298.